Dissertation

submitted to the

Combined Faculties for the Natural Sciences and for Mathematics

of the Ruperto-Carola University of Heidelberg, Germany

for the degree of

Doctor of Natural Sciences

presented by

M. Sc. Alvaro Banderas

born in Copiapó, Chile

Oral examination:

27th of July, 2015

Population-parameter sensing in the mating system of *Saccharomyces cerevisiae*

Referees:

Prof. Dr. Victor Sourjik

Prof. Dr. Sabine Strahl

A mis amigos.

Acknowledgments

I sincerely and deeply thank Victor for accepting me in his lab, for always teaching passively by simply giving the example, for always being optimistic, for always supporting me in science and life matters and most importantly for believing in my scientific ideas and refining them with his always sharp razor of scientific parsimony. It is highly stimulant and motivating to work with someone you basically feel admiration for. I also deeply thank Alex, who always helped me and was willing to share his constructs, strains, knowledge and friendship. Most importantly, I thank his sharp eye for spotting things I many times missed and to be the first one to establish the necessary skepticism on my ideas. To Gabriele, for helping me in my first steps in Germany inside and outside of the lab, for being an optimist and for being a relational buffer and making environments happy. To Misi for all the super-stimulant brainstormings that inspired experiments and ideas, his always thoughtful insights, for his help with math when I needed it, and his permanent willingness to talk about science anywhere. I also thank all the Sourjik lab with no exception, specially to Max who translated the abstract of this thesis to German, Michal who also helped me with thesis revisions, Yu, Olga, Silke and Vladimir for their authenticity which made me feel at home with very simple conversations and Verena with whom I shared good time being the last two people from our lab staying at ZMBH. Also all the staff at ZMBH. My examiners Sabine and Thomas for their always useful comments on the TAC meetings. I want to thank also Edgar for being my friend and sharing a deep interest in epistemology and cognition as I do. To Pame for always helping me when I had problems with algebra and being my most important support in my time here. To Pedro, Tomás and Ricardo for the music. Finally I thank my parents and family for their permanent support.

Summary

Sexual reproduction is a key evolutionary innovation which sets the ground for sexual selection. Sexual selection exhibits a strong dependence on the degree of competition in a mating population. The tie between active perception of competition and sexual behavior is a crucial process for intra and intersexual selection, however, its mechanisms remain largely unknown due to experimental intractability. Unicellular mating occurs under the same constraints but population and environmental parameters can be experimentally controlled and dynamic measurements of molecular and behavioral outputs can be performed. In this work, we propose that on the prototypical chemosensory mating system from *Saccharomyces cerevisiae*, the response magnitude generated by the presence of the complementary sex equals the probability of forming a sexual pair by chance. In chemosensory (pheromonal) mating systems, perception of competition as an indicator of mating likelihood is constrained by the following fact. Given that the most reasonable measure of the degree of competition/mating-likelihood in the population is the operational sex ratio, i.e. the fraction of individuals of a particular sex in the sexually active population (OSR in animals or θ in this work), sensory systems would need information about the abundance of individuals of both sexes, whereas the sexual response is induced by pheromones produced only by the opposite sex. Therefore, the OSR seems sensorially indistinguishable from the absolute number of potential mates, which would make mating likelihood imperceptible. By using experiments where the emitted pheromone concentration is isotropic and therefore does not depend on the distance separating mates, we manipulated population parameters and measured quantitative mating-pheromone pathway outputs to show that yeast is able to effectively sense the population sex ratio (θ) and the absolute mate number as separate cues by using a sensory disentangling mechanism. The mechanism is based on sensory input attenuation, i.e. the enzymatic degradation of the sexual pheromone produced by the opposite sex. As revealed by a simple physical model, the population displays specific sensitivities to sex ratio and cell density by modifying the time profile of pheromone concentration, with its maxima depending linearly on emitter cell density, and scaled by the inverse square root of receiver cell density. We show that in a random collision scenario the sex-ratio of the population indeed determines the likelihood of successful sexual pairing, matching the gene-expression response to sex ratio. Sensing mating likelihood allows control of mating investments, minimizing growth arrest and pathway overstimulation. Pheromone-based mate-sensing constitutes an example of a population-level fractional sensing mechanism, aided by the coupling of population-dependent signal attenuation and internal non-adaptive signal transduction. The study can be framed within the context of quantitative biology in its experimental methodology, and within (cellular) sensory systems, cell-cell communication and sexual selection theory because of its implications.

Zusammenfassung

Sexuelle Reproduktion ist eine zentrale evolutionäre Innovation und maßgebend für die sexuelle Selektion. Sexuelle Selektion korreliert stark mit dem Konkurrenzdruck, der in einer sich fortpflanzenden Population vorherrscht. Der Zusammenhang zwischen der aktiven Wahrnehmung von Konkurrenz und sexuellem Verhalten ist entscheidendend bei der intra- und intersexuellen Selektion. Aufgrund der experimentellen Komplexität sind die zugrundeliegenden Mechanismen jedoch weitestgehend unbekannt. Paarungen unter einzelligen Organismen geschehen mit denselben Einschränkungen, jedoch lassen sich Populationen und Umweltparameter experimentell kontrollieren und molekulare Vorgänge sowie das Verhalten in dynamischen Messungen bestimmen. In der vorliegenden Arbeit wurde die chemosensorische Kommunikation zwischen Zellen verschiedenen Paarungstyps der Hefe Saccharomyces cerevisiae untersucht. Es wurde gezeigt, dass in diesem System die Stärke der Antwort, welche durch den anderen Paarungstyp ausgelöst wird, annähernd der Wahrscheinlichkeit der zufälligen Kollision mit einer andersgechlechtlichen Partnerzelle entspricht. Prinzipiell ist in chemosensorischen (durch Pheromone vermittelten) Paarungssytemen die Wahrnehmung von Konkurrenz als Indikator der Paarungswahrscheinlichkeit eingeschränkt. Das operative Geschlechterverhältnis (OSR = operational sex ratio bei Tieren, θ in dieser Arbeit), welches den Anteil an Individuen des selben Geschlechts beschreibt, stellt die sinnvollste Messgröße für den Grad der Konkurrenz/ Paarungswahrscheinlichkeit in einer Population dar. Zur Detektion der OSR benötigen sensorische Systeme Informationen über die Häufigkeit beider Geschlechter; allerdings wird in chemosensorischen Systemen eine sexuelle Reaktion durch Pheromone induziert, welche nur von andersgeschlechtlichen Zellen produziert werden. Sensorisch scheint die OSR daher nicht unterscheidbar von der absoluten Zahl potentieller Geschlechtspartner, wodurch die Wahrscheinlichkeit einer Paarung nicht wahrnehmbar wäre. Durch Experimente, bei denen die Pheromonkonzentration isotropisch und daher unabhängig von der Distanz zwischen Geschlechtspartnern ist, wurden in der vorliegenden Arbeit Populationsparameter manipuliert und quantitativ die Aktivität des Pheromon-Signalweges gemessen. Dabei konnte gezeigt werden, dass Saccharomyces cerevisiae das Geschlechterverhältnis (θ) und die absolute Zahl potentieller Geschlechtspartner in einer Population als getrennte Hinweise mittels eines sensorischen Mechanismus zur Signalunterscheidung wahrnehmen kann. Dieser Mechanismus basiert auf einer Attenuation des Signals durch enzymatische Degradation des Sexualpheromons, welches von andersgeschlechtlichen Zellen produziert wird. In einem einfachen physikalischen Modell wird gezeigt, dass die Population unterschiedliche Sensitivitäten für Geschlechterverhältnis und absolute Zelldichte besitzt, indem sie die Pheromonkonzentration über die Zeit verändert. Die im Zeitverlauf erreichte maximale Pheromonkonzentration ist proportional zur Zelldichte der sekretierenden Zellen und invers proportional zur Quadratwurzel der Dichte der Empfängerzellen. Es wird gezeigt, dass in einem Szenario zufälliger Kollisionen die Wahrscheinlichkeit einer erfolgreichen sexuellen Paarung tatsächlich vom Geschlechterverhältnis in der Population bestimmt wird, welches wiederum mit der Genexpressionsantwort auf das Geschlechterverhältnis korreliert. Die Abschätzung der Paarungswahrscheinlichkeit ermöglicht eine Kontrolle des Investements in den Paarungsversuch, wodurch Wachstumsarrest und Signalweg-Überstimulierung minimiert werden. Die auf Pheromon basierende Kommunikation zwischen Partnerzellen in Hefe ist ein Beispiel für einen Mechanismus, in welchem das Verhältnis von verschiedenen Zelltypen auf Populationsebene wahrgenommen wird. Erreicht wird dies durch die Kopplung von populationsabhängiger Attenuation des Signals und einer nicht-adaptiven internen Signaltransduktion.

Contents

Abbreviations

Table 1: List of abbreviations

Abbreviation	Meaning
α_s	Initial α-factor concentration needed to observe shmooing in the *bar1*Δ *strain.*
α_{EC50}	Initial α-factor concentration needed to observe half-maximal P_{FUS1} response in the *bar1*Δ *strain.*
α_l	Local α-factor.
α_g	Global α-factor.
θ_α	Fraction of $MAT\alpha$ cells in the mixed population.
ρ_T	Total density of the mixed population.
ρ_a	Density of $MAT\boldsymbol{a}$ cells in the mixed population.
ρ_α	Density of $MAT\alpha$ cells in the mixed population.
Aga2	Adhesion subunit of a-agglutinin of $MAT\boldsymbol{a}$ cells. Interacts strongly with Sag1 from $MAT\alpha$.
Bar1	Pepsin-like endopeptidase only expressed in $MAT\boldsymbol{a}$ cells which cleaves α-factor (named after "barrier")
CFP	Cyan fluorescent protein.
FRET	Fluorescence (or Förster) resonance energy transfer.
Fus1	Protein which opens and expands the fusion pore [78]. Its transcription is strongly pheromone -dependent.
GFP	super-folder yeast codon-optimized monomeric green fluorescent protein (yEmGFP).
GPCR	G-protein coupled receptor.
MAPK	Mitogen-activated protein kinase (Fus3 in *S. cerevisiae*).
MAPKK	MAPK-kinase (Ste7 in *S. cerevisiae*).
MAPKKK	MAPKK-kinase (Ste11 in *S. cerevisiae*).
$MAT\boldsymbol{a}$	Mating-type a haploid yeast.
$MAT\alpha$	Mating-type α haploid yeast.
$MAT\alpha1$	First copy of the α-factor gene. Responsible for $\sim 90\%$ of its production.
$MAT\alpha2$	Second copy of the α-factor gene. Responsible for $\sim 10\%$ of its production.
MPP	Mating pheromone pathway.
PRE	Pheromone responsive element. DNA binding site for the pheromone-responsive Ste12 transcription factor
P_{FUS1}	Promoter from the FUS1 gene [39]. It has four copies of the PRE sequence and acts as the upstream activation sequence *FUS1*
r	Ratio of $MAT\boldsymbol{a}$ to $MAT\alpha$ cells in the mixed population.
Sag1	α-agglutinin. Interacts strongly with Aga2 from $MAT\boldsymbol{a}$.
Spa2	Stands for Spindle pole antigen. A protein that organizes the actin cytoskeleton and recruits cell-wall integrity MAP kinases. Spa2 is critical for shmooing through the default pathway.
Ste2	pheromone receptor (GPCR for the α-factor)
YFP	Yellow fluorescent protein.
wt	Wild-type strain.

List of Figures

List of Tables

Part I

Introduction

1 Yeast mating

The two haploid forms of *S. cerevisiae* cells, $MAT\boldsymbol{a}$ and $MAT\alpha$, mate by means of peptide-pheromone based communication, where $MAT\boldsymbol{a}$ cells secrete a-factor and $MAT\alpha$ cells secrete α-factor. Each mating type responds to the pheromone produced by complementary cells via a signal transduction pathway that activates expression of mating genes and induces mating-specific morphologies [7].

1.1 The pheromone reponse pathway

The molecular mechanisms involved in pheromone transduction and cell polarization have been characterized in great detail using classic biochemical and genetic tools. The signaling pathway used for mating is a mitogen-activated protein kinase (MAPK)-type pathway called the mating pheromone pathway (MPP). This pathway is part of a more complex network of MAPK pathways operating in yeast [71]. The MAPK signaling pathways are well conserved across eukaryotic evolution, for this reason they are prototypical signaling pathways and are subject of intense investigation. Activation of the pathway has several steps and is highly dynamic (Fig. 1) (reviewed in [38, 8]. Mating peptide pheromones bind G-protein coupled receptors (GPCRs) in the plasma membrane, transducing the signal through the MAPK cascade and MAPK Fus3 nuclear translocation, finally activating the both the transcription factor Ste12 which promotes changes in gene expression through pheromone responsive elements (PREs) [18] and the protein Far1, which induces cell cycle arrest in G_1 and morphological development through the guanine exchange factor (GEF) Cdc24 and its target the small rho-like GTPase Cdc42 [15]. Also, internal desensitization processes exist at the receptor level, mediated by the interaction between the Sst2 GTPase and the G-protein Gpa1 after prolonged exposure to pheromone [23] and also downstream, through Fus3 dephosphorylation mediated by phosphatase Msg5. Pathway activation results in dose-dependent morphological development, i.e. cells with increased volume, enlarged cell bodies and displaying mating protrusions, also known as shmoos. Since pheromone gradients are expected to emerge from pheromone-secreting cells, the local concentration of pheromone is generally considered a cue cells can use to estimate the distance that separates them from potential partners (Fig. 2A).

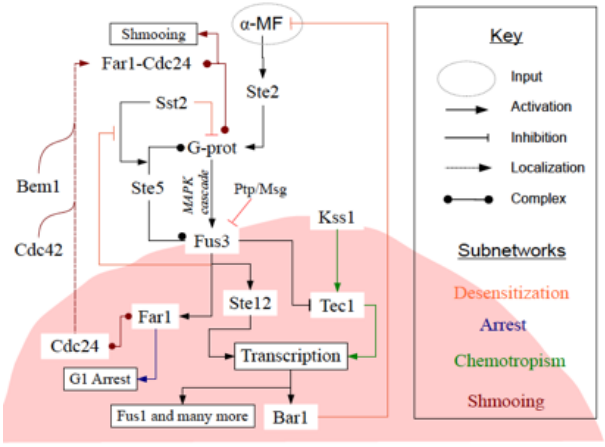

Figure 1: Schematic representation of the mating pheromone pathway components and interactions. The external concentration of α-factor determines a particular cell fate. The pathway transduces receptor (Ste2) ligand occupancy and activates different pathway subnetworks through MAPK Fus3 which induces Ste12-dependent transcription, Far1-dependent cell cycle arrest and morphological development. Several negative interactions (Sst2-Gpa1, Msg5/Ptp3-Fus3, Fus3-Sst2) modify pathway transduction upon activation. Also input concentration is modified by Bar1. The MAPK cascade is composed by MAPKKK Ste11 and MAPK Ste7, which also bind to scaffold Ste5. α-MF is the α-factor peptide.

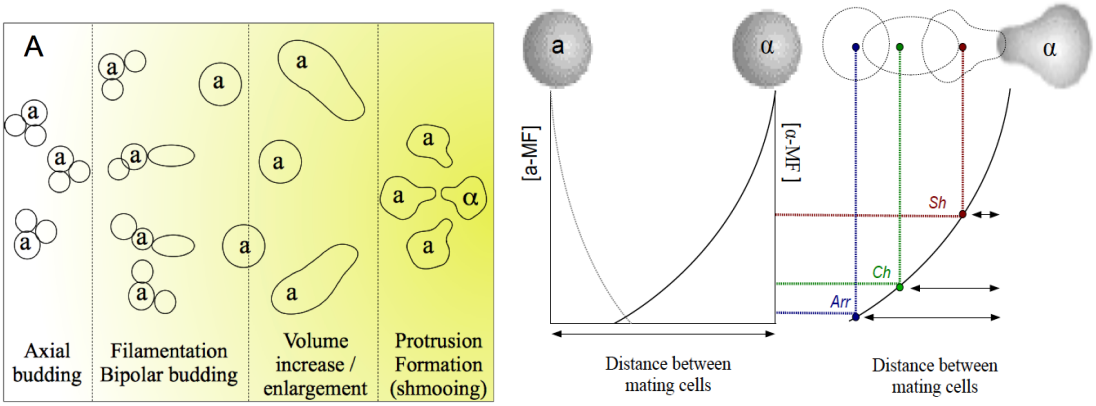

Figure 2: Development of mating morphologies as a function of distance. A. An α-factor concentration gradient (yellow) emanating from a single $MAT\alpha$ cell induces different morphological phenotypes in $MAT\boldsymbol{a}$ cells located at different distances from the source. B. A $MAT\boldsymbol{a}$ cell that senses a low pheromone dose arrests its cell cycle in G_1. If the distance between the cells decreases, the chemotropic and shmooing phenotypes can develop.

1.2 Molecular mechanisms

1.2.1 Transduction

The mating pheromone pathway transduces ligand binding of the pheromone receptor inducing different phenotypic states in a dose-dependent manner. Ste2 and Ste3 are the seven transmembrane-domain receptors from $MAT\boldsymbol{a}$ and $MAT\alpha$ cells, respectively. Ste2 (or Ste3) physically interact with Gpa1, the G-protein α-subunit which when inactive (GDP-bound state), binds to the Ste4 β-subunit and Ste18 γ-subunit. Upon receptor stimulation with α-factor, GDP is exchanged for GTP which leads to the release of Ste4-Ste18 complex from Gpa1. When the basal GTP hydrolytic activity of Gpa1 is initiated by pheromone binding, the unbound Ste4-Ste18 complex is able to tether the scaffold protein Ste5 at the membrane. In addition, the Ste4-Ste18 complex activates protein kinase Ste20 and also the Far1/Cdc24 complex. When Ste20 and Ste5 (which also binds Ste11 MAPKKK and Ste7 MAPKK) are in close proximity, Ste11 gets phosphorylated and starts signal transduction via the MAPK phosphorylation cascade. Ste5 has a critical role as a scaffold protein, keeping the the MAPK cascade (Ste11/Ste7/Fus3) in proximity ensuring that the transmitted signal keeps specificity (reviewed in [27]). From Ste7, the signal is transduced to Fus3 or Kss1. Fus3 and Kss1 have both the ability to get double-phosphorylated and to be imported into the nucleus. Fus3pp and Kss1pp release the inhibitory complex of Dig1, Dig2 and Ste12 on promoters for mating specific responses. Dig2 normally blocks the DNA binding domain of Ste12. Successful binding of Ste12 to mating specific promoters is closely related to the level of Fus3 and Kss1. If Fus3 and Kss1 are knocked out there is no interaction between Ste12 and mating specific promoters (PREs) [110]. Phosphorylation of Fus3 leads to binding of Ste12 on PREs, whereas upon phosphorylation of Kss1, Ste12 binds mostly to filamentation specific elements (FREs) [18]. Fus3 and Kss1 are both able to trigger a wide range of gene expression programs including Fus1 expression. Fus1 localizes at the shmoo tip and is important for the opening and expansion of the fusion pore complex [78]. As many genes that are activated through Ste12, Fus1 expression is enhanced by pheromone stimulation. Fus1 is commonly used as a gene expression reporter because its pheromone-dependent expression is high, making it a sensitive reporter.

1.2.2 Regulation of Transduction

Sst2 can act as a negative regulator of the GPCR [23]. It is a GAP (GTP activating Protein) which hydrolyzes the GTP molecule in Gpa1 and promotes re-assembly of the trimeric G-protein complex, making the Ste4-Ste18 dimer no longer able to recruit scaffold Ste5 to the membrane. This results in decreased signal transduction and gene expression. Sst2 has also been shown to be activated by Fus3, which indicates a negative feedback loop at the MAPK cascade to the

membrane bound receptor [12]. A second reported activity of Sst2 is recruiting Ste5 to the membrane, it has been shown that Fus3 can inhibit this particular Sst2 activity [109]. The phosphatase Msg5 is able to dephosphorylate Fus3, leading to a weaker transcriptional up-regulation in the nucleus. Msg5 and also Gpa1 have been reported to down-regulate the mating response by inhibiting the pheromone-induced increase of phosphorylated Fus3 in the the nucleus [12]. A second phosphatase (Ptp3) also dephosphorylates Fus3 [111]. The Ste12 transcription factor also ubiquitinates and degrades upon continuous stimulation with α-factor [28].

Positive feedbacks also play a role in transduction. Butty et al. showed that local activation of Cdc24 produces Cdc42-GTP, which recruits Bem1. Bem1 then stabilizes Cdc24 at the site of polarization, leading to apical growth [16]. In another example, Takahashi et al. showed that pheromone-induced membrane localization of Ste5 is involved in the gradual rather than ultra-sensitive MPP transcriptional response [97]. Also, a role for pheromone-induced ubiquitination and degradation of Gpa1 has been reported, constituting another example of a positive feedback [41]. On the other hand, feed-forward regulation of Far1 by fast phosphorylation and slower transcriptional induction was demonstrated as the mechanism of persistent cell cycle arrest [24]. Apart from strong up-regulation of protein expression involved in mating execution (e.g. Fus1, Prm1, Aga2), there seems to be also a generalized transcriptional up-regulation of practically all pathway components involved in transduction [37] as well as the pheromone-producing genes. The role of the degree of expression of signaling components has yet no clear role in transduction.

2 Functional properties of the mating pheromone pathway

The molecular mechanisms described above provide the ground for understanding the functional properties that the input-output relationships have. The essential character of each particular feedback structure for the default input-output behavior of the pathway is a different problem than that of what are the constraints that allowed such a behavior to evolve. The input-output function (or functions), should be intimately related with its (their) suitability to perform successfully within the input landscape that yeast encounter during mating.

2.1 Functions of input-output properties

Well characterized signalling systems as the MPP provide a mechanistic basis for an understanding of signal transduction at its topological level. Pathway-level properties define an intermediate level of causality between the pathway's topological structure and biological behavior. The topological structure of the pathway is expected to exert outputs that cohere with typical input distributions. Functions of signalling input-output relations have been proposed for the yeast mating response [109, 10, 79, 101]. Functions are ascribed by doing experiments

that use controlled stimulation with purified pheromone and measure the relation between some property of the input and one or several pathway outputs. During isotropic stimulations, the MPP shows a combination of both hyperbolic and sigmoideal α-factor dose response curves, depending on the output measured. The normalized (to its saturation value) steady state intensity of mean population Fus1 transcription, Fus3 activation and G-protein FRET show alignment with the calculated Ste2 receptor occupancy [109, 97]. Dynamic range preservation is argued to be a mechanism for a faithful representation of receptor occupancy [109, 14], i.e. deviations from the alignment (shifts in the output curve respect to the receptor occupancy curve in any direction) would produce sub-optimal information transfer. Contrary to that, other experiments suggest that the dynamic range of sensing can differ from receptor occupancy. By using a fluorescent version of α-factor, Ventura et al. [101] showed that the equilibrium receptor occupancy has a slower timescale than the Ste5 membrane-recruitment response. Given that pathway responses can be faster than the time receptor saturation needs, the authors suggest that the dynamic range of sensing could be expanded above receptor saturation if a negative-feedback based transient response is activated before ligand binding reaches equilibrium. Their model showed that the transient response peaks with high amplitude at early times when stimulated with high α-factor concentration and with low amplitude at later times for lower stimulation values, when receptor-ligand equilibrium is reached slowly. For this reason, compared to the receptor occupancy curve, the dynamic range of the maximal transient response is broader, at the expense of sensitivity-loss (i.e the EC_{50} shifts right)

By using Immunoblots of activated Fus3, Behar et al. [10] observed that roughly equal activation rates for Fus3 are observed across different stimulation intensities. They propose a negative-feedback based model based on a "dose-to-duration" encoding, i.e. the equilibrium receptor occupancy produces an intermediate output which if transduced through a slow biochemical reaction, the effect of the different concentrations rather differing in their duration. The authors however do their experiments in a wild type strain harboring its native *BAR1* copy, implying the possibility of the alternative explanation: that the rate is equal because the lowest α-factor concentration is high enough to saturate the receptors but, with time, Bar1 reduces the input value, generating different durations. In fact, in a different work [40], the same authors show that in the *bar1*Δ the rough slope invariance is lost. Dose response alignment and dose-to-duration encoding seem irreconcilable [14]. Different from the mentioned outputs, the frequency of shmooing cells (thin mating projections) in the population is ultrasensitive [73, 69] as are outputs of other MAPK pathways [31]. An interesting, and potentially important feature is that ultra sensitivity occurs at the level of Fus3-Ste5 dissociation, and as noted before, Fus3 activation approaches saturation linearly. Different thresholds for transductional sub-networks could explain the transcription/shmooing difference in sensitivity. Alternatively, transductional

signal-processing schemes could extract different attributes of the ligand binding process.

In yeast mating, the great majority of the work is performed considering the input as a steady state spatial gradient or isotropic and constant in time. Crucially, considering that low dilution rates for the extracellular-medium is a plausible scenario and that pheromones are actively secreted by numerous cells, the understanding of how the pathway topology performs in reality, lacks data for the temporal component of the background (or global) concentration (α_g). The existent evidence provides an interesting possibility i.e. Bar1 could be an extracellular adaptation mechanism that allows the pathway to extend its dynamic range without sensitivity loss.

2.2 Sensory input reshaping by Bar1

A key feature contributing to the α-factor concentration profile in space is the ability of the $MAT\boldsymbol{a}$ cells to degrade it by releasing the Bar1 protease to the extracellular environment. Experimental work shows that Bar1 apart from allowing $MAT\boldsymbol{a}$-cells to recover from arrest[19] has more active roles in mating behavior as for example allowing them to avoid each other during chemotropism [51]. This last property is explained by localizing pheromone degradation to the a-cell surface, making cells pheromone "sinks" , a feature that generates gradients of pheromone around cells that can be detected by neighboring $MAT\boldsymbol{a}$ cells. Theoretical work shows that an homogeneous distribution of Bar1 in a mating reaction can limit diffusion of pheromone from its emitting sources, this allows $MAT\boldsymbol{a}$ cells to correctly align to a pheromone-emitting source and not to a pheromone local maxima built by contributions from multiple cells and located in an irrelevant position [9]. However this property does not work robustly when modeling geometries where distances are less than one cell diameter[81]. These distances exist between germinating spores confined in an ascus or between cells in a sexual aggregate. In that situation, the model shows that homogeneous Bar1 would not be able to limit diffusion at sufficiently high rate, making equidistant sources generate a single local maxima between them. The problem is solved by considering the $MAT\boldsymbol{a}$-cells as perfect sinks of pheromone (the pheromone diffusional flux equals the pheromone degradation rate at the cell surface), with the result that net diffusional flux lines bias their direction towards the emitting source producing the necessary two local maxima [81]. As in the study by Jin et al. [51], the sink function needs localized Bar1 activity. Taken together these studies suggest that in a real mating scenario free fraction of Bar1 should maintain the pheromone levels below receptor saturation and limit diffusion of distant emitting sources. On the other hand, the cell-wall bound fraction of Bar1 could sharpen existing gradients in the $MAT\boldsymbol{a}$-cell proximity allowing the disentanglement of pheromone sources.

2.3 Fractional sensing

An understanding of the pathway sensory functions at work requires an understanding of adaptation processes. Microorganisms seem to sense input properties different from the concentration alone, for example, In *E. coli* chemotaxis both the mean population maximal amplitude of pathway activity and the mean chemotactic drift velocity are sensory outputs showing a linear dependency on the logarithm of the stimulus magnitude, allowing a broad dynamic range of sensing[91, 53]. In eukaryotic *wnt* signalling, responses to the fold-change in nuclear to cytoplasmic concentration of β-catenin, allows robust developmental and gene expression outputs in *Xenopus,* whereas the noisy absolute value of nuclear concentration is ignored [35]. The mechanism in the described systems relies on changes in pathway sensitivity at the receptor level or specific pathway topologies which result in a adapted response. These systems can be phenomenologically described by a biochemical version of the Weber-Fechner relationship [30], originally an account of perceptual magnitudes in humans.

In *S. cerevisiae*, the work by Paliwal et al. [79] suggests that *S. cerevisiae* is able of maintaining constant precision of positive chemotropism while growing towards the source of pheromone, if the gradient separating both cells is exponential. This result implies a form of fractional sensing, by which measurements of concentration and concentration differences must be performed. The evidence that supports fractional sensing in yeast chemotropism is the following. First, the authors classified the population of yeast cells present along linear gradients of different steepness into "bad" aligners (cells with the angle formed between protrusion direction and gradient direction grater than 55° are "bad" aligners) and "good" aligners, and then plotted the pheromone concentration and gradient values against each other, observing linear relationships for both groups. This means that for the same average pheromone concentration, good aligners are mostly found in chambers with steeper gradients. This led to the authors to conclude that cells sense the fractional gradient (gradient divided by the average pheromone concentration), rather than the gradient or the concentration alone. Since the value of the scaling factor of the exponent in an exponential function equals the fractional gradient, the authors conclude that the function of fractional gradient sensing is to maintain a constant pathway output in exponential gradients. There is a two-fold problem with this approach. First it is not a direct measure. Second, the classification of the population into two groups assumes that "precision of alignment" is a binary output, so an alternative interpretation is that "poor alignment" is also maintained constant while climbing up an exponential gradient. This in itself is not a problem if the real exponential gradient experienced by the cells has exactly the fractional gradient value observed for the good-aligning population, which remains unknown but it is probably not a unique shape. The authors invoke Bar1 activity to explain exponential gradients, with localized Bar1 acting

as a sink for pheromone, real pheromone spatial profiles separating cells are expected to be exponential and might be less variable in their steepness. The mechanisms involved in this type of fractional sensing do not need to be adaptive. If adaptation mechanisms are maintaining a constant behavioral output upon fold-changes in input, allowed a proper adaptation time, the pathway output should also be maintained constant.

3 Mating behavior

3.1 Inbreeding and outcrossing

Although mating frequently occurs already within the ascus [58], haploid cells that are released by ascus degradation, e.g. in a fruit-fly gut [20], subsequently mate under conditions where pheromone signaling and gradient sensing become critical [83]. Since the yeast spore-wall and not the ascus survives the digestive tract of drosophila [20], the fruit fly or its larvae can work as vector for yeast colonization through their depositions [92]. The scenario without ascus confinement can promote outbreeding [83]. The fruit fly's feces can be seen as an inoculum of yeast spores. After germination, haploids can begin courtship in whatever environment inoculation happened.

3.2 Sexual aggregate formation

The first step in yeast mating in liquid is sexual agglutination, a process dependent on the global pheromone concentration in the mating reaction [29]. Sexual-agglutinin mutants show a three to seven order of magnitude reduction in mating efficiency [67, 65]. In mass mating assays in solid media where cells are in close proximity, agglutination is apparently not essential [49]. However, increasing the moisture in these assays makes agglutination critical [95], probably through increased pheromone homogenization. Therefore, mating requires close contact or at least close proximity between cells. Indeed, even though long lengthed chemotropic cells are commonly observed in artificial gradients [87, 52], chemotropism between cells in solid surfaces is more discrete and happens when cells are close to each other [7, 49]. These results suggest that under environmental conditions that do not promote cell-cell contact but allow pheromone accumulation, both encounter probability and pathway activation, which determine aggregate formation and hence mating efficiency, are expected to be dependent on population parameters. Indeed, it has been shown that both population composition [60] and α-factor pre-stimulation [88, 29] affects mating efficiency. Once cells are in close proximity, precision of alignment plays an important role. It is however not completely essential to mating, since cells using the default mating pathway can indeed mate randomly in the absence of gradients, provided contact between

them [26].

3.3 Courtship and default mating

Jackson and Hartwell [49] distinguished an early interaction between mating cells which they termed "courtship" during which sexual selection can occur i.e. cells prefer stronger pheromone producers. The method involved a mass-mating assay which is similar to a sexual aggregate. They are similar in that they are densely packed and that there is a defined intercellular space geometry which has its narrowest and broadest regions in defined positions. They are different in that in the mass-mating assay there is mono-layer of hydrated cells placed over a hydrophylic filter and the aggregate is 3-dimensional with the intercellular space more precisely defined by the agglutinin complex length. During courtship, the ability of the cells to polarize towards local pheromone concentration maxima allows them to find and choose strong signallers, constituting a simple form of sexual selection [85]. Shmooing is the execution of the "default" mating pheromone pathway (Spa2-dependent) which is activated ultrasensitively [26, 25, 48] at a specific α-factor concentration and results in the formation of a thin protrusion, different from elongation. Yorihuzi et al. isolated mutants defective in what they called *pointed projection* [107], this mutants are *SPA2*, *BNI1*, and *PEA2* defective and show elongation instead of shmooing at high α-factor concentrations. The default mating pheromone pathway randomizes sexual selection when pheromone concentration is above the shmooing threshold and isotropic, and It is only efficient in the context of closely packed cells. Because of the shmoo length, the default pathway produces successful encounters only in close proximity. Sexual-aggregate formation ensures proximity between multiple potential mating partners, and ensures that shmooing effectively reaches a cell. In the probability of a deceptive encounter, it also increases the probability that a second or third shmoo is effective. This default pathway behavior seems to be a modality where no sexual selection occurs but rather mating appears randomized.

In the context of an aggregate, an isotropic composition of the intercellular media would be expected only when it reaches equilibrium with the extracellular media, this can happen fast if *MAT*α cells cease production of α-factor in a well stirred environment. On the other hand, under constant production conditions equilibrium seems difficult. However, within the aggregate we may expect that the higher the rate of pheromone production is, the more homogeneous the source itself is. Under isotropic conditions mating would work under its default, with impaired discrimination abilities. Courtship is expected to happen in the context of an aggregate of cells where the overall ratio of a-cells to α-cells is thought to be consistently 1, independent of the initial ratios mixed in the reaction [54]. To allow courtship to happen, the cells must maintain their sensitivity under this conditions and avoid random mating by maintaining the pheromone concentration below the shmooing threshold. Related to this, here we study how

cells can maintain mating-proficiency.

3.4 Sex-ratio perception.

In sexual selection theory, the strength intrasexual selection is predicted to be high when the degree of competition is high. Operational sex ratio (OSR) theory [21] predicts which sex will compete for mates by relating a single population parameter, i.e. the operational sex ratio (OSR [62]) to the expression of agonistic (aggression) or attractive (courtship) behavioral strategies. Likewise, choosiness (intersexual selection) also depends strongly on the OSR, with inverted dependence respect to competition, which makes intuitive sense [11]. Experimentally (in the field or in the laboratory), the operational sex ratio (OSR) is quantified as the fraction of sexually active males in the sexually active population (females plus males) [62]. It is preferred over the actual ratio (males divided by females) because it provides a finite scale. However useful, operational sex ratio theory lacks a mechanistic account, mainly due to the difficulty of performing quantitative experiments with well defined environmental conditions and more importantly, the difficulty of choosing the right output measurement [104, 21]. Operational sex ratio theory attempts to show that the OSR influences "behavioral propensity" and not just the frequency of observed behaviors, i.e. the OSR is sensorially perceived, and it changes behavior independently of competitor encounter rates. Crucially then, the theory lacks a mechanistic explanation of how the OSR is sensed by the individuals in the first place, even though it has been shown that this is indeed possible [103]. It is sensory perception and its internal relation with behavioral outputs that lies in between the OSR and the observable competing/choosing behavior. Moreover, sensory systems are believed to play a central role in sexual selection both as a pre-existing preference bias and as a physiological determinant of mate discrimination capacities [13, 32, 3, 4]. Both population density and sex-ratio are expected to influence competition, although in different ways [59]. The ability to sensorially distinguish between these two population parameters, should allow individuals to relate responses to real changes in the likelihood to encountering a partner, and not simply the likelihood of encountering any individual. This differential effect of density and sex-ratio has been proven for sexual selection on a fish [103]. It has to be noted that when thought as a sensory input magnitude, the election on whether to use the fraction or the ratio as the OSR scale is not trivial. A change in sex proportion due to changes in mating type availability, e.g. form 2 males/2 females to 3 males/1 female, would produce a change in the ratio (r in this work) of 1 to 3 (3x), whereas the same change would produce a change in the fraction (θ in this work) of 0.5 to 0.75 (1.5-fold), hence care has to be taken when interpreting the functions each scale produces when used as inputs in a sensory input-output measurement.

Here we use single cell and population-level quantitative responses in the yeast mating system to study mate-perception. From a purely probabilistic mating perspective, i.e. mating at

the population level without considering the local effects of gradients, the OSR is expected to determine the likelihood that a given haploid cell encounters a mate, similarly to null ("ideal gas") models for animal encounter rates [47, 42]. In the yeast case, a high competition state is more precisely defined as simply a low mating likelihood state and a high choosiness state equals a high mating likelihood state. By measuring a perceptual (internal) magnitude subject to population-composition dependent pheromone stimulation, we explore the mechanistic basis of mate perception in a quantitative way, and attempt the derivation of mathematical expressions useful for sex-ratio theory.

Part II

Experimental Methods

4 Yeast strains

4.1 Strain construction

Saccharomyces cerevisiae strains used in this study are derivatives of SEY6210$\boldsymbol{a}$ (*MAT***a** *leu2-3,112 ura3-52 his3*Δ*200 trp1*Δ*901 lys2-801 suc2*Δ*9*) or SEY6210 (*MAT*α, otherwise identical to SEY6210$\boldsymbol{a}$), provided by Prof. Sabine Strahl. Strains are listed in Table 4.1.2 and Table 2.

4.1.1 FRET strain construction

We constructed FRET fusions in MAT$\boldsymbol{a}$ cells by taking open reading frames (belonging to the MPP) from the yeast movable open reading frame (ORF) library [34], based on the Gateway cloning system (Invitrogen). Plasmid DNA (pBG1805) was prepared from *E. coli* strains (Quiagen miniprep kit) belonging to the library. Each plasmids harbors an ORF flanked by attB1 and attB2 sites (from the phage lambda recombination system). In a BP reaction, the plasmid DNA is mixed with an entry vector (pDONR221) and the BP clonase enzyme mix II in a 10-15 μl reaction (15 ng-100 ng of pBG1805, 15 ng of pDONR221, 1μl of enzyme mix in 1x TE buffer). Then, the reaction is incubated for 18 hours at 25°C and then the reaction stopped by adding 1μl of Proteinase K (Invitrogen). The reaction is used for transformation via heat-shock into DH5α *E. coli* chemocompetent cells. Transformation reactions are then plated in LB-Kanamycin plates (50 μg/ml). Plasmid DNA (entry clones) is prepared from transformants, and then moved into the destination vectors pABLY or pABUC using a 5 μl LR reaction (1 μl from the entry clone miniprep elution, 50 ng of destination vector and 1 μl of LR clonase mix, in 1x TE buffer) incubated at 25° for 18 hours and stopped by adding 0.5 μl of the Proteinase

K solution and incubating at 37°C for 20 minutes. Reactions are subsequently transformed into DH5α *E. coli* chemocompetent cells and plated in selective LB-Ampicillin plates (100 μg/ml). Plasmid DNA is prepared from transformants to finally yield expression vectors with YFP and CFP C-terminal fusions under the control of the *GPD* promoter P_{GPD}. Recipient plasmids are linearized by endonuclease digestion on single restriction sites at the *URA3* or *LEU2* loci and then transformed serially in the recipient strain using the yeast transformation protocol (see Sec. 4.2.3) and integrated via recombination in the *leu2-3,112* locus for pABLY and the *ura3-52* locus for pABUC. The constructed FRET strains are shown in table 2.

4.1.2 Gene expression reporter strains

All fluorescent reporter strains are based on a construct in plasmid pAA35 (P_{FUS1}-GFP) or pAA30 (P_{FUS1}-mCherry) (Alexander Anders). Constructs retain the 3' and 5' UTRs and in the case of GFP, the construct includes an ubiquitination sequence for faster degradation. The reporter constructs were integrated into the *URA3* and *HIS3* genomic loci, respectively, by means of integrative plasmids (pRS series [90]). Knockout strains where constructed by integrating deletion cassettes amplified from plasmids from the pRS300 series [99] or the pFA series [66], which harbors antibiotic resistance or auxotrophic markers. Amplification was done with primers with 45-50 bp non-hybridizing overhangs with identity to 3' and 5' regions for deletion the gene of interest. In this study the three strains

4.2 Cloning

4.2.1 PCR

DNA sequences were amplified from appropriate plasmids. Polymerase chain reaction (PCR) was performed with a standard protocol. Phusion polymerase (Fermentas) or *Taq* polymerase (Invitrogen) were used to perform PCR reactions. For Phusion polymerase the thermal cycler (Biometra) program used for amplification was the following: Initial denaturation of 98°C for 30 seconds, denaturation at 98°C for 10 seconds, annealing of primers at 58°C for 30 seconds, extension at 72°C for a time dependent on amplicon size (calculated according to manufacturer instructions) and a final extension time of 3 minutes at 72°C. For *Taq* the program used for amplification was the following: Initial denaturation of 95°C for 10 minutes, denaturation at 95°C for 30 seconds, annealing of primers at 58°C for 30 seconds, extension at 72°C for minutes for a time dependent on amplicon size (calculated as one minute per kilobase) and a final extension time of 10 minutes at 72°C. The cycle number used was 30. PCR products were checked for correct size using agarose gel electrophoresis. Colony PCR was performed as for *Taq* except that 35 cycles were used and a final reaction volume of 10 μl using 1 μl of a cell suspension (1 colony

Table 2: List of strains I.

Strain name (yAB)	CFP fusion *ura3*::pABUC[PGPD1-X-CFP LEU2]	YFP fusion *leu2*::pABLY[PGPD1-YFP URA3]
yAB-C1	DIG2	NA
yAB-C2	BEM1	NA
yAB-C3	DIG1	NA
yAB-C4	FUS3	NA
yAB-C5	KSS1	NA
yAB-C6	GPA1	NA
yAB-C7	CDC42	NA
yAB-C8	STE7	NA
yAB-F1	DIG2	FAR1
yAB-F2	BEM1	SST2
yAB-F3	BEM1	DIG2
yAB-F4	BEM1	FAR1
yAB-F5	DIG1	BEM1
yAB-F6	DIG1	FUS3
yAB-F7	DIG1	STE12
yAB-F8	FUS3	SST2
yAB-F9	FUS3	CDC24
yABF-10	FUS3	BEM1
yABF-11	FUS3	DIG1
yABF-12	FUS3	STE12
yABF-13	FUS3	FAR1
yABF-14	KSS1	DIG2
yABF-15	KSS1	CDC24
yABF-16	KSS1	BEM1
yABF-17	KSS1	DIG1
yABF-18	KSS1	FUS3
yABF-19	KSS1	FAR1
yABF-20	GPA1	SST2
yABF-21	GPA1	DIG2
yABF-22	GPA1	BEM1
yABF-23	GPA1	DIG1
yABF-24	GPA1	FUS3
yABF-25	CDC42	SST2
yABF-26	CDC42	DIG2
yABF-27	CDC42	DIG1
yABF-28	CDC42	FUS3
yABF-29	CDC42	KSS1
yABF-30	CDC42	GPA1
yABF-31	CDC42	FAR1
yABF-32	STE7	DIG1
yABF-33	STE7	FUS3
yABF-34	STE7	KSS1
yABF-35	STE7	GPA1

Table 3: List of strains II.

Strain name	Mating type	Genotype	Referred in the text as	Reference
SEY6210a	a	*MAT***a** leu2-3,112 *ura3-52 his3*Δ200 *trp1*Δ901 *lys2*-801 *suc2*Δ9 (Background strain)	N/A	[84]
SEY6210	α	*MATα leu2-3,112 ura3-52 his3*Δ*200 trp1*Δ*901 lys2-801 suc2*Δ*9*(Background strain)	N/A	[84]
yAA24-1	a	*ura3*::pAA35[P_{FUS1}-Ubi(I)-sfGFP-3'*FUS1 URA3*]	wild type	Alexander Anders
yAA28	a	*bar1*Δ::*kanMX6* *ura3*::pAA35[PFUS1-Ubi(I)-sfGFP-3'*FUS1 URA3*]	*bar1*Δ	Alexander Anders
yAA57	α	his3Δ::pAA30[P_{FUS1}-mCherry-3'*FUS1 HIS3*]	wild type MATα (used in mixing experiments)	Alexander Anders
yAA65	a	*mf(alpha)2::hphNT1 mf(alpha)1::HIS3* *bar1*Δ*::kanMX6* *ura3*::pAA35[P_{FUS1}-Ubi(I)-sfGFP-3'*FUS1 URA3*]	*bar1*Δ*matα1/2*Δ, Non autocrine-signaller.	Alexander Anders
yAA156-1	α	*ura3*::pAA35[P_{FUS1}-Ubi(I)-sfGFP-3'*FUS1 URA3*]	wild type MATα (used in a-factor dose-responses to purified a-factor)	Alexander Anders
yAB2	a	*bar1*Δ*::kanMX6* *ura3*::pAA35[PFUS1-Ubi(I)-sfGFP-3'*FUS1* URA3] *aga2*Δ*::hphNT1*	*bar1*Δ*aga2*Δ (non-aggregating strain)	This study
yAB6	a	*ura3*::pAA35[P_{FUS1}-Ubi(I)-sfGFP-3'*FUS1 URA3*] *BAR1*-mCherry-kanMX6	Bar1-mCherry fusion strain	This study
yAB09	α	*his3*Δ::pAA30[P_{FUS1}-mCherry-3'*FUS1 HIS3*] *afb1*Δ::natNT2	*afb1*Δ	This study
yAA198	a	*aga2*Δ*::klTRP1* *ura3*::pAA35[PFUS1-Ubi(I)-sfGFP-3'FUS1 *URA3*]	*aga2*Δ	Alexander Anders

in 10 μl) as DNA template. Primers (Eurofins MWG) used in this work are listed in Table 4.

4.2.2 Plasmid construction

Plasmids pABLY was constructed by replacing an AatII/SalI fragment from pAG305GPD-ccdB [5] (which contained the GFP gene) with a similarly digested insert from pGM2 (Gabriele Malengo) which contained the mYFP gene ("m" stands for monomeric, produced by the A206K mutation). pABUC was constructed similarly but replacing a SalI/XhoI fragment from pAG306GPD-ccdB [45] with a SalI/XhoI fragment from pDK342 (David Kentner) which contained the mCFP gene. Restriction endonuclease reactions (Enzymes from New England Biolabs or Fermentas) and DNA gel-purifications (Quiagen) were performed according to manufacturer's instructions. Plasmids pABLY and pABUC were used to transform the strains in Table 2. The plasmid names obtained through the Gateway cloning are simply named pABUC-X, where the "X" is replaced with the gene name, e.g. pABUC-FUS3. Plasmids used in this work are listed in Table 5.

4.2.3 Yeast transformation

Transformation was performed by adding 10-20 μl of purified plasmid or concentrated PCR products solution into 200 μl of frozen competent yeast cells. Mixtures were incubated for two hours on a thermoshaker at 37°C and 800 rpm. Afterwards, cells were heat-shocked for 20 minutes at 42°C and finally plated on appropriate selective SD plates when auxotrophic markers are used and on YPD plates with no selection when antibiotics are used. For transformations harboring auxotrophic markers, transformant colonies were re-streaked on selective plates again after 2 or 3 days of growth. For colonies with antibiotic resistance, colonies were transferred to antibiotic-containing plates the next day. Successful integrations are confirmed with either fluorescence microscopy, colony PCR or genomic prep PCR.

4.3 Growth conditions

In general, the synthetic defined medium (LoFlo-SD) for growing yeast in liquid was used, which is composed of low-fluorescence yeast nitrogen base (LoFlo-YNB, Formedium) with complete supplement mix (CSM, Formedium) and 2% glucose. Routinely, cells from glycerol stocks or selective agar plates where inoculated in 10 ml LoFlo-SD in 100 ml flasks and incubated overnight at 30°C on an orbital shaker set to 200 rpm for 12-16 hours. These overnight cultures where diluted 1:100 v/v in fresh LoFlo-SD and grown as explained above to reach the exponential growth phase with a doubling time of ~100 minutes. The exponentially growing cultures where reinoculated again at a final optical density (OD_{600}) of 0.05 and allowed to grow to OD_{600} of 0.1 or ~0.5 prior to further processing for dose-response and mixing experiments, respectively.

Table 4: Primers used in this work.

Name	Sequence (5'-3')	Description	Usage
198AA	ATATATTTGATATTTATATGCTATAAAGAAATTGTACTCCAGATTTCTTAATCGATGAATTCGAGCTCG	S1-type primer[50]	Amplifies mCherry tagging cassette
AB_Bar1_S3	CTGTCACGAAGTATTCTACAGTCTTAATAAATGTCTGTAAACCAACATATCGTACGCTGCAGGTCGAC	S2-type primer[50]	Amplifies mCherry tagging cassette
AB_p_S1Afb1	ATCCAGTTACGAACCATTTACAACATTCCTGAAAATATTGCGTATCAATGCGTACGCTGCAGGTCGAC	S1-type primer	Amplifies *AFB1* deletion cassette
AB_p_S1Afb1	ATGGCGGACCTCCCATGGAATTAAATTGTCAAATTTGGTTGAGGCACTTAATCGATGAATTCGAGCTC	S2-type primer	Amplifies *AFB1* deletion cassette
AB Aga2(KO)FW	ACTTGTGTGCCAAAATATTATACCTACTTCATACATTTTCAATTAAGATGCGTACGCTGCAGGTCGAC	S1-type primer	Amplifies *AGA2* deletion cassette
AB Aga2(KO)RV	GTTTATAAGTGTCACGAACGATGAAATGGAAACTTGGGGGGGAAGGCTCAATCGATGAATTCGAGCTCG	S2-type primer	Amplifies *AGA2* deletion cassette

Table 5: Plasmid List.

Plasmid name	Relevant genotype	Marker	Type	Usage	Source
pAA35	PFUS1-Ubi(I)-sfGFP-3'FUS1 *URA3*	*URA3*	Integrative	Integrates GFP reporter construct	Alexander Anders
pAA30	P_{FUS1}-mCherry-3'*FUS1 HIS3*	*HIS3*	Integrative	Integrates mCherry reporter construct	Alexander Anders
pABLY	P_{GPD}-*CCDB*-CFP *LEU2*	LEU2	Destination vector	generates protein-YFP fusions	This study
pABUC	P_{GPD}-*CCDB*-YFP *URA3*	*URA3*	Destination vector	generates protein-CFP fusion	This study
pFA6-hphNT1	hphNT1	Hygromycin	Knockout-cassette source	*aga2*Δ strain yAB2	[50]
pFA6-natNT2	natNT2	ClonNAT	Knockout-cassette source	*aga2*Δ strain yAB2	[50]
pMM151	mCherry-ADH1term-KanMX	G418	Tagging-cassette source	Bar1-mCherry tagged strain yAB6	[57]
pAB-C1	P_{GPD}-*DIG2*-CFP *URA3*	*URA3*	Integrative	protein-CFP fusion cassette	This study
pAB-C2	P_{GPD}-*BEM1*-CFP *URA3*	*URA3*	Integrative	protein-CFP fusion cassette	This study
pAB-C3	P_{GPD}-*DIG1*-CFP *URA3*	*URA3*	Integrative	protein-CFP fusion cassette	This study
pAB-C4	P_{GPD}-*FUS3*-CFP *URA3*	*URA3*	Integrative	protein-CFP fusion cassette	This study
pAB-C5	P_{GPD}-*KSS1*-CFP *URA3*	*URA3*	Integrative	protein-CFP fusion cassette	This study
pAB-C6	P_{GPD}-*GPA1*-CFP *URA3*	*URA3*	Integrative	protein-CFP fusion cassette	This study
pAB-C7	P_{GPD}-*CDC42*-CFP *URA3*	*URA3*	Integrative	protein-CFP fusion cassette	This study
pAB-C8	P_{GPD}-*STE7*-CFP *URA3*	*URA3*	Integrative	protein-CFP fusion cassette	This study
pAB-Y1	P_{GPD}-*SST2*-YFP *LEU2*	*LEU2*	Integrative	protein-YFP fusion cassette	This study
pAB-Y2	P_{GPD}-*DIG2*-YFP *LEU2*	*LEU2*	Integrative	protein-YFP fusion cassette	This study
pAB-Y3	P_{GPD}-*FAR1*-YFP *LEU2*	*LEU2*	Integrative	protein-YFP fusion cassette	This study
pAB-Y4	P_{GPD}-*FUS3*-YFP *LEU2*	*LEU2*	Integrative	protein-YFP fusion cassette	This study
pAB-Y5	P_{GPD}-*STE12*-YFP *LEU2*	*LEU2*	Integrative	protein-YFP fusion cassette	This study
pAB-Y6	P_{GPD}-*SST2*-YFP *LEU2*	*LEU2*	Integrative	protein-YFP fusion cassette	This study
pAB-Y7	P_{GPD}-*CDC24*-YFP *LEU2*	*LEU2*	Integrative	protein-YFP fusion cassette	This study
pAB-Y8	P_{GPD}-*BEM1*-YFP *LEU2*	*LEU2*	Integrative	protein-YFP fusion cassette	This study
pAB-Y9	P_{GPD}-*KSS1*-YFP *LEU2*	*LEU2*	Integrative	protein-YFP fusion cassette	This study

5 Cell stimulation

5.1 Synthetic input stimulation experiments

For synthetic α-factor (Sigma) or a-factor (A gift from Dr. Frank Uhlmann, or synthesized according to Dr. Uhlmann's published protocol [82] by BioCat), 100 μl of a day culture was deposited on the bottom of a 96-well glass-bottom flat-bottom plates (Matrical Bioscience) coated with type-VI Concanavalin A (Sigma). Coating was done by exposing the glass surface for 2 minutes to a concentrated solution (6% w/v) of Concanavalin A previously pelleted by brief spinning to remove excess and get a transparent liquid. Stimulation was performed by adding 10 μl of 11x α-factor and 11 μM casein using multi-channel pipettes. Acquisition begun as soon as 2 minutes after stimulation. The time of acquisition initiation varies depending of the experiment.

5.2 Mixed-populations experiments and mating reactions

To ensure isotropic mixing of the mating types and prevent cell aggregation, $MAT\boldsymbol{a}$ cells used were deleted for the gene encoding the a-agglutinin subunit Aga2 and shaken vigorously. Separate cultures of $MAT\boldsymbol{a}$ and $MAT\alpha$ cells were grown as described above, washed once with LoFlo-SD and resuspended in fresh LoFlo-SD medium. OD_{600} was determined and the suspensions were diluted to appropriate densities and mixed at appropriate ratios in a final volume of 800 or 1000 μl. Cell mixtures were incubated in 24-well plates (Costar) at 30°C with orbital shaking at 200 rpm. Following the incubation, single-cell responses were immediately analyzed by fluorescence microscopy or flow cytometry. Mating reactions are performed exactly as the mixed population experiments but using the wild type $MAT\boldsymbol{a}$ strain. Sampling was performed by first homogenizing the reactions by pipeting up and down half reaction-volume twice. Aga2 deletion does not alter α-factor sensitivity of our reporter.

6 Data acquisition

6.1 Fluorescence microscopy

Fluorescence microscopy was performed on a wide-field microscope (Olympus MT20) equipped with a 150W mercury-xenon lamp, a motorized stage, a 40× dry objective (Olympus UPLSAPO N/A=0.95) and a EM-CCD camera (Hamamatsu C9100). The GFP signal was acquired using a 474/23 excitation filter and a 525/45 emission filter and the mCherry signal with 562/40 and 641/75 filters, respectively. Cell suspensions were transferred to a 96-well glass-bottom plate (Matrical Bioscience) and image acquisition was started after allowing cells to settle down grav-

itationally for approximately 5 minutes. For time-lapse experiments with synthetic α-factor stimulation, wells of the glass-bottom plate were coated with type-IV Concanavalin A (Sigma-Aldrich) prior to the transfer of cell suspensions. Synthetic alpha-factor (Sigma-Aldrich) was prepared as 11x stocks in 11 μM casein sodium salt from bovine milk (Sigma-Aldrich) and added to the cell suspensions to reach the desired final alpha-factor concentration and casein at 1 μM. Image acquisition was started immediately after alpha-factor addition and repeated periodically at defined time intervals over the course of several hours.

6.2 Flow cytometry

Flow cytometry measurements for quantifying GFP fluorescence in mixed-population experiments were performed in a FACS Canto II instrument (Becton Dickinson). Samples from mixed-populations experiments or α-factor stimulation experiments performed in 24-well plates were directly analyzed after brief sonication. In mixed populations, $MAT\boldsymbol{a}$ cells were distinguished from $MAT\alpha$ cells by manual gating of cells showing GFP fluorescence since only $MAT\boldsymbol{a}$ cells contain the GFP-reporter construct. Measurements of relative cell densities in cell suspensions were performed by collecting data for a constant period of time at a constant acquisition speed. Thus recorded number of cells was proportional to their density in the suspension. The average sample size was 47000 cells. For mating reactions, and depending on the experiment, 50-100 μl samples were transferred to a 96 well plate and fed to CANTO II-HTS (Becton-Dickinson) flow-cytometer. Half volume is then pipeted up and down 3 times at 180 μl/s by the instrument before analyzing a fixed sample volume of 5 - 10 μl. Gene-expression is quantified in both mating types (P_{FUS1}-GFP for $MAT\boldsymbol{a}$ and P_{FUS1}-mCherry for $MAT\alpha$). Events are quantified by defining a non-overlapping separate gate for each mating-type in a mCherry vs GFP intensity scatter-plot. Fixed gates were drawn to contain complete haploid populations at any stage of gene induction (gate shapes are defined by the time-trajectory of haploid populations). Finally, gate positions were manually corrected at data points with minor misalignments.

7 Data analysis

7.1 Image analysis

Single-cell segmentation was done using CellProfiler (Broad Institute). The OTSU adaptive thresholding method was used for object identification in the fluorescence images. Cell clumps were discarded with an object-size threshold and a form-factor filter to select rounder objects. Segmentation quality was inspected visually and empirically optimized by changing filter and threshold values. Shmooing cells were identified manually as thin protrusions (See sec. 10.3).

To ensure that all shmoos were recognized, cells were followed in time-lapse movies throughout the entire course of their morphological development. The fluorescence intensity of a cell population was defined as the mean of the averaged relative pixel intensities of individual single cells belonging to this population (mean of the single-cell means). The fluorescence intensity of a non-stimulated population with basal fluorescence intensity was subtracted from this value to give a response value as used in this study for quantification of fluorescence-microscopy derived measurements. Plots were generated with the ggplot2 package for R or with MATLAB.

7.2 Calculation of GFP expression rate

The GFP signal accumulation rate shown in the experiments (See Fig. 18, Fig. 19 and Fig. 22) was obtained by fitting the first $\backsim$200 minutes of the mean response of each population to an exponential function with two linear terms (A and B) of the form $y(t) = A(1 - e^{-\beta t}) + B$ (Fig. 3), based on a simple inducible transcription model [6] and then evaluating the derivative of the fitted function ($y' = A\beta e^{-\beta t}$) at different time points.

7.3 Mating-pair quantification

Even though sexual aggregates are a clearly distinguishable population in FACS (Fig 4), an effective quantification of mating pair formation cannot be performed precisely by counting aggregate events due to the size heterogeneity induced by higher-order aggregation (Fig. 42). However, a precise quantification can be done by determining the loss in $MAT\boldsymbol{a}$ or $MAT\alpha$ cell number from their respective gates. Haploid initial cell number loss is expected to be equal to mating-pair number and, at a slower timescale, increases in cell number are expected due to cell growth. Even though direct counting of $MAT\boldsymbol{a}$ cells gives a good qualitative picture, the data is noisy and inappropriate for a precise quantification. A more robust measure of aggregation as a function of $MAT\boldsymbol{a}$:$MAT\alpha$ sex-ratio (r) can be obtained as follows. In the both wt and $aga2\Delta$ strains, $r(t)$ changes its value as strains grow. However, only in the wt the value changes due to mating pair formation. At initial $r = 1$, cell proportions should remain invariant in time. A starting $r < 1$ is expected to get lower as $MAT\alpha$ cells arrest and $MAT\boldsymbol{a}$ cells grow. Similarly, when mating pairs form, a reduction in the underrepresented $MAT\alpha$ cells weights more than a reduction of the same absolute magnitude in the $MAT\boldsymbol{a}$ cell population, also decreasing r with time. The instant sex-ratio in the mating reaction is then:

$$r(t) = \frac{(\rho_{\alpha_0} - m(t))g_\alpha(t)}{(\rho_{a_0} - m(t))g_a(t)} \tag{1}$$

Where $m(t)$ is the instant density of mating pairs and g is a growth function that duplicates the current number of haploids with a generational time set by the initial sex-ratio (r_0). This

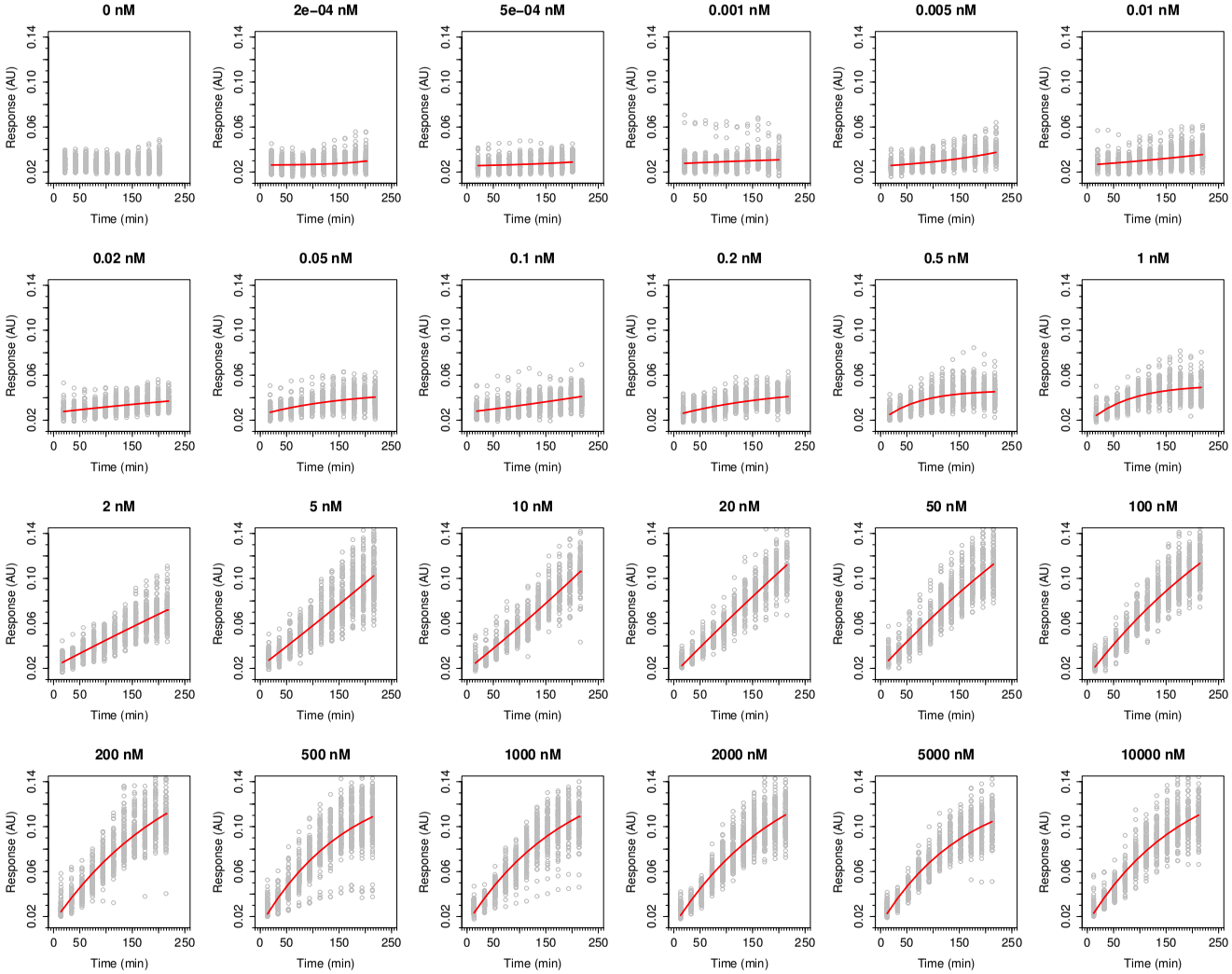

Figure 3: Fitting of P_{FUS1}-GFP expression kinetics to an exponential model. Yeast populations were stimulated with different α-factor doses (top of each plot) and time-lapse movies acquired with a high-throughput fluorescence microscope. The first 200 minutes of each movie where plotted and fitted (red line) to an exponential function according to a simple gene-regulation model. Each dot on each plot represents a single cell. Each time point consists of ~50-100 cells. Fitting failed for the 0 nM α-factor sample.

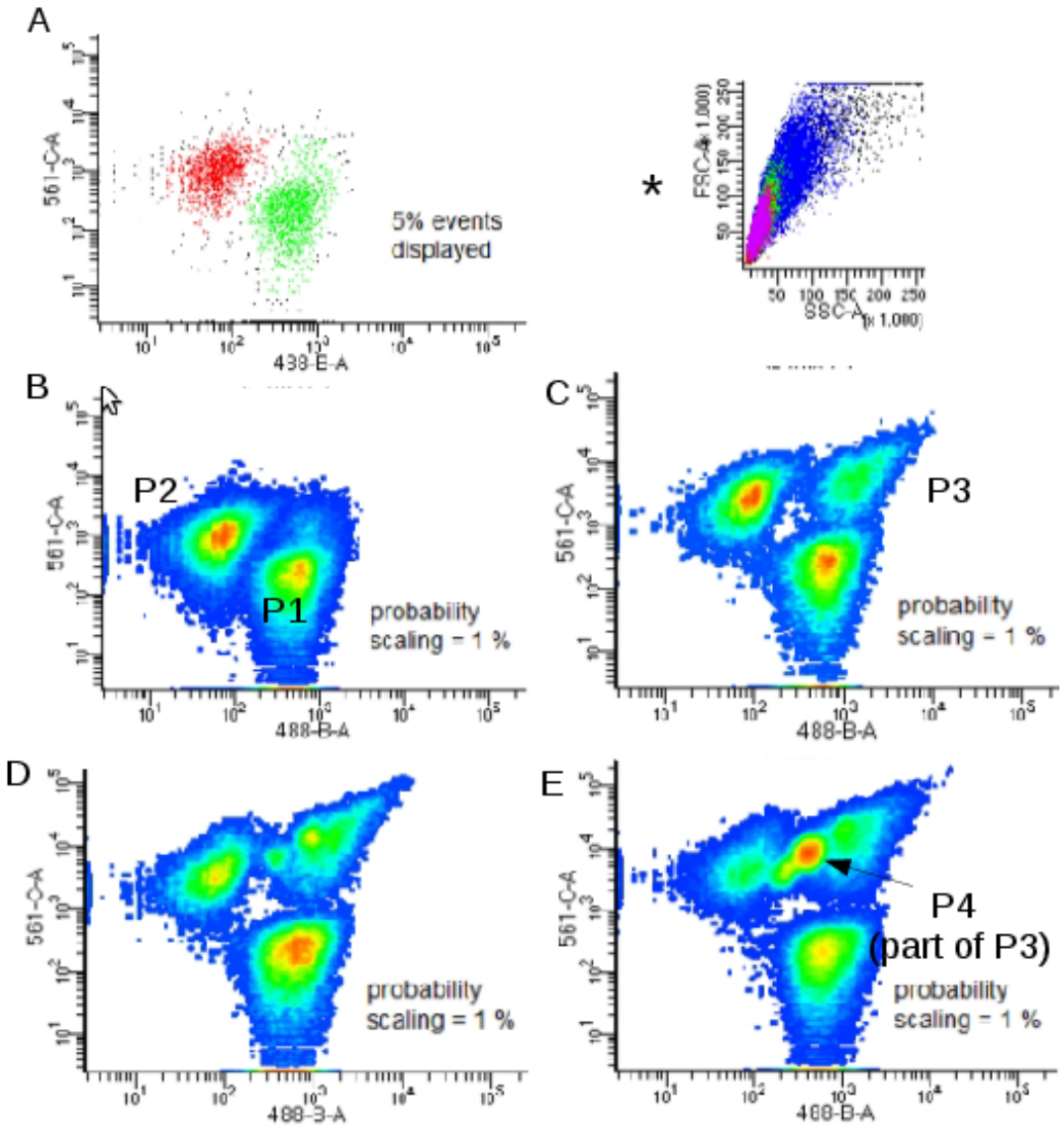

Figure 4: FACS subpopulations. Mating reaction development at ρ_T=0.34 at an example θ_α value near to 0.5, shown as mCherry (561-C-A) versus GFP (488-B-A) intensity scatter plots. A. P1 gate ("green gate") corresponds to $MAT\boldsymbol{a}$ (GFP) and P2 ("red gate") to $MAT\alpha$**.** B. Density plots showing the same data in A at t=33 min C. At 100 min the aggregate population is clearly distinguishable ("P3"). D. At 160 min a fourth population starts appearing, characterized by a sharp distribution of fluorescence values and correlated intensity of fluorophores. E. At 220 minutes, P4 reaches higher densities than its neighbors. (*) denotes an independent example showing P3 forward and side scattering compared to P2, P1 and P4.

formula assumes a timescale separation between the rate of cell growth and pair formation, a fair assumption considering cell growth is substantially slower (a maximum of two duplications are expected during experimental time). $MAT\boldsymbol{a}$ growth is:

$$g_a(t) = 2^{t/\tau(r_0)} \tag{2}$$

Where $\tau(r_0)$ is the generation time. We can further assume $MAT\alpha$ arrests equally with $1/r_0$. Then, $MAT\alpha$ growth is

$$g_\alpha(t) = 2^{t\tau(r_0)} \tag{3}$$

We next define $r_g(t)$ and its theoretical value as

$$r_g(t) = \frac{g_\alpha(t)}{g_a(t)} = 2^{t\left[\tau(r_0) - \frac{1}{\tau(r_0)}\right]} \tag{4}$$

Then solving m(t) in equation 1 and further normalizing $r(t)$ and r_g by r_0 we obtain the density of mating pairs (Fig 36A,C,D):

$$\rho_{MP}(t) = m(t) = \frac{\rho_{a_0}\bar{r}(t) - \rho_{\alpha_0}\bar{r}_{\mathrm{g}}(t)}{\bar{r}(t) - \bar{r}_{\mathrm{g}}(t)} \tag{5}$$

By running control mixing experiments (no agglutination) in parallel to mating reactions under the exact same conditions, we can experimentally determine $r_g(t)$. In these controls, $m(t) = 0$ in equation 1. Then,

$$r_g = \frac{r(t)}{r_0} \tag{6}$$

and

$$\bar{r}_g = \frac{r(t)}{{r_0}^2} \tag{7}$$

By using a separate specific *aga2*Δ control for wt and *bar1*Δ strains, we avoid complications caused by differential arrest sensitivities. The value of $\bar{r}_g$ used is then strain specific. It has to be noted that at $r(t) = 1$, since no sex-ratio changes are expected while mating pairs form or strains (equally) grow (Fig 5), $\bar{r}(t)$ is theoretically equal to $\bar{r}_{\mathrm{g}}(t)$ and equation 5 gets undefined. Even though an exact measured ratio of 1 is difficult to obtain, experimental error is expected to produce noisy data on the vicinity of r_0=1 (θ_α=0.5). For this reason, in the results section, an evident outlier was removed from the data displayed in Fig 36A (but not from Fig. 36B, where the same point is harmless). Fused events (ρ_M) were calculated by counting events on gate "P4"

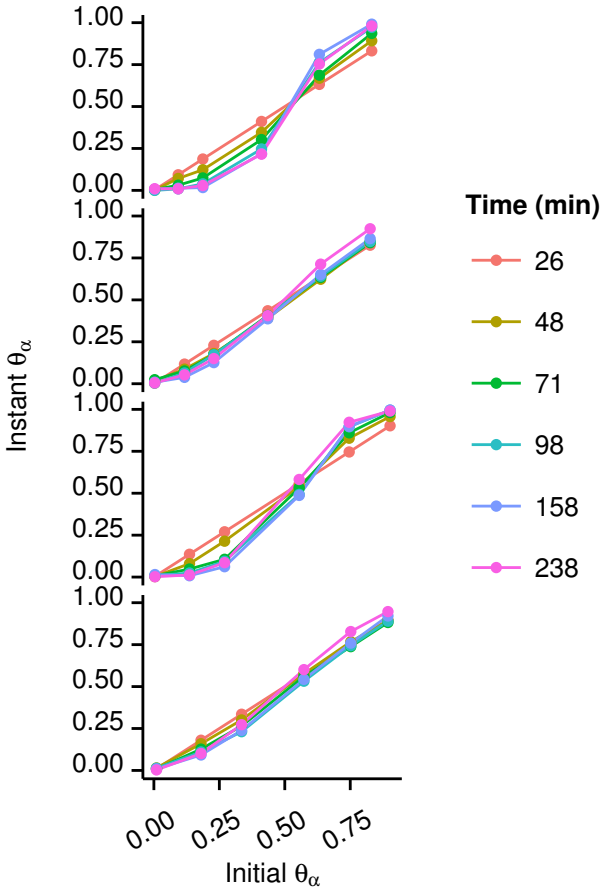

Figure 5: Instant sex-ratio changes at a constant ρ_T=0.34 in different strains. From top to bottom: wt, *aga2*Δ, *bar1*Δ and *bar1*Δ*aga2*Δ.

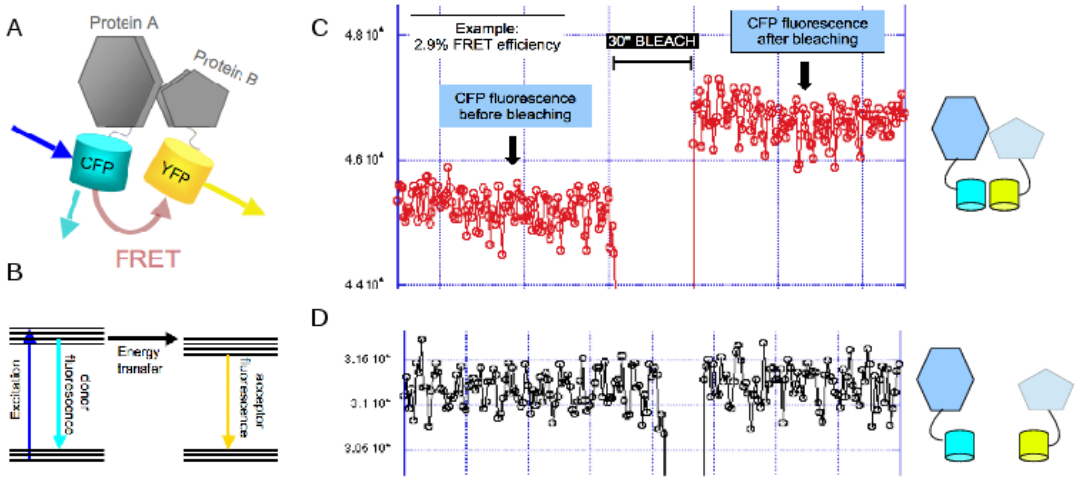

Figure 6: Acceptor photobleaching FRET. A. Fluorescent protein fusions experience FRET upon emitter excitation (CFP) if in close proximity to the acceptor (YFP). B. Fluorescence is generated when the excited fluorophore (CFP) returns to its ground state. Non radiative energy transfer excites the acceptor (YFP), generating a similar fluorescent signal. C. In positive samples (cartoon in the right), loss of energy transfer is seen as an increase in CFP emission upon bleaching of YFP for 30 seconds using a 532-nm laser. Bleaching eliminates energy transfer to the YFP acceptor, causing un-quenching of CFP emission and a concomitant increase in its signal. D. Negative interactions (cartoon on the right) show equivalent CFP intensities before and after bleaching.

(Fig. 4), which is characterized by being rich in prezygotes and diploid cells as determined by cell sorting. Unlike the aggregate cloud, it has a fixed position in the GFP-mCherry scatter plot independent of the degree of stimulation of the haploid clouds, suggesting late fusion or first diploid daughter cells. Although useful qualitatively, gate "P4" is not a precise count of mating events, due to the presence of considerable background from the aggregate cloud and diploid incipient growth.

8 Acceptor photobleaching FRET

Acceptor photobleaching FRET [102] (Fig. 6) was performed on monolayers of exponentially growing yeast cells settled on the surface of a thin 0.5% agarose pad in SD media containing or not α-factor. The microscope configuration is equivalent to that of a previous work [55]. Acquisition was done with photomultiplier tubes (Hamamatsu H7421-40). Photons are counted through a counter function of the PCI-6034E board, controlled by a custom program written in LabView 7.1 (National Instruments). YFP and CFP fusion proteins were expressed under the control of the *GPD* promoter using integrative plasmids harboring auxotrophic markers (Sec. 4.1.1).

Part III

Results

9 Physical interactions of pathway components

With the aim of finding appropriate reporters of mating pheromone pathway (MPP) activity that can be monitored in real-time, we first explored the suitability of reporters of physical interactions between pairs of pathway proteins, i.e. proteins that change their physical proximity when the pathway gets activated after stimulation with the α-factor pheromone. An overview of the physical interactions between pathway proteins can be obtained by measuring the physical proximity between two fluorescent proteins fused to pathway components through Fluorescence Resonance Energy Transfer (FRET) measurements. Strains harboring pairs of CFP and YFP tagged versions of MPP protein pairs in addition to the native ones, were screened for interactions using acceptor photobleaching FRET, as previously done with the chemotaxis and chaperone protein networks in *E. coli* [55, 61]. We placed the gene chimeras downstream of the promoter of the glycerol 3-phosphate deshydrogenase gene (*GPD1*) gene. The *GPD* promoter (P_{GPD}) is a strong promoter [33]. Levels for most components can be considered as corresponding to overexpression, although not as high as with high-copy plasmid based experiments. We screened for interactions with reproducible FRET efficiency measurements that might sensitively report internal pathway interactions, either by association or dissociation.

9.1 Sub-cellular localization of fusion proteins

The localizations of the fusion proteins (Fig. 7) constructed shows strong agreement with previously reported localization of chromosomal fusions of MPP proteins under native expression conditions [46] (Table 6). Since protein overexpression might lead to artefactual interactions or recruitments, we explicitly show that in general proteins keep their localization independent of the overexpressed partner protein (Table 6).

9.2 FRET data distribution and quality estimation

We cloned FRET pairs in a semi-randomized way, i.e. favoring interactions involving the MAPK Fus3 but otherwise doing random combinations. We screened 35 interactions and observed the statistical properties of the dataset. The complete dataset shows a long-tailed distribution (Fig. 8A). When plotted with logarithmic axis, the distribution shows a bell-shape, suggesting a log-normal distribution (Fig. 8B). The mean FRET efficiency is roughly 1% (Fig. 8C, dashed line), including several examples with 0% FRET efficiency. There are three types of

Table 6: Comparison of fusion protein localization. Each row represents a strain with two fluorescent proteins. The localization of a set of pathway fusion proteins obtained in this study is compared with the results of a previous high-throughput localization study of natively expressed chromosomal fusions [46].

CFP fusion	Localization (this study)	Localization [46]	YFP fusion	Localization (this study)	Localization [46]
DIG2	nucleus	cytoplasm,nucleus	FAR1	nucleus	nucleus
BEM1	bud, cytoplasm	ambiguous,bud neck,cell periphery,bud	SST2	cytoplasm	cytoplasm
BEM1	bud, cytoplasm	ambiguous,bud neck,cell periphery,bud	DIG2	nucleus	cytoplasm,nucleus
BEM1	bud, cytoplasm	ambiguous,bud neck,cell periphery,bud	FAR1	nucleus	nucleus
DIG1	nucleus	nucleus	BEM1	periphery, cytoplasm	ambiguous,bud neck,cell periphery,bud
DIG1	nucleus	nucleus	FUS3	cytoplasm,nucleus	cytoplasm,nucleus
DIG1	nucleus	nucleus	STE12		nucleus
FUS3	cytoplasm,nucleus	cytoplasm,nucleus	SST2	cytoplasm	cytoplasm
FUS3	cytoplasm,nucleus	cytoplasm,nucleus	CDC24	cytoplasm, nucleus	cytoplasm,nucleus
FUS3	cytoplasm,nucleus	cytoplasm,nucleus	BEM1	periphery, cytoplasm	ambiguous,bud neck,cell periphery,bud
FUS3	cytoplasm,nucleus	cytoplasm,nucleus	DIG1	nucleus	nucleus
FUS3	cytoplasm,nucleus	cytoplasm,nucleus	STE12		
FUS3	cytoplasm,nucleus	cytoplasm,nucleus	FAR1		
KSS1	nucleus	cytoplasm, nucleus	DIG2	nucleus	cytoplasm,nucleus
KSS1	cytoplasm, nucleus	cytoplasm, nucleus	CDC24	cytoplasm, nucleus	cytoplasm,nucleus
KSS1	cytoplasm, nucleus	cytoplasm, nucleus	BEM1	periphery, cytoplasm, bud	ambiguous,bud neck,cell periphery,bud
KSS1	cytoplasm, nucleus	cytoplasm, nucleus	DIG1	nucleus	nucleus
KSS1	cytoplasm, nucleus	cytoplasm, nucleus	FUS3	cytoplasm,nucleus	cytoplasm,nucleus
KSS1	cytoplasm, nucleus	cytoplasm, nucleus	FAR1	nucleus, punctuate in cytoplasm	nucleus
GPA1	cell periphery, vacuole lumen, vacuole membrane, vesicles?	cell periphery	SST2	cytoplasm	cytoplasm
GPA1	cell periphery, vacuole lumen, vacuole membrane, vesicles?	cell periphery	DIG2	nucleus	cytoplasm,nucleus
GPA1	cell periphery, vacuole lumen, vacuole membrane, vesicles?	cell periphery	BEM1	bud, cytoplasm	ambiguous,bud neck,cell periphery,bud
GPA1	cell periphery, vacuole lumen, vacuole membrane, vesicles?	cell periphery	DIG1		nucleus
GPA1	cell periphery, vacuole lumen, vacuole membrane, vesicles?	cell periphery	FUS3	cytoplasm,nucleus	cytoplasm,nucleus
CDC42	cytoplasm	not visualized	SST2	cytoplasm	cytoplasm
CDC42	cytoplasm	not visualized	DIG2	nucleus	cytoplasm,nucleus
CDC42	cytoplasm	not visualized	DIG1	nucleus	nucleus
CDC42	cytoplasm	not visualized	FUS3	cytoplasm,nucleus	cytoplasm,nucleus
CDC42	cytoplasm	not visualized	KSS1	cytoplasm, nucleus	cytoplasm, nucleus
CDC42	cytoplasm	not visualized	GPA1	cell periphery, vacuole lumen, vacuole membrane, vesicles?	cell periphery
CDC42	cytoplasm	not visualized	FAR1	nucleus	nucleus
STE7	cytoplasm, punctuate in cytoplasm	cytoplasm	DIG1	nucleus	nucleus
STE7	cytoplasm, punctuate in cytoplasm	cytoplasm	FUS3	cytoplasm, not in nucleus?	cytoplasm,nucleus
STE7	cytoplasm, punctuate in cytoplasm	cytoplasm	KSS1	cytoplasm, not in nucleus?	cytoplasm, nucleus
STE7	cytoplasm, punctuate in cytoplasm	cytoplasm	GPA1	cell periphery, vacuole lumen, vacuole membrane, vesicles?	cell periphery

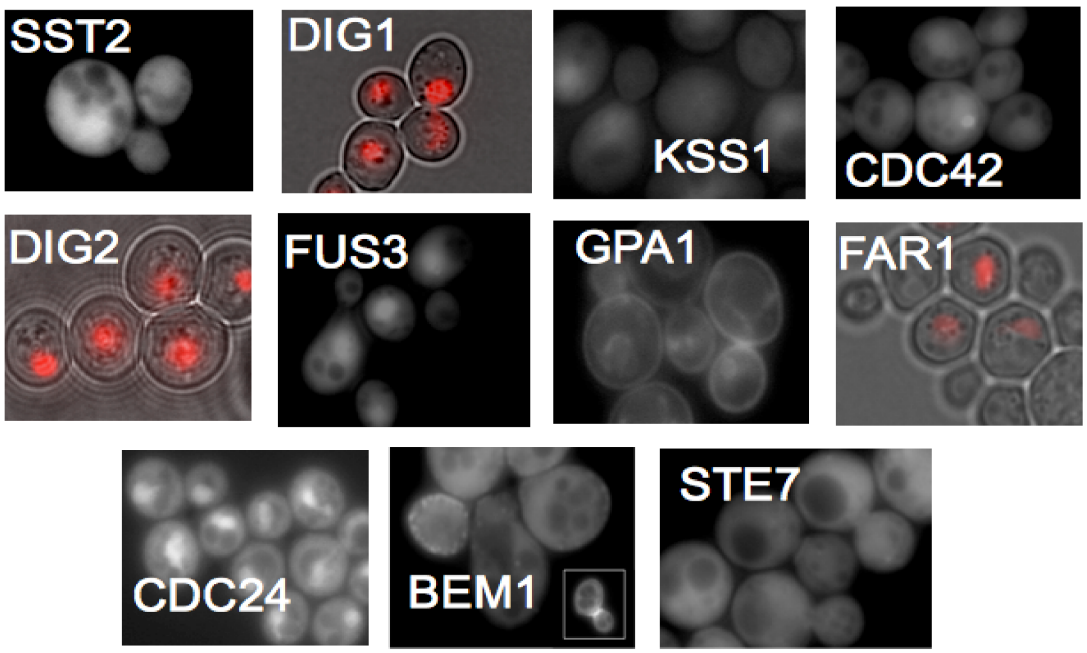

Figure 7: Localization of overexpressed versions of pathway proteins. Nuclear localizations are shown as bright-field/fluorescence merges to facilitate visualization. Correct localization were confirmed by comparison with a previous study in which genomic GFP-fusions were used [46] (See Table 6).

variability in the data set (Fig. 8C). First, technical replicas have extremely low variability (acquisitions in different parts of the mono-layer) and hence these error bars are not shown. Second, biological replicates (same strain assayed on different days) show higher variability. Those above 1% FRET efficiency (dashed line in Fig. 8C), show less-variable efficiencies (note logarithmic y-axis) than negative interactions, i.e. those below the dashed line, which show higher variability. A third type of variability is composed of measurements performed on strains that should yield similar but not necessarily identical results, i.e. strains re-isolated from single colonies of already constructed strains (FRET pairs marked "b" in the x-axis labels (Fig. 8C)) or FRET pairs cloned with swapped CFP/YFP fusions orientation (Fig. 8C, see caption). For further analysis, we only consider those interactions that have enough biological replicates (at least 2) and average the efficiencies of "equivalent" strains.

9.3 FRET interaction map.

We consider the subset of interactions that have enough quality as described in the previous section. The results are summarized in Figure 9. Interactions are classified on the basis of reproducibility given they show a non-zero value. All strains used to construct the map showed some degree of polarization when stimulated with pheromone and no polarization when unstimulated, suggesting that the pathway is operational in these strains. However functional, we did not observe pathway activation leading to changes in FRET efficiency in the strains forming part

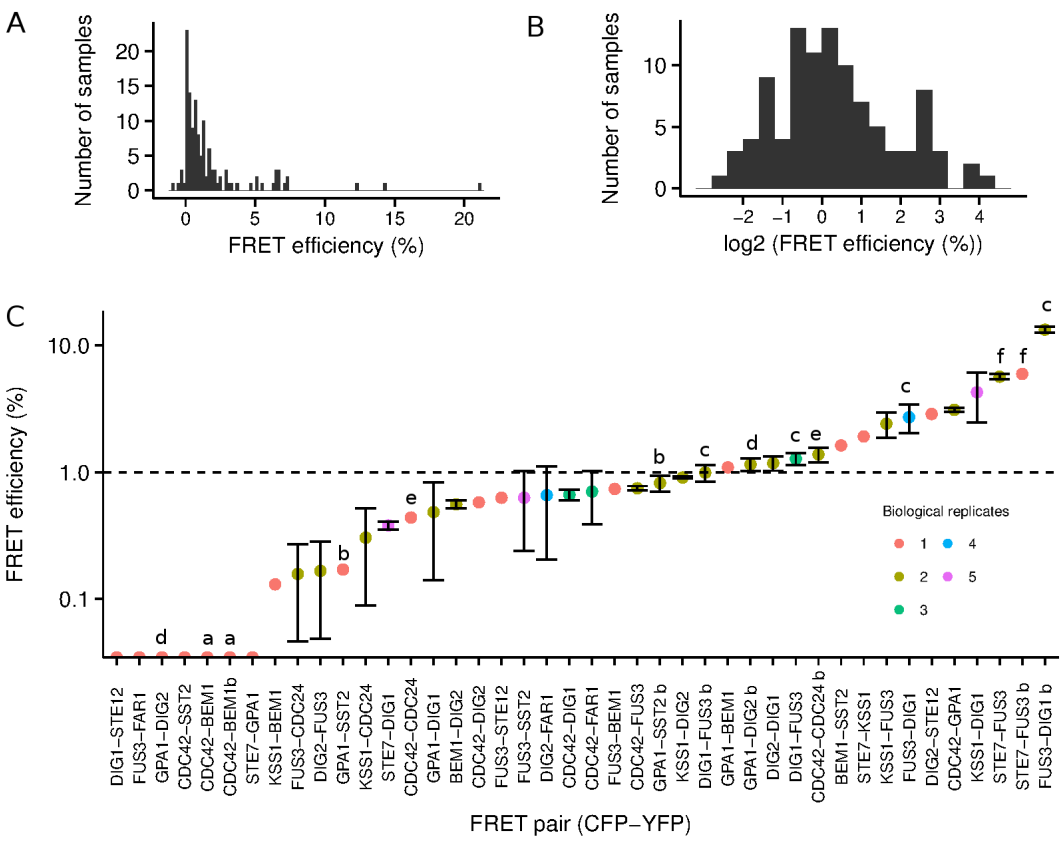

Figure 8: Bleach FRET data distribution and reproducibility. A. Histogram for the Bleach-FRET dataset, including technical and biological replicas. B. Same data as in A with base 2 logarithm in the x-axis. C. Confidence of detected interactions. Screened pairs are ordered in the x-axis according to their FRET efficiency values. The line defines the modal value in B. All biological replicates are the mean of at least 2 technical replicas. Small letters (a-f) group "equivalent" strains. A "b" letter on strain names means a re-isolation of a single colony from that strain.

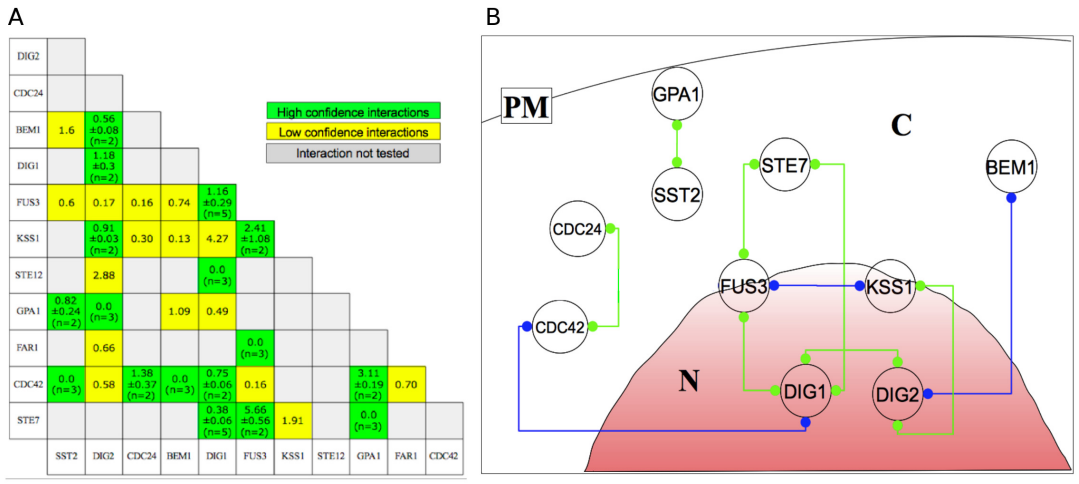

Figure 9: Bleach-FRET map of protein-protein interactions. A. Summary of the screened interactions between pairs of proteins belonging to the mating pheromone pathway. Two levels of confidence are defined according to the amount of biological replicates performed. B.Scheme showing the resultant protein-protein physical interaction map. Only high confidence interactions (green in panel A) are shown. Green lines represent expected interactions (reported in the literature). Blue lines represent unexpected interactions (not reported in the literature) PM: plasma membrane. C: cytoplasm. N: Nucleus.

of the high confidence map (9 A, green and 9 B) after stimulation with 500 nM α-factor in liquid and then deposited on an agarose containing α-factor (5 μM). We also attempted screening for transient changes in FRET by using 96-well plates and α-factor step-increase stimulations with real-time acquisition of fluorescent signals, however, no significant changes in FRET where measured, i.e. no opposite-direction changes in CFP and YFP upon α-factor stimulation (not shown). Given that monitoring real time stimulus-dependence is crucial for measuring pathway activity, we opted to monitor pathway activity by different means (See next section), however a more exhaustive screening involving changes in dose could led to a successful reporter.

10 The *MATa* response to α-factor.

Given the unsuitability of the constructed FRET strains as stimulus-dependent real-time pathway activity reporters, we decided to use pathway outputs known to report pathway activity with high sensitivity, i.e. the transcriptional and morphological outputs of the pathway, We characterized these by measuring the MPP response dynamics to varying synthetic α-factor at the single cell level which allowed us to define phenotypic thresholds and identify the concentration of pheromone at which the cells commit to mating, i.e. the "shmooing" concentration. We used two types of outputs of the pathway known to respond differently to the dose of purified α-factor, i.e. the P_{FUS1}-dependent gene-expression and the the frequency of shmooing cells in the population (as well as other morphological changes like elongation or budding). The transcriptional output of the cells (Fig. 10) was quantified in a strain where we integrated in the

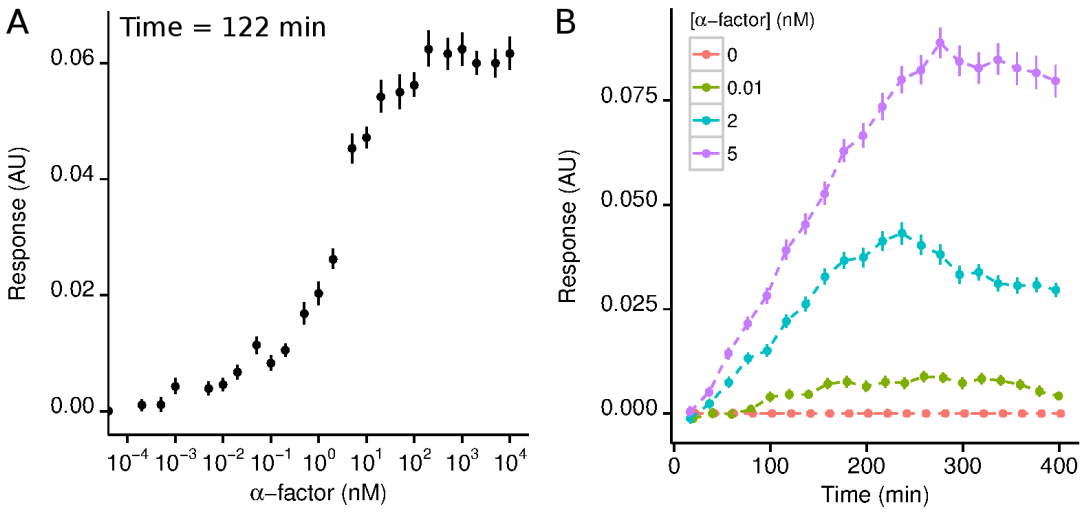

Figure 10: Dynamic gene expression analysis. A. An example of an α-factor dose response at t=122 minutes after stimulation on the *bar1*Δ strain. B. Examples of response kinetics at three different α-factor concentrations. Points represent the mean cell intensity of a population of ~100 individuals. Error bars are the standard error of the mean. Fluorescence intensity corresponds to the mean pixel intensity gray value as a fraction of the maximal intensity. Note that the time of the dose response in (A) corresponds to an intermediate time in (B). The basal response is subtracted (response to 0 nM α-factor) from all time traces.

genome a copy of the *FUS1* promoter controlling the expression of super-folder yeast-enhanced monomeric green fluorescent protein (P_{FUS1}-GFP). The construct maintains the native 3' and 5' UTR regions of the *FUS1* gene and included a degron sequence for faster protein degradation (constructed by Alexander Anders, see Experimental Methods). The construct was integrated in the wild type and *bar1*Δ strains keeping the native copy of the *FUS1* gene for proper mating behavior [78]. We measured the intensity of the GFP signal in cells from yeast populations exposed to different concentrations of nearly isotropic α-factor, i.e. cells attached to the bottom of glass-bottom flat-bottom micro-wells (96-well plates) stimulated with α-factor at different concentrations and then calculated the per-cell average pixel intensity (single cell response) (see Experimental Methods) and the mean cell intensity (defined as "response") as the population-level gene-expression output. We next analyzed the temporal properties of pheromone-dependent gene induction in both wt and *bar1*Δ strains.

10.1 Wild type and *bar1*Δ response behavior

Some contradictions in experimental results and interpretations of the dependency of the pathway activity on pheromone dose can be found in the literature. For example, bimodal distributions of the *FUS1* reporter gene expression where found [79] when exposing cells to pheromone gradients. Using mathematical modeling Paliwal et al. suggested that bimodality is a consequence of bistable *FUS1* gene expression. Other works, also quantifying gene expression in single cells reports similar P_{FUS1} gradual dependency, but without any bimodality [80, 98].

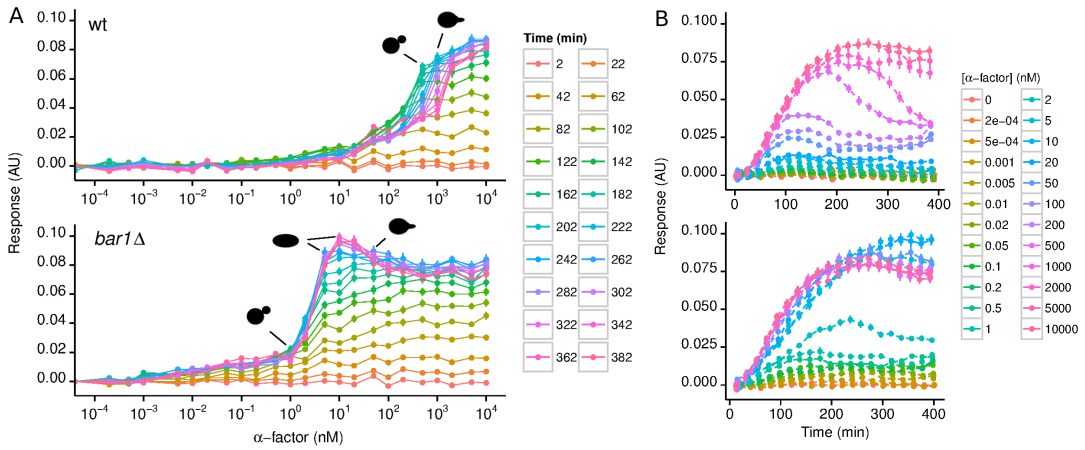

Figure 11: Dynamic response of the P_{FUS1}-GFP reporter to purified α-factor in wt and *bar1*Δ *MAT***a** cells. A. An α-factor dose response at different times from stimulation. Black yeast diagrams indicate populations that show a cumulative (in time) phenotypic frequency $> 95\%$. In the *bar1*Δ strain, from left to right the diagrams show budding, elongating and shmooing populations. Fluorescence was quantified in microscopy time-lapse series. B. Data from A shown as the response kinetics to different concentrations of α-factor. The response to 0 nM α-factor is subtracted from all responses.

Also it is not clear what is the dose-dependency relation between gene expression and morphological development and how these are related as outputs of a single extracellular input. To clarify these issues, we performed an extensive characterization of the P_{FUS1}-GFP reporter response dynamics to α-factor stimulations in single *MAT***a** cells. We performed long time-lapse experiments (600 min) resolving a wide range of isotropic pheromone concentrations in both the wt and the *bar1*Δ *MAT***a** strains. First, we measured induction of the mating pathway using the P_{FUS1}-GFP reporter and determined the population's arresting dynamics (See Experimental Methods, Fig. 11 and Fig. 12). We analyzed how does the response's absolute value, i.e. its fluorescence intensity in arbitrary units, behave in both wt and *bar1*Δ strains (Fig. 11). Consistent with previous studies [80, 98], the P_{FUS1}-GFP reporter showed a clear dose-dependent induction by the purified α-factor (Fig. 11A). Importantly, shmooing of *bar1*Δ cells occurred at doses of α-factor that were above saturation of the transcriptional response. The P_{FUS1}-GFP reporter population mean is thus an ideal marker to resolve the cell response prior to the ultimate commitment to mating. We further observed that in the wild type, the pathway induction strongly shifts over time to higher initial α-factor concentrations as compared to the *bar1*Δ strain (Fig. 11A). This confirms Bar1-mediated degradation of α-factor as the dominant mechanism of attenuation of the *MAT***a** cell mating pathway response at sub-saturating pheromone concentrations. There are three main differences between the responses of both strains. The first one is the response down-regulation with time due to to α-factor proteolysis and the concomitant time-dependent increase in the "sensitivity" difference between the wt and the *bar1*Δ strain (Fig. 11A and B. Note: even though the word "sensitivity" is often used in the literature,

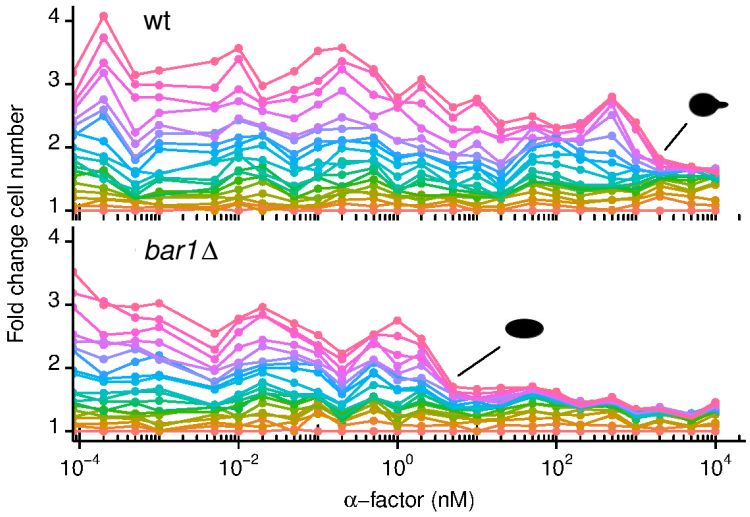

Figure 12: Cell cycle arrest sensitivity in wt and *bar1*Δ strains. Data from Fig. 11 now showing the cell-cycle arrest dose-response. Phenotypes (as defined in Fig. 11) present at the transition to full arrest (less than one cell division during experimental time) are indicated with a line and a cell scheme. Colors represent time, exactly as in Fig. 11 A.

Bar1-dependent changes in the EC_{50} of α-factor dose responses respect to the *bar1*Δ are not related to sensitivity changes but rather to signal availability, hence the quotes in the word). The second difference, which has not been reported in the literature, is a response overshoot at late times observed only in the *bar1*Δ strain precisely at α-factor concentrations where the elongation phenotype is observed. Third, when we analyzed the phenotypic frequencies on both strains we found that the wt is perfectly capable of performing the shmooing switch observed for the *bar1*Δ (Fig. 11, note the difference between concentrations generating 100% elongated and 100% shmooing cells), however it does not show clear elongation at concentrations below the shmooing threshold (See section 10.3). It has to be noted that, in the literature, un-budded cells are usually classified as arrested cells [105, 73]. Even though true, cells do recover from arrest in both strains, making this phenotype transient. The degree of arrest (measured as the population-level relative growth) is dose-dependent (Fig. 12). Full arrest, i.e. absence of a full duplication in the population number during experimental time is indeed observed in both strains, however the phenotype expressed at the full-arrest threshold is different in both strains, consistent with the phenotypes observed in Fig. 11.The non-monotonic (overshooting) α-factor dose response at late times observed in the *bar1*Δ strain (Fig. 11A) implies that maximum P_{FUS1}-GFP levels are not necessarily obtained at signalling saturation. Moreover, the absence of shmooing at the α-factor concentration corresponding to the overshoot suggests that a property different from the maximal expression level attained is the determinant of this particular cell-fate decision. In order to clearly interpret the data it is necessary to define the timescale of the P_{FUS1}-GFP reporter turnover, i.e. an estimate of the combined degradation and dilution rates due to proteolysis and cell growth/division.

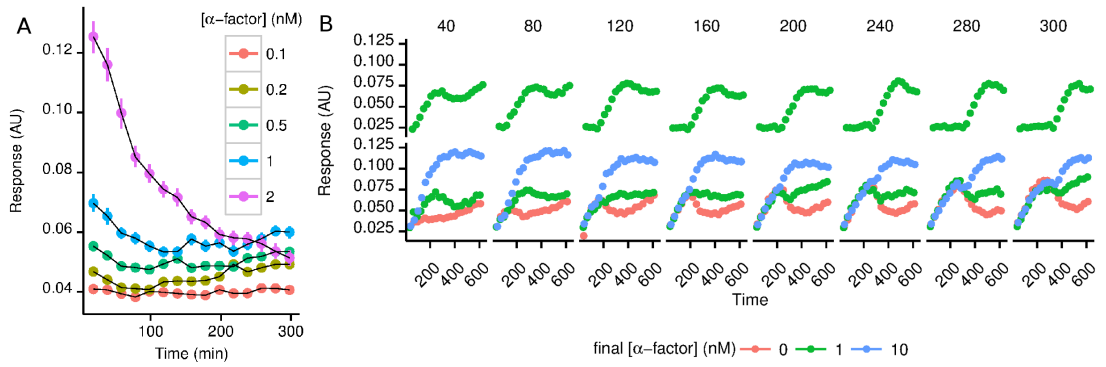

Figure 13: P_{FUS1}-GFP reporter turnover in the *bar1*Δ strain. A. Signal decrease kinetics for prestimulated P_{FUS1}-GFP reporter upon removal of α-factor. Colors indicate population subject to α-factor stimulation at the indicated concentrations. B. $MAT\boldsymbol{a}$ response to α-factor addition and removal is independent of prestimulation time. Upper row. Time traces showing of non-prestimulated cells stimulated with 1 nM α-factor at different times (in minutes indicated at the top of each plot), indicating the correct functioning of cell signalling across experimental time, i.e. independent of the time they get stimulated, the response is equivalent. Bottom row. At time = 0 min, 1nM α-factor is added to all samples. Then the α-factor solution is replaced with media (red), a solution with 1 nM α-factor (green) or a solution with 10 nM α-factor (blue), at the time points corresponding to the control stimulation (upper row).

10.2 Reporter turnover

We defined the timescale in which P_{FUS1}-GFP is useful to report dynamic changes in α-factor. The timescale for pheromone-induced activation of P_{FUS1}-GFP RNA expression is tens of minutes [109]. The maturation half-time for our version of GFP (obtained from Prof. M. Knop, ZMBH) in *S. cerevisiae* is 6 minutes [56] and it includes a degron sequence for faster degradation (See Experimental Methods). The time needed for the GFP intensity to decay its half-maximal value after removal of α-factor is roughly 100 minutes (Fig. 13 A). Also, when prestimulated near its saturation value, the P_{FUS1}-GFP reporter shows equal response times to either depletion or full stimulation (Fig. 13 B) with α-factor, independent of the pre-stimulation time the cell populations are subject to. This shows that the combined degradation and dilution rate for GFP allows for the monitoring of pathway inactivation given that the experimental measuring time exceeds at least 100 minutes, as can be seen in the decay kinetics of the P_{FUS1} response observed when Bar1 is present (Fig. 11 B). Given the comparatively slow GFP degradation kinetics (~100 min) and the faster ligand-receptor equilibration curve (~10 minutes for values near K_d) [101], it is reasonable to assume that the GFP production rate in our construct reports the equilibrium Ste2 occupancy as reported before [109] and not a dynamic pre-equilibrium property, as the case of upstream pathway outputs like Ste5 membrane localization [101].

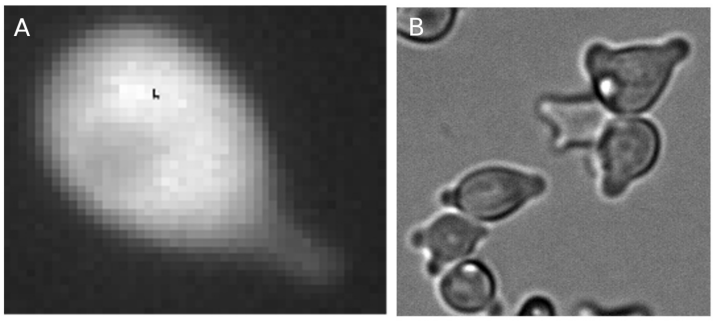

Figure 14: Examples of shmooing morphologies. A. A single shmoo showing decreased fluorescence when compared to the rest of the cell body. B. Multiple shmoos are observed at saturating α-factor concentrations.

10.3 Developmental thresholds in mating morphologies.

The second output considered is the morphological fate of yeast populations subject to isotropic α-factor stimulations, e.g. the frequency of shmooing cells in the population. In the literature, the word "shmooing" is usually used indiscriminately to designate any type of distinguishable symmetry-breaking in stimulated cells. For the sake of precision, "shmooing" refers in this work to the Spa2-dependent polarization which causes the randomly polarizing non-chemotropic protrusion, as defined by Dorer et al. [26] (See section 3.3). The shmoo (thin protrusion) displays the following properties. First, cytoplasmic GFP fluorescence shows dimmer intensity within the thin protrusion region, probably because of its reduced thickness compared to the cell-body which sums up several layers of GFP proteins (Fig. 14 A). Second, multiplicity of thin protrusion occurrences are possible (Fig. 14 B, see also [43, 74]). Third, in the wt strain a shmooing event generally precedes an elongation event, in this case one can directly compare how different these two are (See Fig. 15 C for an example). On the other hand, "elongation" refers to any polarization which does not correspond to the properties mentioned for shmooing. Elongating cells (See Fig. 17 B for an example) show a wide protrusion, display chemotropic capacity and no defined maximum length in artificial gradients [51, 87]. Other mating phenotypes are "bipolar budding" where a daughter cell emerges from the opposite side of the previous bud, and "volume increased" cells with no symmetry breaking, i.e. isotropic volume-increased cells (See Fig. 39).

As shown above (Fig. 11), the wt and *bar1*Δ strains express different phenotypes at equivalent regions of the dose response as a consequence of Bar1-induced α-factor depletion. Notably, the wt strain does not show clear elongated phenotypes at concentration below shmooing. Table 7 summarizes the observed frequencies of phenotypes for the *bar1*Δ strain as a function of the pheromone concentration. Unlike *bar1*Δ, the wt shows elongating populations only after a shmoo has been completed (Fig. 15). On the other hand, shmooing is executed only when the *FUS1* transcriptional output is saturated ([26], Fig. 11B), which strongly indicates receptor

Table 7: Phenotypic thresholds in *MAT* **a** *bar1*Δ.

Threshold	α-factor concentration $[\alpha]$	Approximately equals
Full Arrest, elongation and delayed steady state ("shmooing onset"): -Population does not double when the non-stimulated control has doubled twice. -Population elongates. -During the first 200 minutes the GFP signal grows linearly, contrary to higher or lower α-factor concentration where it looses rate.	2 nM$<[\alpha]<$10 nM	Ste2·α-factor dissociation constant (K_d) = 5.4 ± 2.5. Averaged from 9 different experimental measurements (See Ste2 K_d in yeastpheromonemodel.org [108]).
Transient arrest with isotropic growth: Cells increase their volume isotropically before returning to budding in a bipolar manner.	1nM$<[\alpha]<$2 nM	2/5 x K_d
Rate-loss: Loss of GFP accumulation rate happens within the first 200 minutes of the response.	10 nM$<[\alpha]<$20 nM	4 x K_d
Shmooing: Cells execute the default mating pathway by shmooing instead of increasing volume	20nM$<[\alpha]<$50 nM	10 x K_d

saturation [109]. Indeed, the P_{FUS1} response EC_{50} in *bar1*Δ corresponds exactly to the reported dissociation constant K_d for the Ste2 - α-factor interaction (Table 7).

The P_{FUS1}-GFP response to isotropic α-factor in the *bar1*Δ strain shows a clear overshoot at concentrations corresponding to elongation (Fig. 11, see Fig. 37 for a replica). It can be observed only as the dose-response develops in time, the reason being that the steady state level of the mean GFP intensity is higher in elongating cells than in shmooing cells. In the former, the GFP accumulation rate even though lower than in the latter, is maintained constant during the elongation time reaching a higher steady-state level. This means that whatever loss-of-rate mechanism operating during shmooing has a more discrete or no contribution in elongating cells or that there is a gain of rate mechanism operating when cells elongate which is somehow suppressed when cells shmoo. Unlike elongation, shmooing cells do not reach the highest possible mean GFP value, although its initial accumulation rate is higher than that of elongating cells (Fig. 19, Section 10.5).

10.4 Cell-cell variability in gene expression and morphological fate

The full characterization of the response dynamics and dose-dependency allowed us to define developmental thresholds by combining the data from the measured outputs. It seemed possible that the phenotypic response and the gene expression response are controlled by different properties of the input function. Although the mean population P_{FUS1}-GFP intensity can be clearly correlated with the type of morphology the cells develop, the intensity distribution displayed

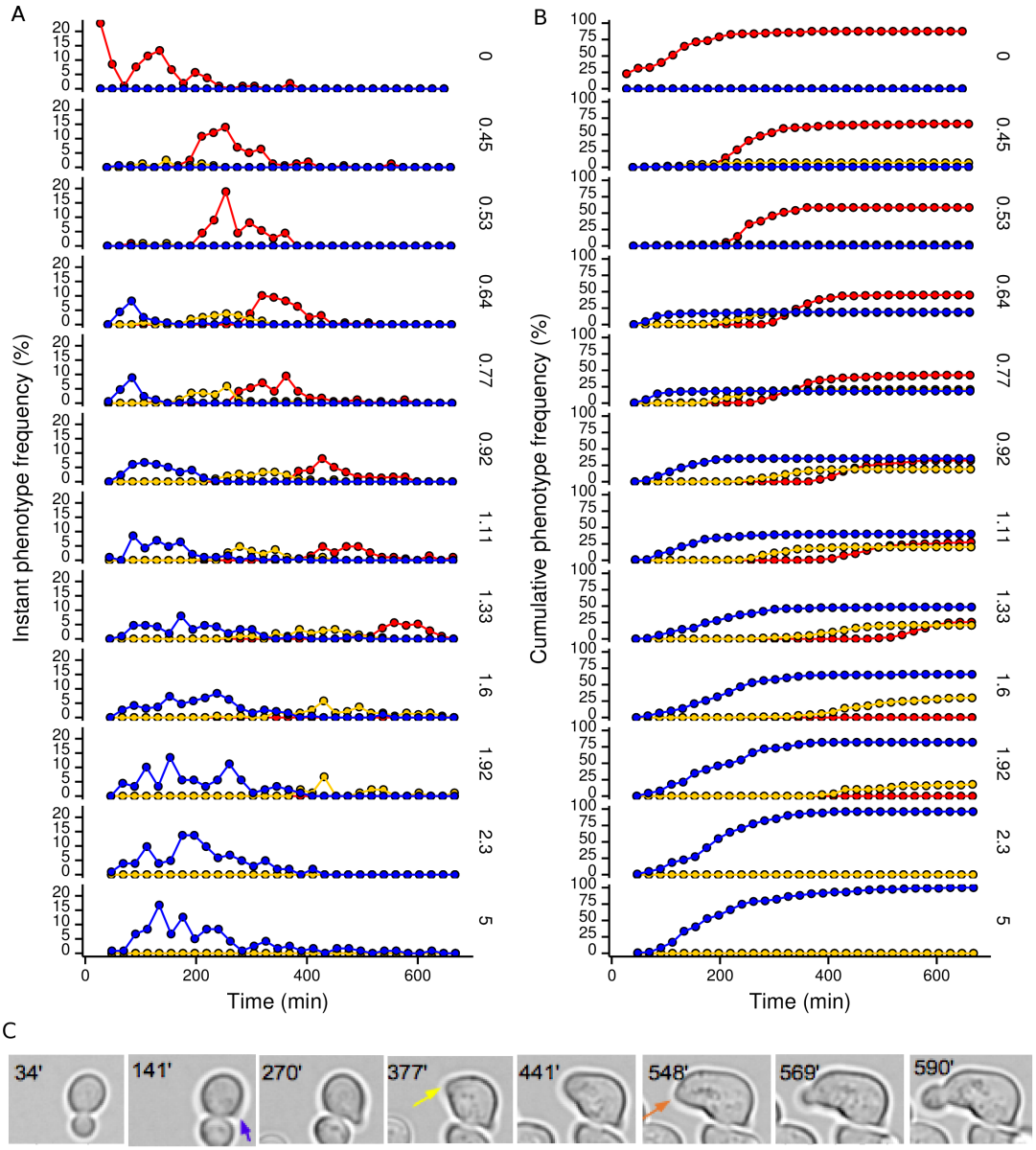

Figure 15: Wild-type phenotypic trajectories. A. Instant frequency of first-buds (red), elongation (yellow) and shmooing (blue) at different α-factor concentrations (rows, in μM). First-buds means that only the first bud generation from every cells in the three fields of view considered were counted, i.e. the second bud emerging from any given cell during experimental time was ignored. Phenotypes and not cells are counted. i.e., One cell can display several phenotypes in time (a phenotypic trajectory). Each phenotype is scored at its initiation, as determined from the time-lapse analysis. B. Cumulative frequencies of mating phenotypes plotted using the data from A. C. An example of a phenotypic trajectory. A cell starts shmooing at 141 min, then starts elongation at 377 min and finally starts budding at 548 min. Arrows indicate the position of the incipient developing phenotype. Colors correspond to colors in panels A and B.

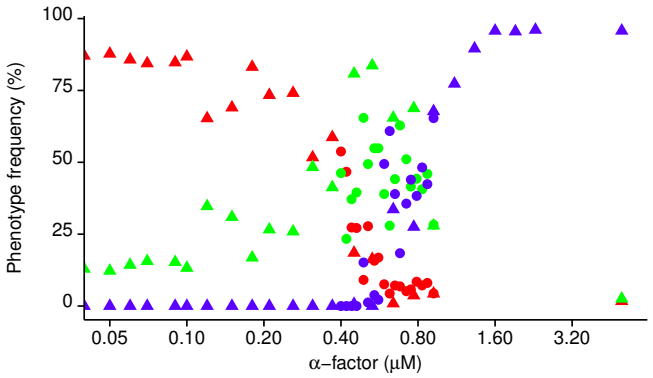

Figure 16: Phenotypic transitions in the wt strain. Budding (red), shmooing (blue), and transitional (green) cumulative phenotype frequencies. The transitional phenotypes consist of bipolar budding, isotropically volume-increased cells and non-shmooed elongated cells. Unlike Fig. 15, only one phenotype is assigned to a given cell, i.e., the first one appearing. Different symbols (triangles and circles) correspond to different experiments.

by the population overlaps with that of populations expressing a clearly different phenotype (Fig. 17). For example, cell populations with 100% shmooing cells (Fig. 17C) are composed of individuals having P_{FUS1}-GFP output values characteristic of the mean intensity shown by cells displaying elongation (Fig 17B). The relation between the instant absolute value of pheromone-dependent gene expression and the morphological output is hence not directly causal. We then decided to track individual cells in populations displaying 100% of elongating or 100% shmooing cells (Fig. 18) in the *bar1*Δ strain. If the determinant of the developmental fate cannot be correlated with the intensity displayed by the maximal gene-expression output level, it is reasonable to think that it is rather a dynamical property, e.g. its activation rate, what correlates with the fate chosen. The already shown lack of response down-regulation in the sensitive range in the *bar1*Δ strain, which generates the overshoot (Fig. 11A and B, bottom) contrasts with the lower maximal value observed for shmooing at higher concentrations in the same strain, consistent with shmooing-dependent downregulation. However the starting accumulation rate in the shmooing population is significantly higher suggesting that the shmooing decision is made early, when the maximum gene-expression rate is obtained. This confirms that shmooing occurs at levels of activation at or above saturation of the gene-expression rate, and that molecular mechanisms different from those determining the absolute level of the gene-expression output must be operating when cells shmoo. In summary, shmooing correlates with a Bar1-independent gene-expression response down-regulation an occurs at maximal P_{FUS1}-dependent expression rate and elongation occurs below saturation of the P_{FUS1} expression rate with a weaker downregulation that generates higher maximum expression levels.

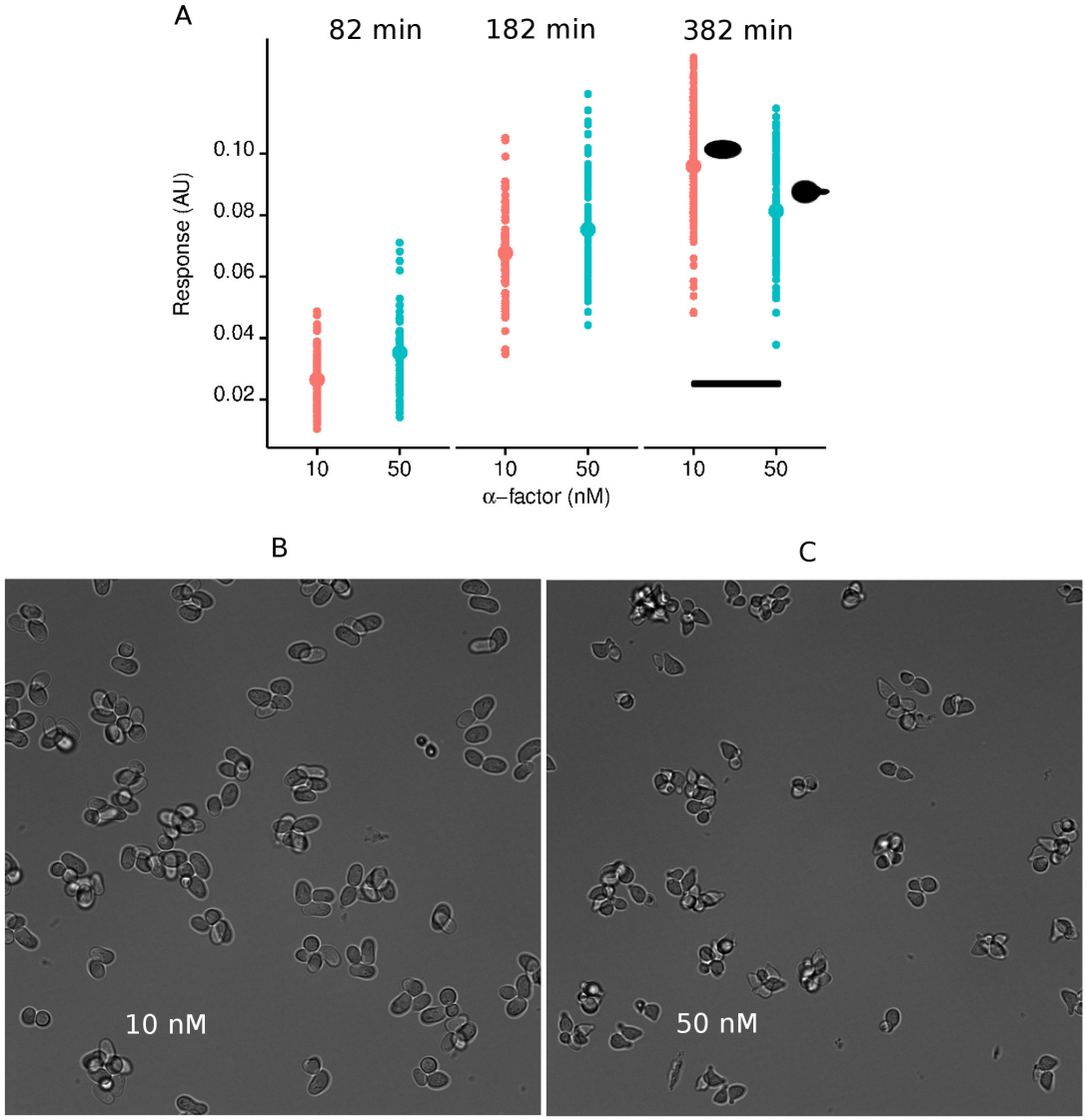

Figure 17: Responses show differential heterogeneity. A. *MAT**a** bar1*Δ response signal intensity distributions in shmooing and elongating populations at two α-factor concentrations inducing phenotypic cumulative frequencies $>$ 95%. B, C. Example time-frames (382 min) of the elongating (B) and shmooing (C) samples shown in panel A. Fluorescence was quantified in microscopy time-lapse series as described in Experimental Methods.

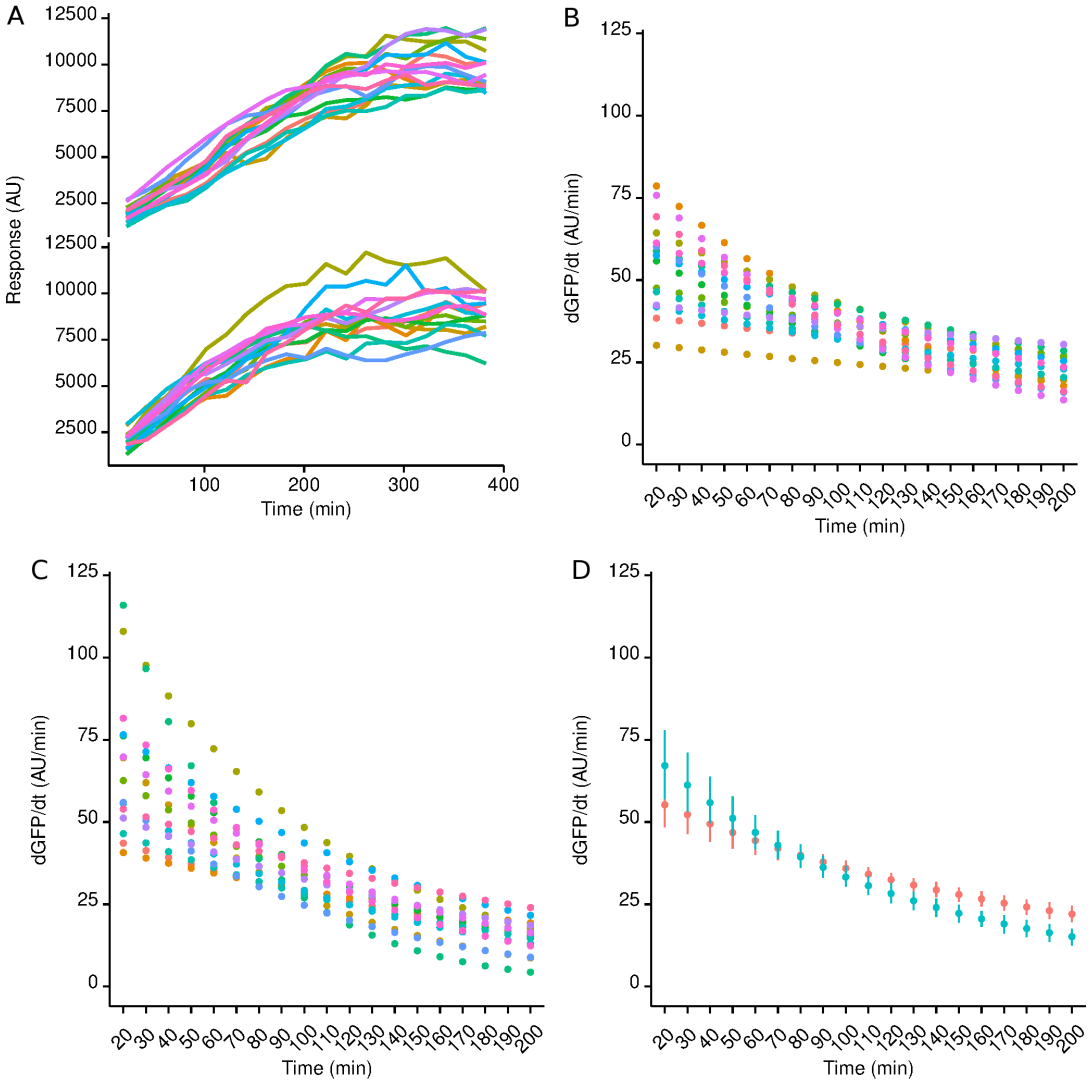

Figure 18: Single cell tracking during α-factor stimulation. A. The average pixel intensity of a fixed area inside cells was quantified in each one of 19 time-frames for a 100% elongating (top) and a 100% shmooing (bottom) population of $MAT\boldsymbol{a}$ $bar1\Delta$, corresponding to the time-lapse movies shown in Figure 17. B, C. For each one of 15 cells exponential fits where performed on the time-traces (See Experimental Methods), and the instant rate calculated at different time points for the elongating (B) and the shmooing (C) populations. D. The mean response rate for both elongating (red) and shmooing (blue) populations was calculated. Error bars are the standard error of the mean

10.5 Response maximal amplitude above shmooing-inducing inputs.

At α-factor concentrations higher than those corresponding to the shmooing threshold, the steady-state response values in the *bar1*Δ strain stabilize at a sub-maximal value smoothly as the dose increases (Fig. 11, Fig. 37). This implies that even though shmooing development obeys a threshold concentration (α_s), presumably equal to the concentration causing receptor saturation at equilibrium, maximal P_{FUS1}-dependent GFP expression level does not need to be achieved to trigger its development, but maximal P_{FUS1}-dependent GFP expression rate does. On the other hand, dose-responses performed on the wt show that cells do not visit the elongation morphological state but the transition to shmooing is intact (Fig. 11 and Fig. 15), suggesting that elongation needs a time-persistent activation rate and shmooing only a transient high one. Hence, the frequency of the elongation phenotype is insignificant in the wt strain, but shmooing is normal (Fig 15). At concentrations below the shmooing switch the wt shows rather heterogeneous phenotypes (*transitional phenotypes*, Fig. 16), but no clear elongation. Cells will execute shmooing when α-factor is high enough by saturating signaling, therefore showing maximal response rate and cells execute elongation when α-factor factor does not decrease in time.

In summary, in this section (10) we first showed that the mean population response rate is indeed an appropriate reporter of the α-factor concentration. Second, we showed that within its dynamic range all developmental fates (See section 10.3) are observed, supporting the idea that particular developmental fates respond to pathway activation thresholds. We also describe how fixed signal degradation by Bar1, i.e. at a fixed $MAT\boldsymbol{a}$ density, modifies the properties of the dose-response, not only modifying its sensitivity dynamically but also modifying the expression of mating morphologies. In the next section (11) we explore the role of internal adaptation (in opposition to Bar1 mediated attenuation). A full picture of the response dynamics to α-factor is necessary to interpret the results obtained in mixing experiments shown later (Section 13).

11 Absence of effective pathway adaptation

To further understand the pathway's response dynamics to α-factor downstream of receptor stimulation, we used the *bar1*Δ strain to explore the adaptive capacities of the MPP. Our motivation came from two different experiments. The first one deals with response deceleration in wt and *bar*1Δ strains (Sec. 11.1) and the second from autocrine pheromone signalling (Sec. 11.2)

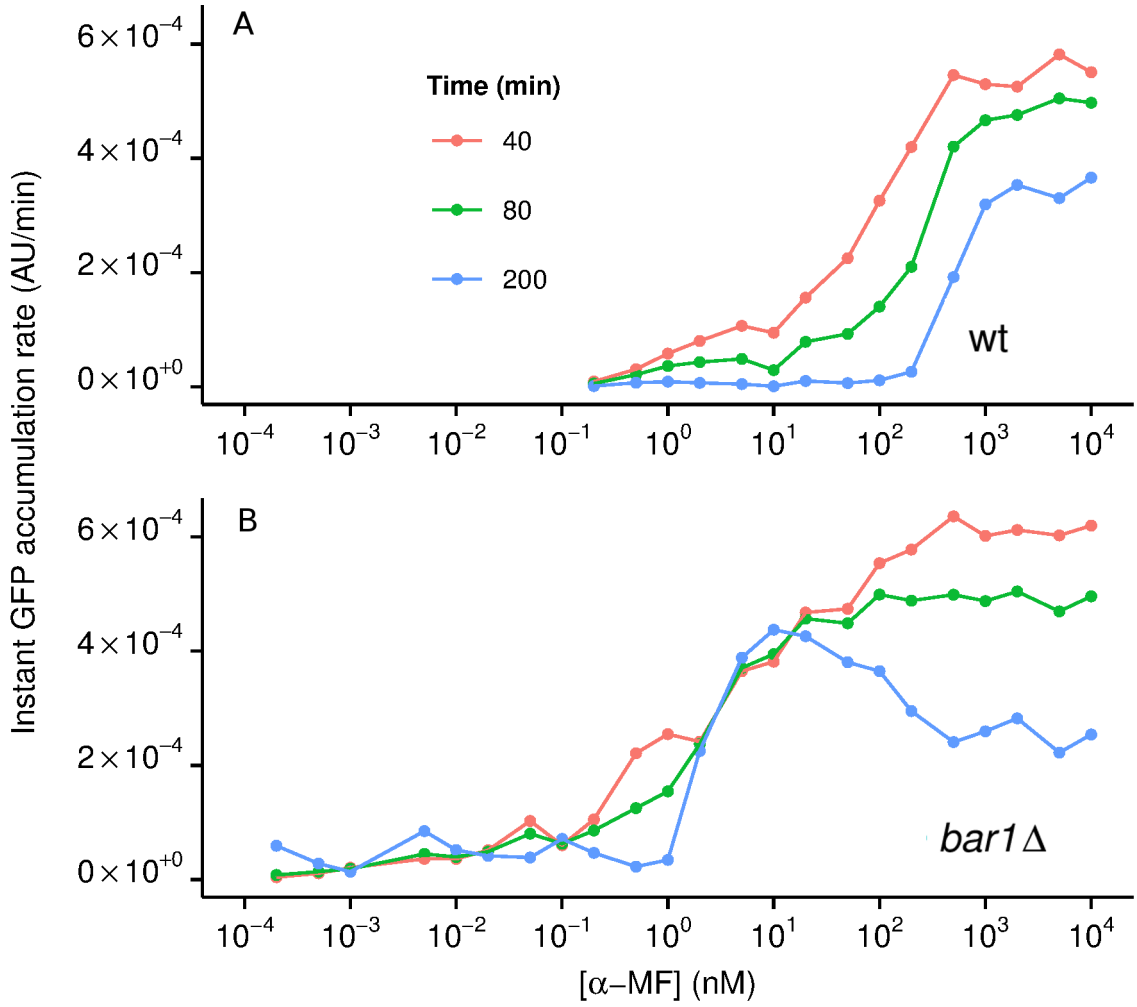

Figure 19: . Instant gene expression response rate to α-factor. A. wt (upper panel) and *bar1*Δ (lower panel) response rate to constant α-factor stimulation. Note region where the curves collapse in the *bar1*Δ strain.

11.1 Bar1-mediated input attenuation is essential for proper down-regulation

From our characterization of P_{FUS1}-GFP, we expected the initial rate of GFP accumulation to be an appropriate reporter of the α-factor concentration, as no negative feedbacks nor saturation effects should be present at early time points. Also, since the construct includes a degron sequence (see Experimental Methods) we expected the GFP signal to be unstable enough to allow us to follow decreases in α-factor concentration when appropriate experimental times are used (See Sec. 10.2). We first compared the dynamics of the P_{FUS1} response in wt and *bar1*Δ cells and discovered that there is an α-factor concentration range in which extracellular signal degradation by Bar1 is crucial to achieve an even response deceleration across the input range (Fig. 19 A). When Bar1 is absent, the pathway shows persistent activation with strongly attenuated deceleration at precisely the range where mating morphologies develop, i.e. 2-10 nM

(Fig. 19A, Table 7, Sec. 10.3). In the *bar1*Δ strain, the dose response curve for the response absolute value shows, as a consequence, an overshoot (Fig. 11). This range (2-10 nM or the "sensitive range") corresponds to that of phenotypes engaged in mating activities showing clear elongation (Fig. 11 and Sec. 10.3) which correlates with persistent activation. The wt does not elongate in the same way but rather following a different phenotypic trajectory under these conditions, being observable only in cells "recovered" from shmooing (Fig. 15, see also Movie S1 in Jin et al. [51]) clearly above the sensitive range of the P_{FUS1} response. On the other hand, at α-factor concentration ranges both below and above the shmooing onset, deceleration seems to mirror the wt behavior. These observations led us to the question of whether its external input degradation only rather than internal processes regulating response down-regulation at precisely the relevant range for mating. We reasoned that weaker internal negative feedbacks in that region could mean that the relevant response needs to perform in a non-adaptive manner or, in other words, to retain its sensitivity.

11.2 Autocrine prestimulation does not alter pheromone sensing

We observed that when allowed to grow in the absence of external α-factor the *bar1*Δ strain shows a significant increase in fluorescence levels within experimental time (Fig. 20 A). The increase comes in its majority from the effect of autocrine pheromone signalling, i.e. the production and detection of α-factor in $MAT\boldsymbol{a}$ cells, because when both $MAT\alpha 1$ and $MAT\alpha 2$ genes are deleted in a *bar1*Δ strain, the increase is lost. On the other hand, Bar1 seems to suppress the basal autocrine activation (Fig. 20 A). Furthermore, the increase is not related to differential growth between these strains (Fig. 20 B). Given that the native system harbors Bar1 and hence suppresses the basal autocrine response, the physiological meaning of autocrine signaling is not clear, but perhaps more important is the observation that pre-stimulated cells do not seem to change their sensitivity to further additions of α-factor, i.e. dose-responses performed on both the autocrine (*bar1*Δ) and the non-autocrine strains (*bar1*Δ $mat\alpha 1\Delta$ $mat\alpha 2\Delta$) are indistinguishable from each other (Fig. 20C). This is somewhat surprising because a common feature of sensory systems is their ability to change the pathway sensitivity once they adapt to a newly experienced stimulation level (See Sec. 2.3), and also because several pathway desensitization mechanisms have been proven to operate in yeast mating (See Sec. 1.2.2). Taken together with the argument exposed above (Sec. 11.1), our data suggests absence of adaptation mechanisms in the sensitive response range. This sensitivity invariance might be important for a proper mating response.

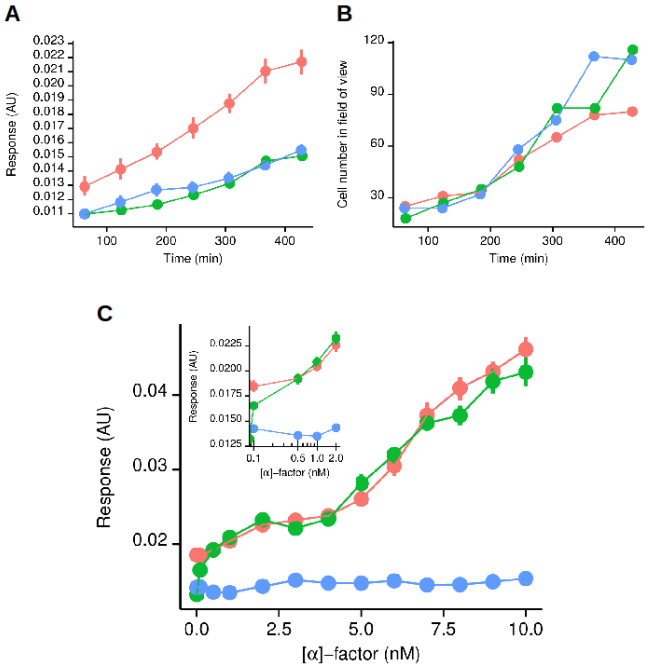

Figure 20: Autocrine signalling through incomplete silencing of α-factor expression. A. P_{FUS1} response kinetics in unstimulated samples of the wt (blue), *bar1*Δ (red) and *mat*α1/2Δ *bar1*Δ triple mutant (green). B. Growth curves for the same three strains. C. Dose responses at 308 after stimulation for the three strains. The inset shows the same response in the low α-factor concentration range. [show rather the 3 panels in a row]

11.3 Absolute pheromone sensing

To test the adaptive abilities of yeast, we performed controlled pre-stimulation experiments on the *bar1*Δ *mat*α1Δ *mat*α2Δ strain within the sensitive range of the response, i.e. between 0.1 and 10 nM α-factor. We provide evidence that supports the idea that the instant response amplitude of the MPP depends on the absolute value of the current α-factor concentration and not on the fractional change from the prestimulation value. We continued by considering that sensory systems and a few recently described cellular sensory systems display what can be called in general fractional sensing or sensory input scale invariance. Sensory input scale invariance assures that the characteristic broad dynamic range of the perceived physical magnitudes can, within certain limits, have a faithful representation in the perceived magnitude used for response elicitation (See Sec. 2.3). With this background, we investigated the possible role of fractional sensing from a sensory-adaptive perspective and asked weather inner mechanisms are able to (i) adapt the pathway output back to basal levels and (ii) modify the sensitivity to input changes in adapted cells. We observed that when pre-stimulated with input values within the sensitive range of the response, cells are not able to do neither during experimental time (Fig. 13 B and Fig. 21). On the other hand, removal of α-factor from the media results in an efficient reduction of the response, with a similar time scale as full induction does (Fig. 13 B), indicating that a slow time scale for GFP degradation ($\sim$100 minutes) is not the cause of the observed sustained

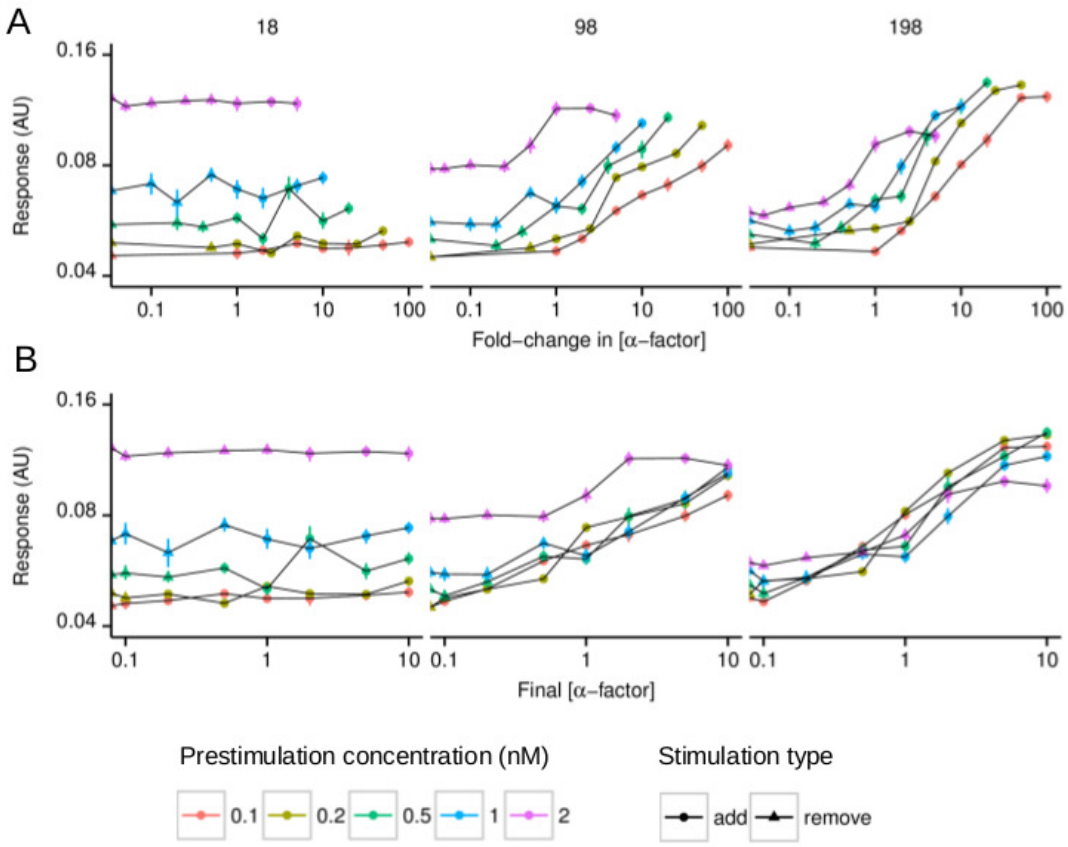

Figure 21: Pathway responses to changes in α-factor concentration in the *bar1*Δ strain. P_{FUS1}-GFP expression plotted as the absolute signal intensity in response to the fold-change (A) or the final (B) concentration of α-factor at 3 different time points (in minutes, indicated at the top of each column) in cell populations pre-stimulated with 0.1 (red), 0.2 (yellow), 0.5 (green), 1 (blue) or 2 (pink) nM of α-factor for 320 minutes prior to performing step concentration changes. Triangles correspond to removal and circles to no changes or additions of α-factor.

activation in response to sustained (320 minutes, Fig. 21) prestimulation. Hence, the response to either additions or subtractions from the current steady value of α-factor should represent input modifications to the system in a non-adapted state (i.e where the output does not go back down to basal levels during experimental time). Nevertheless, as long as prestimulation values lie in the sensitive range of the MPP, there is no reason to assume that the lack of output signal adaptation implies an invariance in sensitivity to further changes in input concentration. However, this seems to be the case (Fig. 21, Fig 40) since all prestimulation values shown except one (pink points) keep sub-saturated outputs after the prestimulation time (320 minutes). When changed to a different concentration, the prestimulated populations response equivalently only when the response is plotted against the final α-factor concentration and not to the fold-change in α-factor (Fig. 21, for a more complete analysis including response fold-changes and input absolute changes see Fig 40, note however the linear x-scales in the mentioned figure). Our results indicate absence of logarithmic sensing in the gene expression output of the yeast mating pheromone pathway. This is surprising because cellular sensory systems have been shown to

follow fractional rather than absolute changes in input concentration (See 2.3). If α-factor gene expression follows the current absolute α- factor concentration, independently of the time it has been exposed to a pre-stimulation, it means that cells are unable to modify their sensitivity and are vulnerable to premature overstimulation by the global pheromone concentration. When Bar1 is present, as with input depletion, the cells can return to basal levels. The inability of the cells to adapt the pathway fast to constant input and, in turn, its ability to follow the current input value could mean that it is the external α-factor concentration which determines the physiologically relevant pathway output, and not purely internal adaptation dynamics. Relying on external signal attenuation rather than internal adaptation to prevent overstimulation is an equally effective strategy, however it bears the consequence that fractional changes in concentration can not be distinguished from absolute changes, suggesting that adaptation is not involved in the fractional gradient sensing reported in the literature [79]. Importantly this makes the response strictly dependent on population parameters since signal attenuation and emission depend on the density of $MAT\boldsymbol{a}$ and $MAT\alpha$ cells respectively, with the input being re-scaled by the relevant environmental variable (mate availability) and not the response re-scaled according to a previous internal state of the system. This makes sense for mating reactions, where the input is expected to increase and accumulate in time making adaptation useless. Furthermore our result suggests that *Saccharomyces cerevisiae* senses population parameters by instantly following the concentration of α-factor in the extracellular medium. In relation to that, the following sections address the sensing of population parameters in mating where we propose an additional form of fractional sensing.

12 Bar1 works with first order kinetics

Given the importance that Bar1 has in regulation of the response at input values at the onset of mating commitment, i.e. α-factor concentrations between the P_{FUS1}-GFP EC_{50} and the concentration determining shmooing (α_s) it is necessary to understand the mode of action of Bar1 in our experimental setup. We determined experimentally whether Bar1 works in the linear range of its substrate dependency curve at input concentrations within the sensitive range of the response. A simple calculation suggests that the crucial assumption of the Michaelis-Menten equation should hold for our purified α-factor stimulation experiments (at least for the range of concentrations near the receptor K_d value), i.e. that the substrate concentration exceeds that of the enzyme considerably. In our experiments the number of $MAT\boldsymbol{a}$ cells stimulated is around 1×10^5 (1 OD_{600} unit $\sim 1 \times 10^7$ cells/ml). A purposeful overestimation for the secretion rate of Bar1 is 1000 molecules per cell per second (two times that of α-factor [86]). Given these assumptions, after 40 minutes of secretion the concentration of Bar1 lies within the femtomolar

range in our reaction volume (100 μl), and hence well below the concentrations of α-factor in the response sensitive range (2 nM). Given that the concentrations of α-factor in the sensitive range of the response are well below (1-10 nM) the reported K_M (30 μM) [77], and that Bar1 induction by pheromone is weak in the sensitive range of P_{FUS1} (Fig. 29), Bar1-induced degradation rate (v_{deg}) should fall in the linear range of a Michaelian hyperbola ($v_{deg} = k_{\mathrm{cat}} B_0 \frac{\alpha}{K_{\mathrm{M}}+\alpha}$), because the condition $\alpha \ll \mathrm{K_M}$ makes α disappear from the denominator, approximating first order kinetics as:

$$v_{deg} = -\frac{d\alpha}{dt} = k_{\mathrm{cat}} B_0 \frac{\alpha}{K_{\mathrm{M}}} \tag{8}$$

Where B_0 is a fixed concentration of Bar1. In our experiments, however, the concentration of Bar1 changes with time due to active secretion. Nevertheless, we can experimentally add a fixed amount of Bar1 exogenously and measure the degradation rate of α-factor by following P_{FUS1} activity in a *bar1*Δ strain (Fig. 22). If the highest concentration of Bar1 encountered in our experiments allows degradation of α-factor with first order kinetics, we can be certain that lower Bar1 concentrations also do. Integrating Eq. 8, we get the expected concentration profile of α-factor in time:

$$\alpha(t) = \alpha_0 e^{-kB_0 t} \tag{9}$$

Where k is the unknown Bar1 specificity constant ($\frac{k_{\mathrm{cat}}}{K_M}$) and α_0 the initial α-factor concentration. Then, if first order degradation is true under the proposed conditions, then at any time point the α-factor concentration should be a constant fraction of α_0. Since the rate of GFP accumulation in *bar1*Δ reports the α-factor concentration, a shift to the right in its dose-response when Bar1 is added is expected if the dose is plotted in logarithmic scale. Also, since the mean lifetime of α-factor is:

$$\tau = \frac{1}{kB_0} \tag{10}$$

, the magnitude of the shift should also increase with time at a rate proportional to B_0 and independent of the initial α-factor concentration, so the slope of the dose-response in with logarithmic x-scale should be equal to that of the *bar1*Δ strain. We observed the shift and its acceleration by comparing the wt, the *bar1*Δ strain and the *bar1*Δ supplemented with exogenous Bar1 (Fig. 22). In this last mentioned sample, we used the Bar1 concentration which is present in supernatants of cultures at a density of OD_{600}=2 , after day growth starting from a 1% v/v inoculation from a saturated culture. The exogenous Bar1 represents then a concentration value of B_0 above its upper limit in our experimental datasets, and hence the linearity assumption of the attenuation model can be verified to a substantial degree under these conditions. Our data

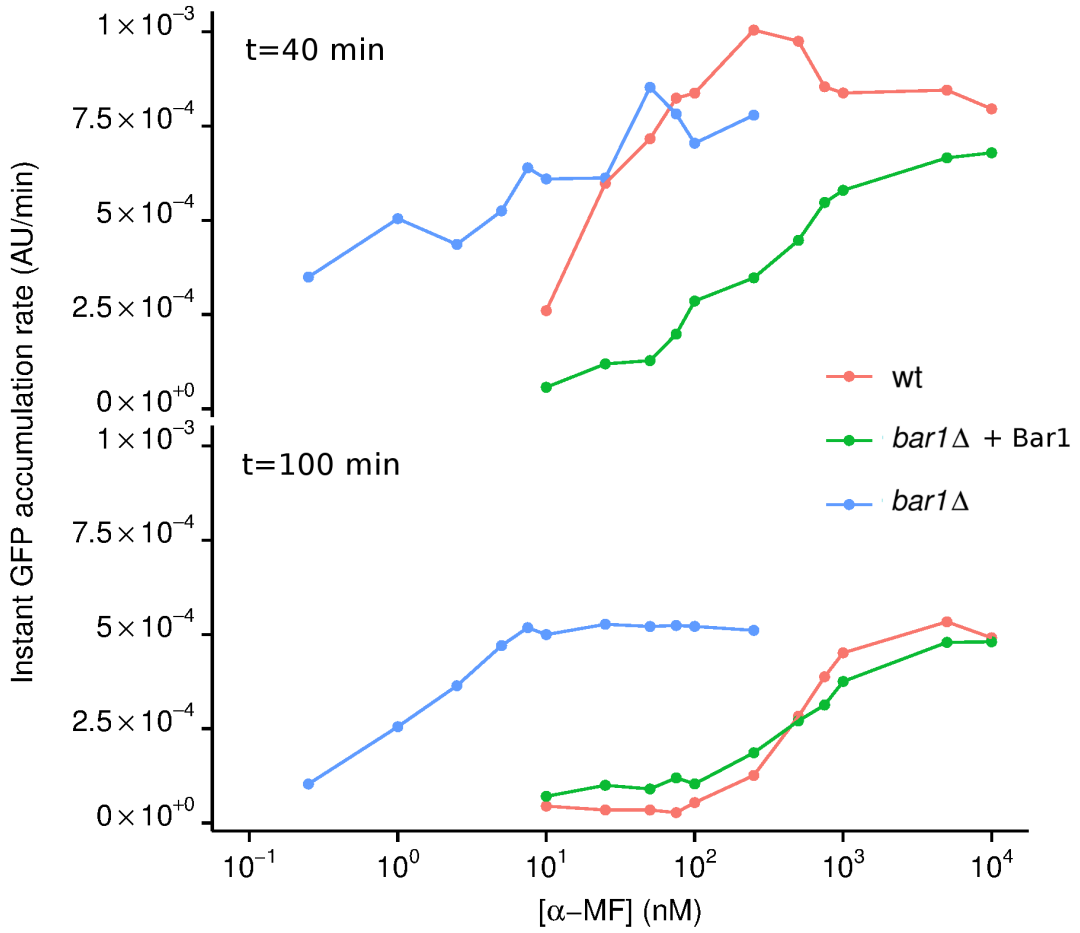

Figure 22: Bar1 works on the linear range of its Michaelis-Menten curve. Experiments shows the shift in the GFP accumulation rate dose-response for the wt (red) and the *bar1*Δ (blue) and the exogenously added Bar1 (Supernatant of a OD_{600}=2 wt culture, green) at 2 different time points.

suggests that Bar1 indeed works on its linear range of its Michaelis-Menten curve, producing the expected shift in log-scale. The wild-type, shows a slower shift than the case where Bar1 is added exogenously (Fig. 22), as expected. The magnitude of the shift at 40 minutes is at least 1.5 orders of magnitude (Fig. 22) for the exogenous Bar1, suggesting a extremely low α-factor mean lifetime. With time, the wild-type is able to produce a similar shift, probably because of accumulation of Bar1 through active secretion. Moreover, the similar shapes of the wt and supplemented *bar1*Δ curves confirms the weak, if any, influence of Bar1 α-factor mediated induction. Importantly, in this model one can see that modifying the concentrations of α_0 result in linear increases in α-factor concentration when examined at a fixed time. Changes in Bar1 produce on the other hand produce linear decreases on the mean lifetime (or half life). Changes in the ratio of these quantities would produce linear changes in either direction when examined at a fixed time, i.e. linear reductions in pheromone concentration with Bar1 and linear increases with α-factor. This means that equivalent increases on both quantities should produce an invariant pheromone concentrations at a fixed time. At late times, substrate exhaustion

causes the P_{FUS1}-GFP response to peak and decay to a lower amplitude steady-state (Fig. 11), this produces the switch like appearance of the dose-response curve. The new steady state is higher than the baseline for unknown reasons.

13 Sensing of population parameters during yeast mating

The mating pheromone pathway of a $MAT\boldsymbol{a}$ cell reacts to the presence of the peptide pheromone α-factor in its extracellular environment. During a mating reaction, the concentration of α-factor that a Ste2 (α-factor specific) receptor is subject to during a given time, depends on its position relative to the spatial profile of pheromone concentration, which is determined by the position and strength of pheromone emitting-sources ($MAT\alpha$ cells) and sinks (Bar1 proteases and adsorptive surfaces). We reasoned that if a mating reaction occurs under well stirred (isotropic) incubation, the concentration that the population of Ste2 receptors in a given $MAT\boldsymbol{a}$ cell is subject to depends only on the temporal profile of α-factor concentration which is determined by the number of α-factor emitting-sources and the number of Bar1 emitting sources. In environments were diffusion is strong (liquid), the primary function of the mating pheromone pathway communication system could be that of sensing the number of mates and doing so, crucially, in a way that also depends on the number of same-sex cells. This idea strongly resonates with the fact that animals are known to adaptively adjust their sexual behavior dependent on the abundance of mates and particularly on the sex ratio of the population. To get quantitative insight into this process, we used the characterized P_{FUS1}-GFP and morphological outputs to measure the effects of population composition on the pathway input function and on the mating process.

13.1 Input attenuation as sensory strategy

Gradients formed by the pheromones provide spatial cues that allow yeast to direct mating projections ("shmoos") towards their respective partners (Fig 23 A). Shaping of the pheromone gradients has been proposed as the major function of the peptidase Bar1 that is secreted by $MAT\boldsymbol{a}$ cells and degrades α-factor [68]. Such degradation can limit pheromone diffusion from the source and therefore steepen the gradients, improving precision of alignment and partner discrimination [9, 74, 79, 51, 22]. In addition to providing directional cues, pheromones induce dose-dependent changes in tropic morphologies and gene expression already at concentrations below the threshold for shmooing [51, 69]. Consequently, pheromone gradients provide distance information so that a mating attempt is only triggered in close proximity to potential mates (Fig. 23A). We speculated that such dose-dependent induction by the secreted signals might also serve a completely different function, providing cells with information about the density

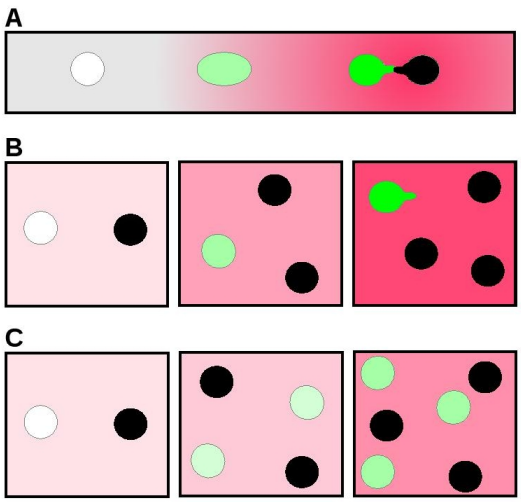

Figure 23: Sensory entanglement of mating cues in pheromone signaling. **A.** When the environment allows establishment of gradients, $MAT\boldsymbol{a}$ cells (white/green) can use the concentration of α-factor (pink) secreted by $MAT\alpha$ cells (black) as a cue for distance to the mating partner and adjust their phenotype and gene expression accordingly. Mating projection (shmoo) is only formed in the immediate proximity to the complementary mating type. Induction of mating genes in the $MAT\boldsymbol{a}$ cells (green) is dose-dependent and occurs already at concentrations of α-factor below the shmooing threshold. Such sub-threshold concentrations also stimulate chemotropic growth towards the mating partner and cell-cycle arrest. **B.** Within the homogeneous population, the α-factor concentration should increase with the density of $MAT\alpha$ cells. Such increase will induce both changes in gene expression and ultimately shmooing even in absence of a direct proximity to a mating partner. **C.** Attenuation of the mating signal dependent on the density of $MAT\boldsymbol{a}$ cells may prevent overstimulation and premature commitment to mating. It would also make response dependent on the ratio of the mating types within the population (compare corresponding panels in (A) and (B)).

and composition of the mating population, and therefore about the likelihood of successful mating. Indeed, for a uniformly mixed population and without additional regulation, the level of a pheromone in the medium should be directly correlated with the density of emitter cells (Fig. 23B). However, although the density of mates is an important determinant of the mating probability, the latter is expected to depend strongly on the density of the same-sex individuals, a crucial prediction of *operational sex ratio theory* [21]. Moreover, high pheromone concentrations can induce unproductive shmooing even in absence of a nearby mate [43, 26], with negative consequences for cell growth, survival and further mating attempts [22, 112, 17]. These problems could be potentially solved if the mate-emitted signal is attenuated by the receiver cells (Fig. 23C), with the Bar1-mediated pheromone degradation providing an attractive mechanism for such attenuation.

To experimentally investigate the mating response as a function of composition and density of a mixed population we used the characterized P_{FUS1} reporter in an isotropic assay where $MAT\alpha$ and $MAT\boldsymbol{a}$ cells were co-cultured under uniform mixing (Fig. 24). Under isotropic conditions, all cells in the population are stimulated only by the global α-factor (α_g) concentration independent of the distance separating mates, because gradients are not allowed to form. The pheromone

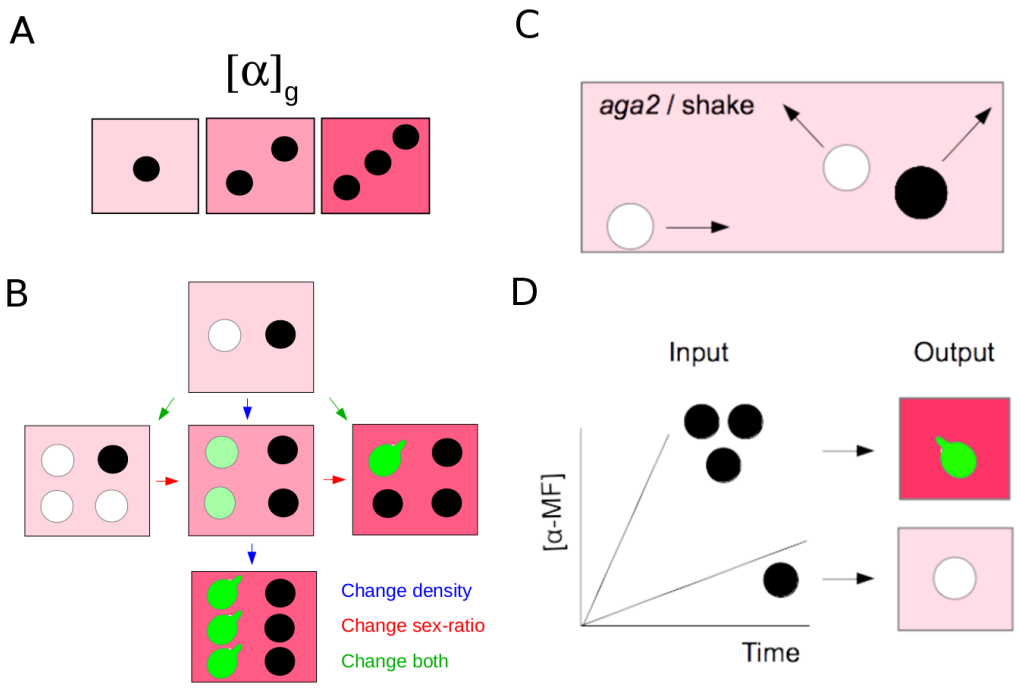

Figure 24: Population parameters and mixing experiments. A. The global α-factor concentration ($[\alpha]_g$) is expected to depend on the density of emitter cells ($MAT\alpha$, black). B. In the absence of gradients, and without further regulation, $MAT\boldsymbol{a}$ cells (green) respond to the $MAT\alpha$ density independently of their number (three black cells induce mating commitment). Arrows show the different ways population composition can be experimentally varied. Red arrows show changes in population composition (sex ratio). Blue arrows show changes in density. Green arrows show changes in recipient (left) and emitter (right) densities. Shmooing in alpha-cells is not considered C. In a *mixing experiment*, *aga2*Δ $MAT\boldsymbol{a}$ strains cells colliding with complementary mating-type cells are unable to form sexual aggregates. D. In *mixing experiments* pheromone accumulation rate is expected to be isotropic and proportional to the density of emitter cells.

concentration is a function of the amount of α-factor emitting cells ($MAT\alpha$ cells) (Fig. 24 A). Then, variations of population parameters such as density and composition of mating-type mixtures can be easily assayed and individual cell responses as shmooing or gene expression can be measured (Fig. 24 B). Since wt yeast cells have the capacity to perform sexual agglutination through sex-specific agglutinin proteins (Aga1:Aga2 complex in MAT$\boldsymbol{a}$ and Sag1 in MATα), a fully isotropic condition is achieved through disruption of this interaction. For this purpose, we used *aga2*Δ $MAT\boldsymbol{a}$ cells (Fig. 24 C, top) in what we call a "mixing experiment". In this way cell collisions do not result in sexual pairing (For mating reactions, where we explicitly measure sexual pairing see Sec. 14). Under constant α-factor production rate, the kinetics of accumulation of α-factor in our assay is expected to be linear in time with a slope value proportional to the amount of emitter cells ($MAT\alpha$), if no modification of the α-factor concentration by Bar1 is present (Fig. 24 D). The response of $MAT\boldsymbol{a}$ cells was induced by increasing total density at

which $MAT\alpha$ and $MAT\boldsymbol{a}$ cells were mixed (ρ_T), at a fixed 1:1 ratio of $MAT\alpha$:MAT$\boldsymbol{a}$ (Fig. 25 A, B). However, in wild-type cells the response flattened at higher density well below the reporter saturation and became nearly density-independent at later time points. Importantly, the response remained below the shmooing threshold and no shmooing was observed over the entire density range and time course (Fig. 25 B). When the relative abundance of $MAT\alpha$ to $MAT\boldsymbol{a}$ was varied at a fixed population density of $OD_{600} = 2$ (approximately 2×10^7 cells/ml), the response of wild-type $MAT\boldsymbol{a}$ cells showed a roughly linear dependence on the fraction of $MAT\alpha$ cells (θ_α), i.e. the sex ratio of the population [62], again without shmooing (25 B, C). In contrast, *bar1* knockout cells (*bar1*Δ) showed saturated reporter induction, shmooing and the concomitant growth arrest already at low densities and low θ_α values (Fig. 25 A-C).

13.2 Robust sex-ratio sensing through sensory input disentanglement

We next systematically explored the dependence of the $MAT\boldsymbol{a}$ cell response on the densities of $MAT\alpha$ and $MAT\boldsymbol{a}$ cells (Fig. 26, Fig. 27). By using our mixing experiments, we varied the composition and total density of cells and measured the response of *wt* and *bar1*Δ $MAT\boldsymbol{a}$ cells at 140 minutes (See Fig. 26 for an overview of population composition and responses). When we plot the $MAT\boldsymbol{a}$ response against the density of partner cells, i.e. $MAT\alpha$ cells, a clear pattern is observed. Contrary to the *bar1*Δ strain (Fig. 27 A and C, bottom), the wt strain (Fig. 27 A and C, top) is clearly able to respond proportionally to the amount of partner cells (ρ_T) when these are varied with a concomitant decrease in same-sex cells, i.e. changes in sex-ratio (θ_α) without changes in total density (ρ_T). Crucially, they do so with a sensitivity that depends on ρ_T (Fig. 27 E). As a consequence, when the data is plotted highlighting the ρ_T values (Fig. 27 B and D), the wt cells show a stable maximal response which only depends on θ_α and does not increase above this level even though ρ_T increases. The *bar1*Δ is therefore unable to distinguish θ_α and ρ_T, and simply responds to the absolute value of partner cell density. Consequently when the response is plotted against θ_α, different ρ_T values tend to collapse to a single curve in the wt, whereas in the *bar1*Δ strain it doesn't. We call this property input-attenuation dependent sex-ratio sensing. As time progresses, the sex-ratio response keeps its dynamic range in the wt, whereas the *bar1*Δ strain shows strong saturation even at very low ρ_T values, where the sex-ratio response is initially possible (Fig. 28). In summary, Bar1 seems to work below saturation even when the pheromone concentration is high enough to saturate signalling.

Our results demonstrate that Bar1-dependent input attenuation allows cells to prevent over-stimulation, premature commitment to mating and unproductive growth arrest at higher density of $MAT\alpha$ cells, as well as to ensure controlled induction of the costly mating response dependent not only on the density but also on the sex ratio of the population.

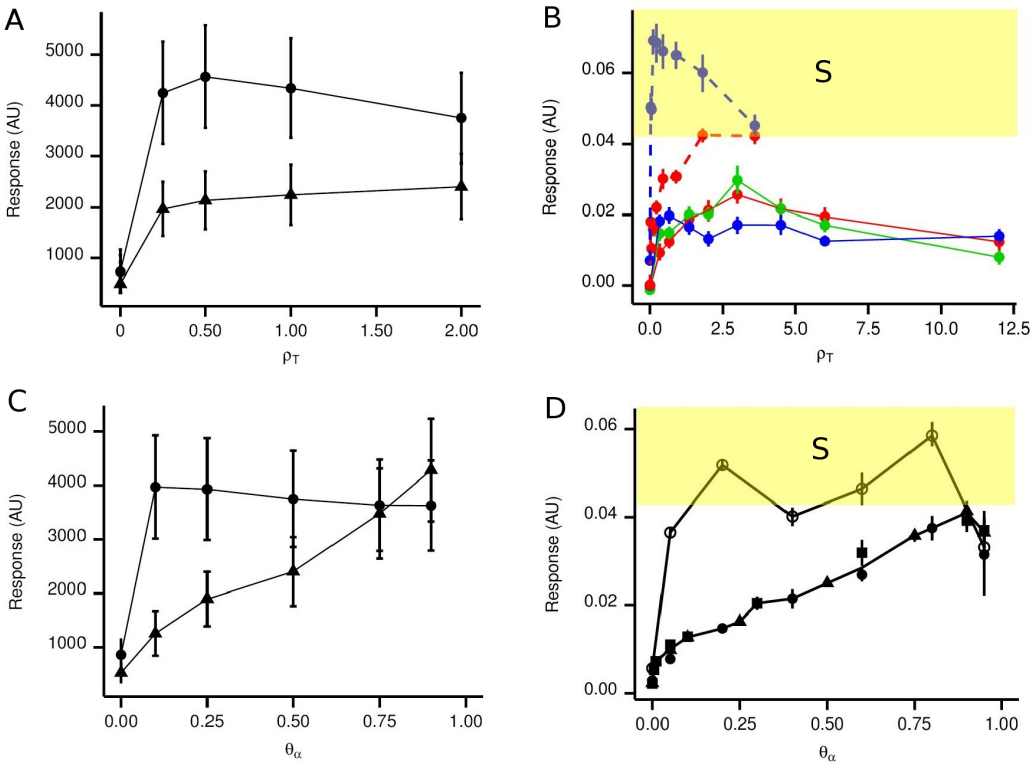

Figure 25: P_{FUS1}-GFP reporter and shmooing response in $MAT\boldsymbol{a}$ cells in mixed-population experiments. A-D. Activity of the P_{FUS1}-GFP reporter in $MAT\boldsymbol{a}$ cells in a mixed population with a fixed 1:1 ratio of $MAT\alpha$ to $MAT\boldsymbol{a}$ cells as a function of the population density at mixing (ρ_T) (A,B) and as a function of the sex ratio (θ_α) at fixed population density (ρ_T = 2 OD_{600}) measured with flow cytometry (A,C) and fluorescence microscopy (B,D). With flow cytometry (A,C), the wild-type (triangles) and *bar1*Δ (circles) where measured at 120 min after mixing of $MAT\alpha$ and $MAT\boldsymbol{a}$ cells. For flow cytometry experiments error bars indicate standard deviation of the responses of individual cells in the experiment, which are more informative (SEM bars are smaller than the symbol). With microscopy (B,D), the P_{FUS1}-GFP reporter response dependence on density of a mixed population at 1:1 ratio of $MAT\boldsymbol{a}$ to $MAT\alpha$ cells was measured over time on both $MAT\boldsymbol{a}$ wt (solid line) and *bar1*Δ (dashed line) (B). The wt response is shown at 100 min (red), 175 min (green) and 250 min (blue) after mixing. The *bar1*Δ response is shown at 80 min (red) and 310 min (blue). The value at zero density indicates the reporter activity in absence of $MAT\alpha$ cells**.** Likewise, The response of $MAT\boldsymbol{a}$ cells to a varying fraction of $MAT\alpha$ cells (θ_α) within the population at constant ρ_T (OD = 2 $\pm$ 0.2) (D) was measured. Different filled symbols indicate three independent measurements of the wt $MAT\boldsymbol{a}$ cell response. The response of *bar1*Δ cells from an experiment performed at OD = 2.3 is also shown for comparison (open symbols). Yellow regions (also noted with an "S") symbol indicate shmooing cells. For microscopy experiments error bars indicate standard errors of the responses of individual cells in the experiment, since there are less sampled cells in this case (50-100) the SEM is more appropriate, to estimate the precision with which the mean is determined.

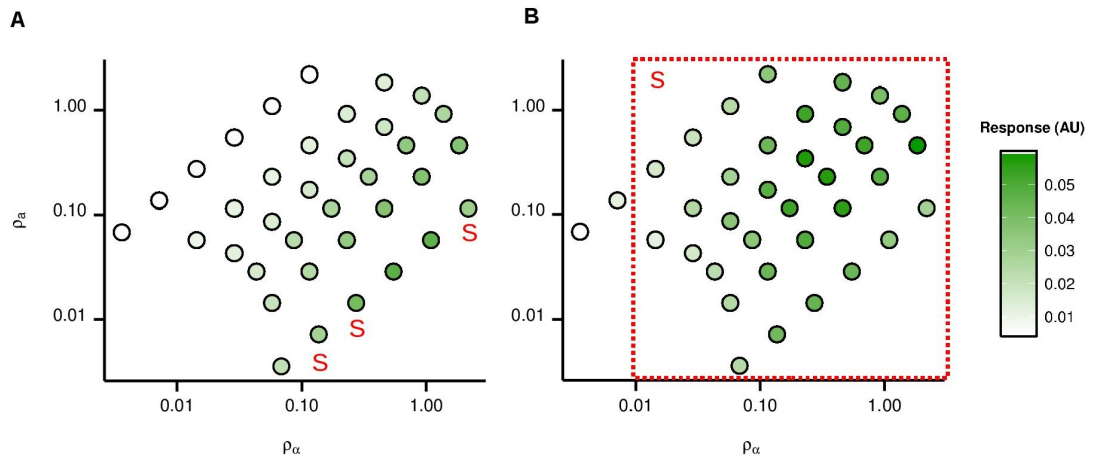

Figure 26: Overview of the $MAT\boldsymbol{a}$ cell response dependence on densities of mating types. **A,B.** Response of wild-type (A) and *bar1*Δ (B) $MAT\boldsymbol{a}$ cells in the mixed populations of $MAT\alpha$ and $MAT\boldsymbol{a}$ cells at different initial values of density and sex ratio, measured using microscopy at 140 min after mixing. Shmooing populations are indicated by "S" or a red frame. Activity of the P_{FUS1}-GFP reporter is indicated by the intensity of the green color.

13.3 Effect of Bar1 localization and regulation

We further demonstrate that the observed response attenuation requires neither the known pheromone-dependent regulation of Bar1 expression [70] nor its cell wall associated activity [75] (Fig. 29). In agreement with previous reports [39], we observed that a Bar1-mCherry fusion protein is induced at much higher pheromone concentrations than the P_{FUS1}-GFP reporter (Fig. 29 A), suggesting that production of Bar1 remains roughly constant in the studied range of the mating response. Consistently, a strain that constitutively expresses Bar1 under the promoter of the *TEF1* gene (translational elongation factor EF-1 α), which yields strong Bar1 expression, shows sensing of the $MAT\alpha$ cell fraction that is very similar to that of the wild-type strain (Fig. 29 B). Also the cell-wall associated fraction of Bar1 [75] appears to play no significant role in the response attenuation, because mixed populations of the wild-type and *bar1*Δ $MAT\boldsymbol{a}$ cells that share a common pool of diffusive Bar1 show identical responses to purified α-factor (Fig. 29 C).

13.4 The attenuation model

Figure 30 shows data replotted from Fig. 27 as a function of additional population parameters and the fits to the attenuation model we will see in this section (Sec. 13.4). $MAT\boldsymbol{a}$ cells clearly respond to the increase in the $MAT\alpha$ cell density (ρ_α), but this response is attenuated dependent on the density of $MAT\boldsymbol{a}$ cells (ρ_a) (Fig. 30 A), because the pheromone signal emitted by $MAT\alpha$ cells becomes balanced by the Bar1-dependent pheromone degradation. Consequently, the response to ρ_α also depends on other population parameters such as the total cell density ($\rho_T = \rho_a + \rho_\alpha$) as mentioned before (Fig. 30 B) and the ratio of $MAT\alpha$ to $MAT\boldsymbol{a}$ cells (r) (Fig. 30 C). For the same reason, the response to ρ_T at fixed r is strongly attenuated at higher densities

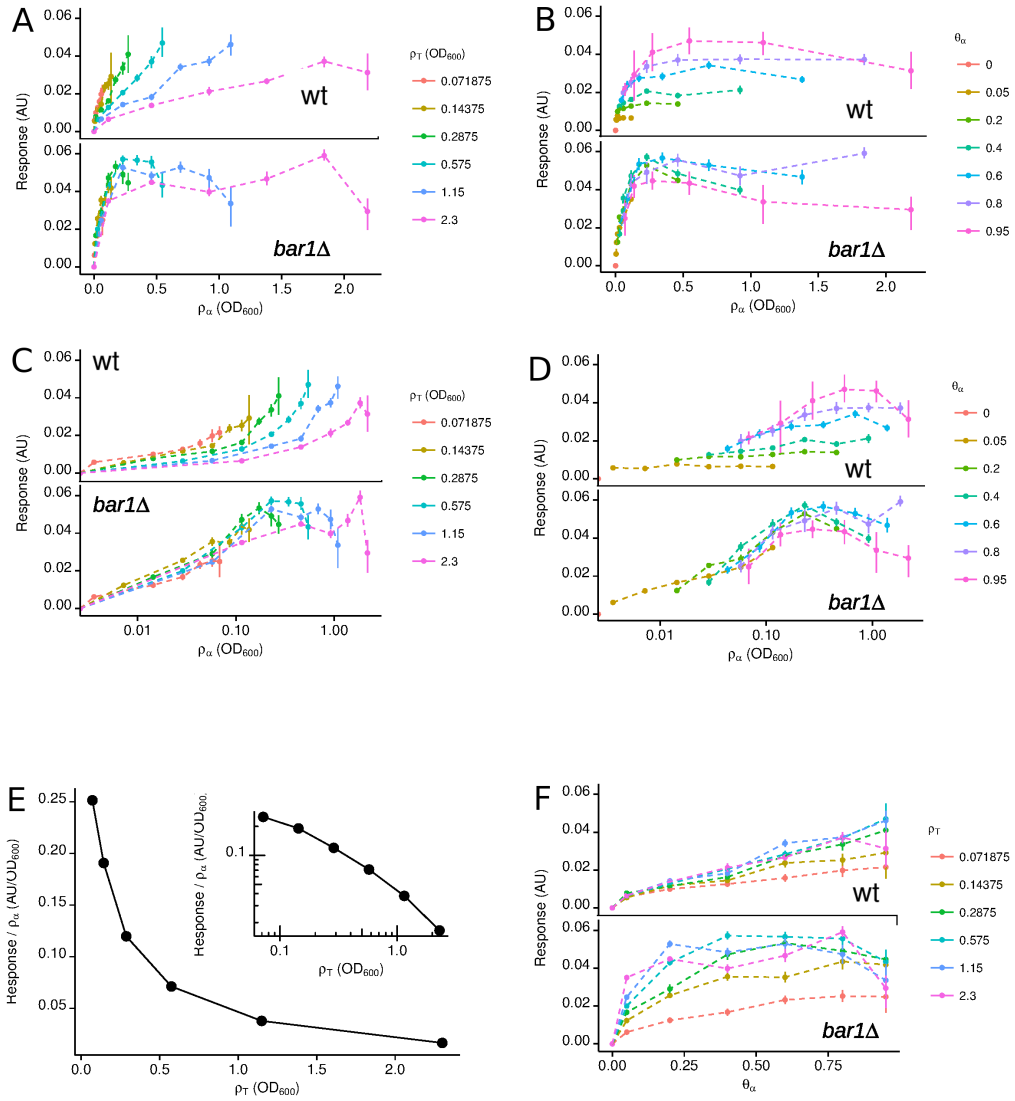

Figure 27: Pathway sensitivity to mate abundance. A-D. *MAT**a*** P_{FUS1} wt (upper plot) and *bar1*Δ (lower plot) response to *MAT*α density (ρ_α) in either linear (A,B) or log (C,D) scale when the total population density (ρ_T) (A,C) or the fraction of *MAT*α (θ_α) (B,D) is kept constant. E. Response sensitivity to partners at different total densities, taken fro linear regressions performed over the traces in panel A. Also shown in log-log scale (inset). F. Response to θ_α at different total densities in the wt (upper panel) and the *bar1*Δ (lower panel) strains. The error bars are the SEM of single cells in the population.

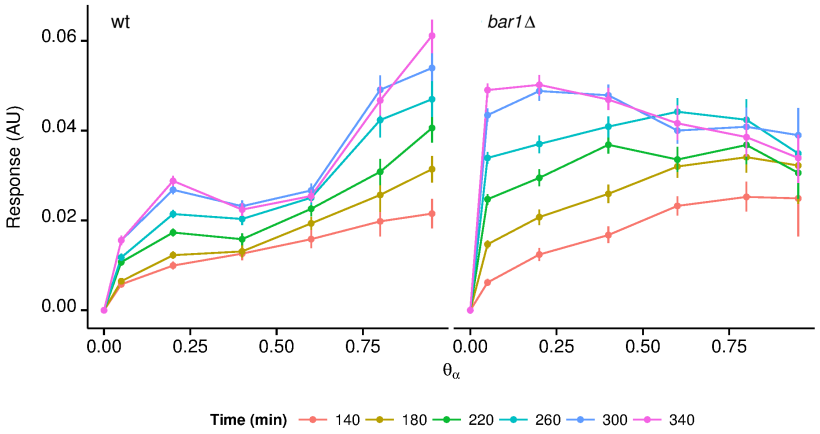

Figure 28: Time-persistence of the sex-ratio response. Response to θ_α in the wt (left panel) and the *bar1*Δ at ρ_T=0.07 (OD_{600}) at different time points after mixing. The error bars are the SEM of single cells in the population.

and flattens below saturation (Fig. 30 D). In the absence of pheromone degradation, the response of the *bar1*Δ strain simply follows the absolute density of the emitter cells, ρ_α, independently of ρ_a, ρ_T or r, and becomes fully saturated already at low densities of $MAT\alpha$ cells (Fig. 30 F-H) as well as at low total density (Fig. 30 I). Consistent with that, while the wild-type response remained below the shmooing threshold in a wide range of parameters, *bar1*Δ showed saturated response and shmooing over most of the parameter range (Fig. 26). Conversely, when the response is plotted as a function of the $MAT\alpha$ cell fraction in the population, θ_α, wild-type responses at different higher densities nearly perfectly align to the same linear relation (Fig. 30 E), whereas response of *bar1*Δ to θ_α is strongly density-dependent (Fig. 30 J). Taken together, these results demonstrate that at low density of the population, induction of the mating genes in $MAT\boldsymbol{a}$ cells depend on both the density and the ratio of the mating types, with the sex ratio sensing becoming dominant at higher densities. In contrast, *bar1*Δ simply senses the absolute density of the emitter cells, meaning that perception of θ_α and ρ_α as separate cues relies on input attenuation. To verify the proposed mechanism, we used a minimal ordinary differential equation (ODE) model (Done by Mihaly Koltai) to simulate the dynamics of pheromone accumulation and the resulting mating pathway response in a mixed population of $MAT\boldsymbol{a}$ and $MAT\alpha$ cells. The model takes into account the number of pheromone sources (i.e., ρ_α), the number of Bar1 sources (i.e., ρ_a), the rates of α-factor and Bar1 production, and Bar1 activity. It further assumes that Bar1 operates far from saturation, since the reported K_M value of Bar1 (30 μM) [77] is much higher than the levels of α-factor in the sensitive range of the mating pathway response (Fig. 11, Section 12). The analytical solution of the model shows that α-factor concentration rises peaks and decays. The maximal levels of α-factor reached in the population in presence of Bar1 are defined, up to a constant, as $\rho_\alpha/\sqrt{\rho_a}$. Thus, the level of the signal that is emitted by

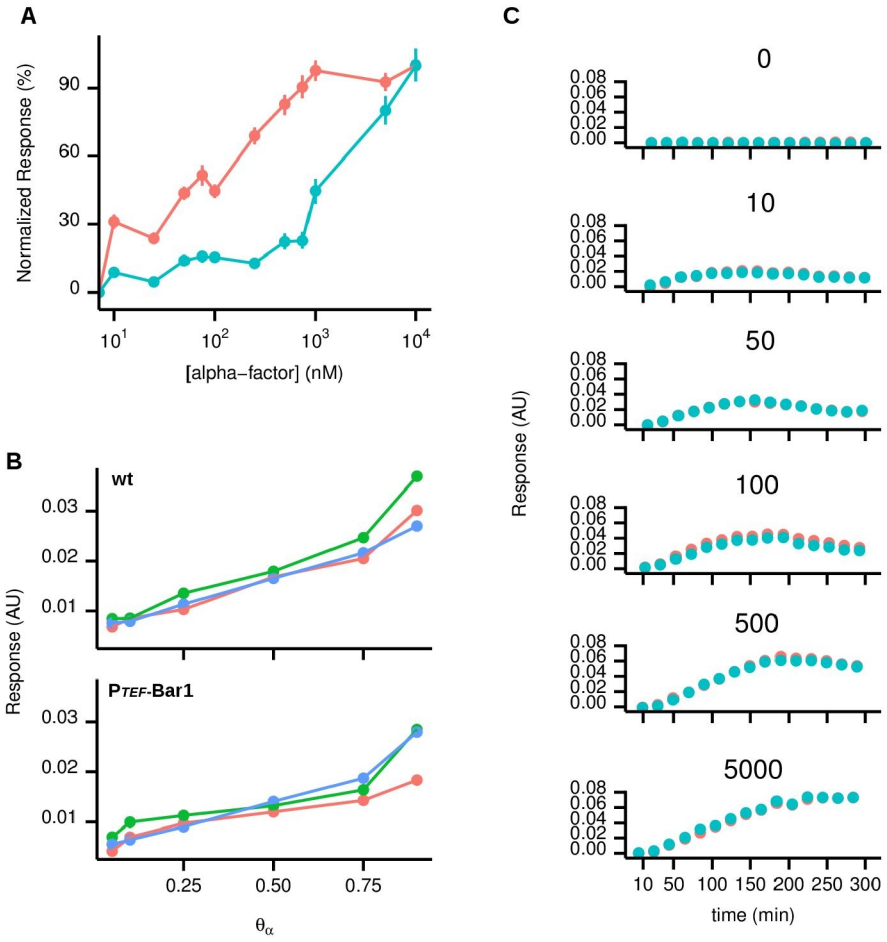

Figure 29: Transcriptional regulation and putative cell-wall associated fraction of Bar1 do not affect pathway response. **A.** Bar1 expression is less sensitive to α-factor than P_{FUS1}-GFP expression. A strain carrying both the P_{FUS1}-GFP pheromone reporter (red) and an mCherry-tagged functional version of Bar1 (blue) was exposed to different α-factor concentrations and fluorescence was plotted normalized to maximal response for each fluorophore. **B.** Bar1 induction by α-factor is not important in determining the sex ratio response and the insensitivity to density. The *BAR1* promoter was replaced with a strong constitutive yeast promoter (P_{TEF}) and the response to density and ratio in the mixed population of $MAT\alpha$ and $MAT\boldsymbol{a}$ cells was measured and compared with the wild type at different starting ρ_T values (OD_{600}) of 0.18 (red), 0.54 (green) and 4.9 (blue). **C.** The effect of cell-wall associated Bar1. Plots show the P_{FUS1}-GFP response kinetics in wild-type (blue) and *bar1*Δ (red) $MAT\boldsymbol{a}$ cells mixed in equal proportion and exposed to different α-factor concentrations (indicated above each plot, in nM). The global extracellular pool of Bar1 is shared by both cell populations, however the cell-wall associated activity is exclusive to the wild-type. Data were acquired using microscopy. Error bars indicate the standard errors of responses of individual cells in the experiment.

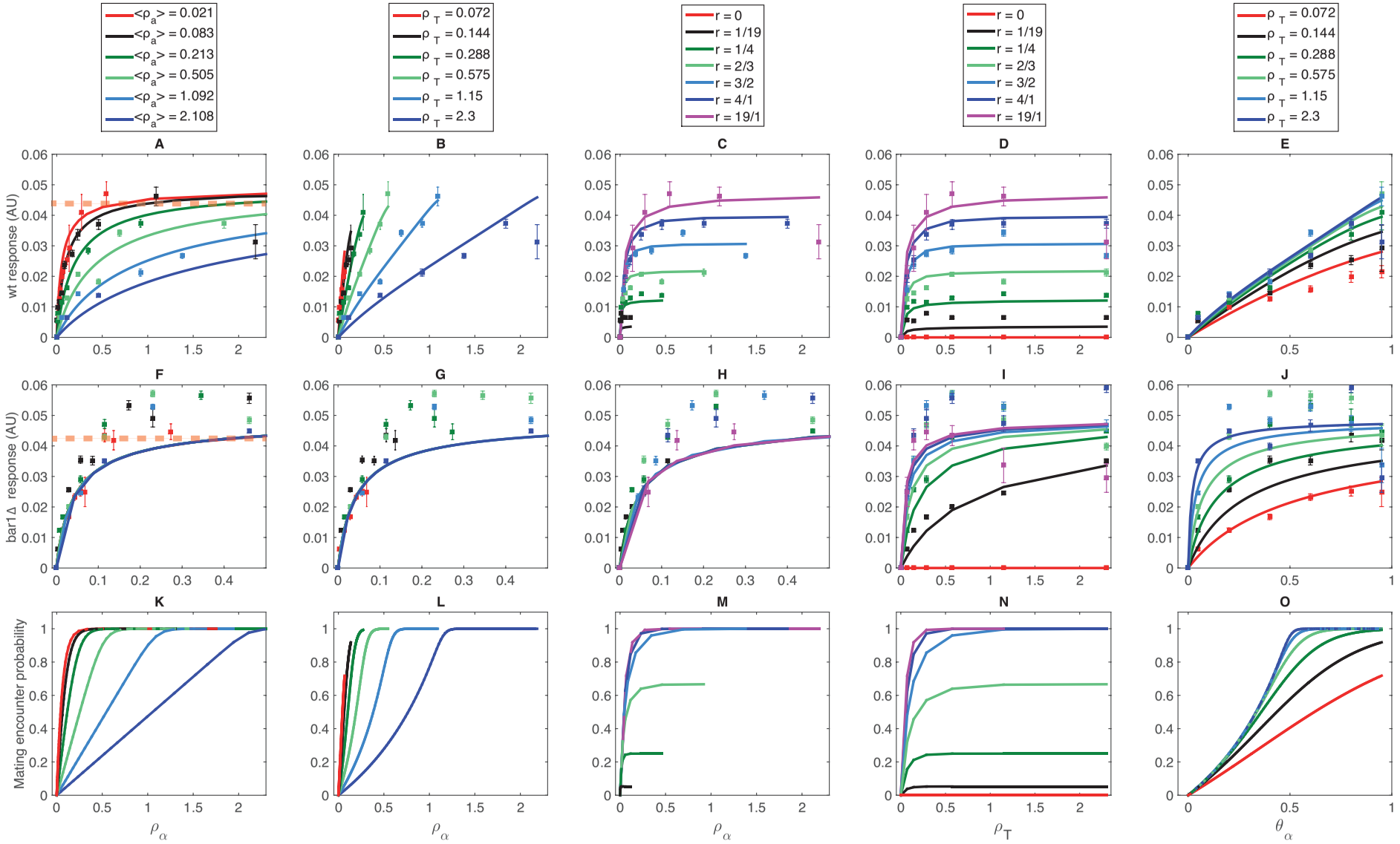

Figure 30: Dependence of mating pathway response and mating encounter probability on population parameters. A-E. Activity of the P_{FUS1}-GFP reporter in wild-type *MAT* **a** cells as a function of ρ_α (A-C), ρ_T (D) or θ_α(E) and at fixed values of other parameters (indicated by colors) in a mixed population of *MAT*α and *MAT* **a** cells. Reporter activity was measured using microscopy at 140 min after mixing. Error bars indicate standard errors of the responses of individual cells in the experiment. Dashed lines mark the characteristic mean response value at which cells shmoo, as determined by image examination. Solid lines show fits to the data using a computational model of the mating pathway response (see Supplementary Text). F-J. Corresponding response of the *bar1*Δ strain. Note the difference of the x-axis scale between (F-H) and (A-C). K-O. Simulated probability of mating encounters at varying parameter values, shown for one time point. Data is the same as in Figure 27.

MATα cells is attenuated by Bar1 dependent on the square root of the *MAT**a*** cell density. This behavior is well consistent with experimental data, taking into consideration the dependence of the P_{FUS1}-GFP activity on the α-factor concentration (Fig. 11). For example, in absence of Bar1-dependent attenuation, the level of α-factor no longer depends on ρ_a and simply increases proportionally to ρ_α (Fig. 30A, F). This solution can be reformulated as $\sqrt{r\rho_\alpha}$ or$\sqrt{\rho_T}r/\sqrt{1+r}$, explaining the sub-sensitive behavior of the response with regard to ρ_α or ρ_T at fixed r, as well as the dependence of the plateau on r (Fig. 30C,D). Alternatively, the wild-type level of α-factor can also be expressed as a function of ρ_T and θ_α as $\sqrt{\rho_T}\theta_\alpha/\sqrt{1-\theta_\alpha}$, in agreement with the nearly linear dependence of the response on θ_α (Fig. 30E). We further used the model to fit the experimental data, using the measured dose-dependence of the reporter response (Fig. 11) to convert the levels of α-factor into the activity of P_{FUS1}-GFP. The model can indeed fit well both the wild-type and *bar1*Δ response data using either the analytical solution for GFP levels (Mihaly Koltai) or the numerical solution that treats GFP as a time-dependent dynamic variable (Fig. 30A-J). We have further considered mutual induction of the pheromone production [1, 94] in our model, but this did not substantially improve the quality of the fits (not shown, Mihaly Koltai) and was neglected for simplicity. The observed dependence of mating gene expression on the relative and absolute densities of the mating partners may have a straightforward physiological meaning. Assuming that for a suspension of yeast cells formation of mating pairs is primarily determined by probability of cell encounters, both the sex ratio and population density provide useful cues for the likelihood of successful mating. At low population densities, the probability for a *MAT**a*** cell to collide with a *MATα* cell and to form a mating pair is expected to increase with the population density and with the fraction of the *MATα* cells. However, the dependence on density should saturate at higher densities when all cells are likely to collide at least once with a mating partner over a given period of time. The likelihood of mating success at high population densities should thus be solely determined by the sex ratio of the population, in a perfect agreement with the observed dependence of the mating response on these population parameters (Fig. 30D,E). A simulation of mating encounters, performed using a model of an irreversible two-species chemical reaction (Mihaly Koltai), shows a striking similarity to the experimentally observed dependence of the mating pathway response on the density and ratio of the partners (Fig. 30K-O). This similarity suggests that the yeast mating system exhibits simple predictive behavior, utilizing the available population cues to estimate the probability of successful mating and to adjust the investment of mating resources accordingly.

13.5 Growth-expression trade-off

Pathway induction may further carry a cost of resource investment [63] and reduced haploid growth due to pheromone-induced cell-cycle arrest on the G_1 stage of the cell-cycle at levels be-

low shmooing induction. On the other hand, cell-cycle arrest is absolutely essential for mating. We observed that the time it takes for the wt population to re-start budding after pheromone exposure is clearly proportional to the dose of α-factor with the time of recovery being heterogeneous in the population (Fig. 15), this arresting dynamics causes the fraction of unbudded cells to decrease proportionally to α-factor when phenotypes are scored after they develop for a fixed amount of time (Fig. 16, [106]). Then, the population growth rate appears inversely proportional to the α-factor concentration (Fig. 12). Cell cycle arrest is a necessary but "risky" behavior, because if mating is not successful haploid lineages that invest their resources (activate the pathway and arrest in G_1) would decrease their overall fitness, i.e. no haploid nor mating-derived diploid growth is achieved. Considering then that arresting time is proportional to pathway expression, we hypothesized that a relation exists between the pathway induction level (arrest-strength) and the likelihood of finding a partner. In other words, cells only "sacrifice" their haploid growth when the chances to mate are high. Likewise, if the chances are low, only a transient and more discrete degree of arrest would be experienced by the population, which would reduce the risk of reduced haploid growth. We indeed observed a reduction of growth for cells stimulated with purified α-factor or grown in a mixed culture, with a clear correlation between the degree of arrest and the strength of the mating pathway response (Fig. 31). This shows the existence of a trade-off between gene-expression induction and haploid growth. The investment of resources in sexual reproduction is therefore costly, it harbors the risk of decreased overall reproductive success if mating is not achieved. The observation confirms that the response bears the cost of reduced haploid fitness at all levels, and needs to be tightly controlled.

13.6 *MAT*α mating behavior

13.6.1 *MAT*α cells show sex-ratio sensing

Motivated by the mate-sensing model described for the *MAT***a** mating-type, we asked weather the *MAT*α mating-type could behave similarly. Indeed we observed that the main features of mate sensing are present in this mating-type (Fig. 32). Although the *MAT*α response seems to differ in terms of the sensitivity to mates, the main feature is indeed present, i.e. there is a range of ρ_T values at which the response does not increase further, with this stable magnitude being proportional to θ_α. Furthermore, when co-incubated with wt or *bar1*Δ *MAT***a** cells, the *MAT*α population has similar responses, indicating that the positive feedback loop for pheromone production which we neglected in the model, indeed does not play a role in the *MAT*α sex-ratio response. Even though an a-factor degrading activity was reported for a gene called *AFB1* [44], we measured no increased sensitivity to a-factor when comparing *MAT*α wt and *afb1*Δ strains (Fig. 33 A). Moreover, we could not detect a pheromone-degrading activity

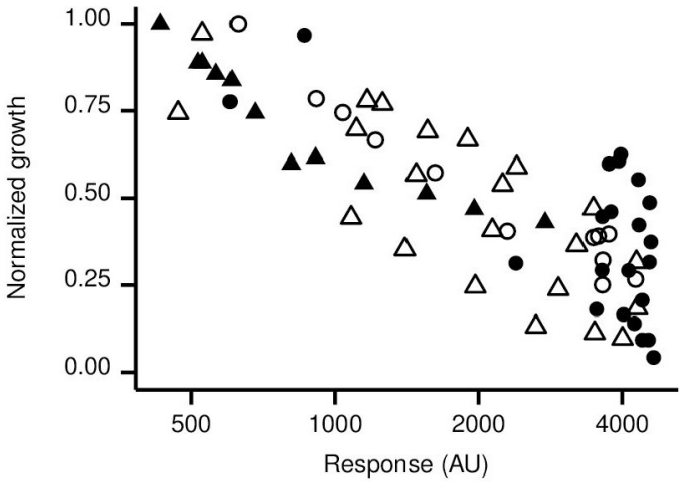

Figure 31: Growth-gene expression trade-off. Population growth for the wild-type (triangles) and *bar1*Δ (circles) as a function of the P_{FUS1}-GFP reporter activity, measured as in Fig. 25. Data are from experiments using stimulation with varying concentrations of purified α-factor (open symbols) or from mixed-population experiments with varying density and ratio of the mating types (closed symbols). For each sample, the $MAT\boldsymbol{a}$ cell density was determined by measuring cell count in flow cytometry and the change in ρ_a from stimulation/mixing time to sampling time was normalized to the corresponding density change of the unstimulated/pure $MAT\boldsymbol{a}$ populations at equivalent starting ρ_a values.

similar to that of Bar1 in $MAT\alpha$ (Fig. 33 B), suggesting the absence of an a-factor protease activity in supernatants or cell-surface from $MAT\alpha$ cells. Density of cells during the incubation performed to detect an a-factor degrading activity seems to relate directly with the a-factor availability after cell removal (See legend of Fig. 33 B), this effect could be explained by a lower adsorption to surfaces of the a-factor when more cells are present or less-likely a density-dependent downregulation of the response which is independent of the cell-type. On the other hand, we also observed that the dose-response of MATα to a-factor tends to attenuate in time (Fig. 34) in a similar way to the wt $MAT\boldsymbol{a}$ (Fig. 11). We also though that the concentration of a-factor could be considerably overestimated (due to ligand adsorption during preparation). For this reason we show that $MAT\alpha$ cells show similar sensitivity to purified pheromone as $MAT\boldsymbol{a}$ does even if the condition for ligand adsorption to surfaces is changed, suggesting that the calculated concentration of a-factor is in the correct range. If overestimated, ligand adsorption would be more likely to shift the dose response to the right, as seen with α-factor in the $MAT\mathbf{a}$ *bar1*Δ strain (Fig. 35). In summary, we cannot rule out completely the existence of a a-factor degrading activity, although internal adaptation mechanisms in $MAT\alpha$ could also explain the observed downregulation. In general the $MAT\alpha$ response to pheromones is similar to its $MAT\mathbf{a}$ counterpart. Sex-ratio sensing in $MAT\alpha$ behaves similarly to the $MAT\boldsymbol{a}$ system, but has to work with a much weaker (if any) Bar1-like activity. Then, an a-factor protease might have a secondary role and a different mechanism could be involved.

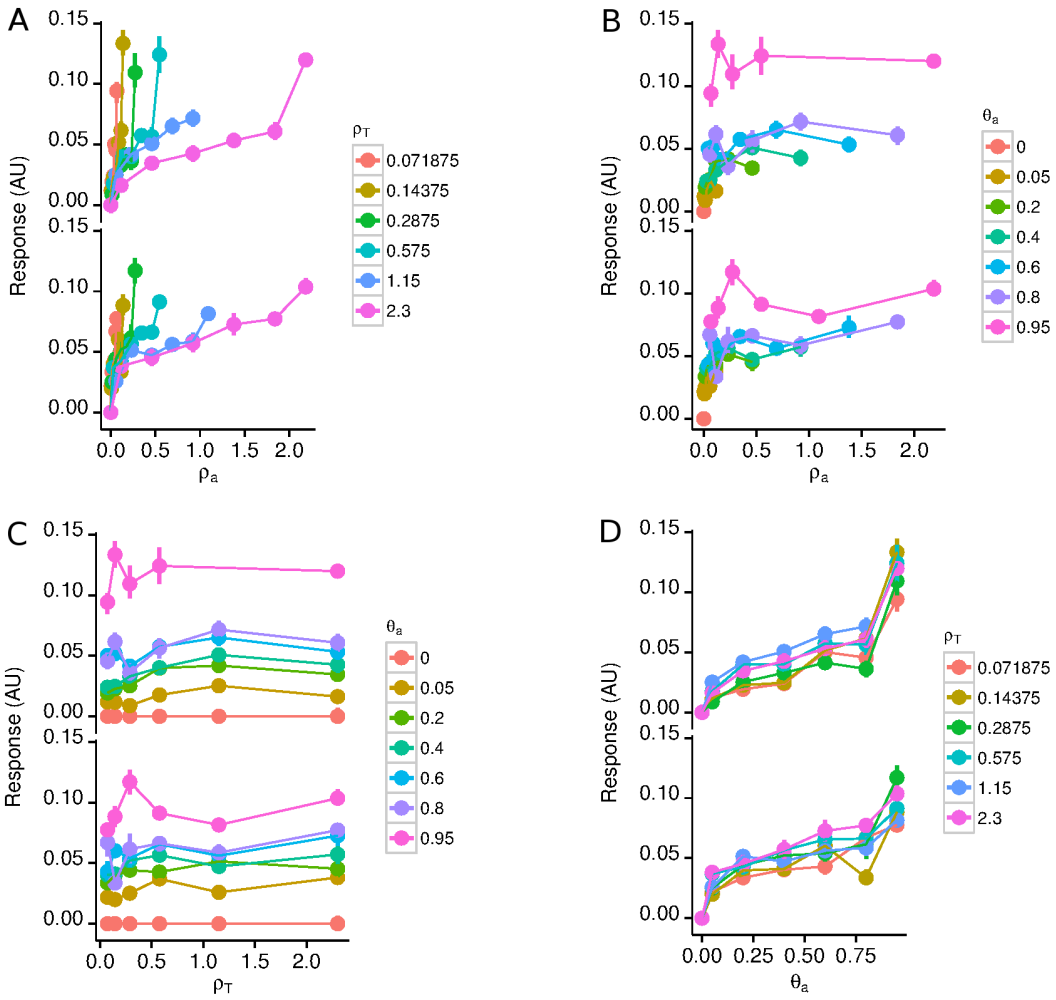

Figure 32: Mate number sensing in $MAT\alpha$ cells. A-B. $MAT\alpha$ response to wt or *bar1*Δ $MAT\boldsymbol{a}$ cells at different total densities (ρ_T) (A) and a:α sex-ratios (θ_a) (B). C. Response to total densities (ρ_T) at different sex ratios (θ_a) (C). D. Sex-ratio sensing. Data comes from the same experiment as in Fig. 27, but the response measures the intensity of P_{FUS1}-mCherry (see Experimental Methods) in $MAT\alpha$ cells

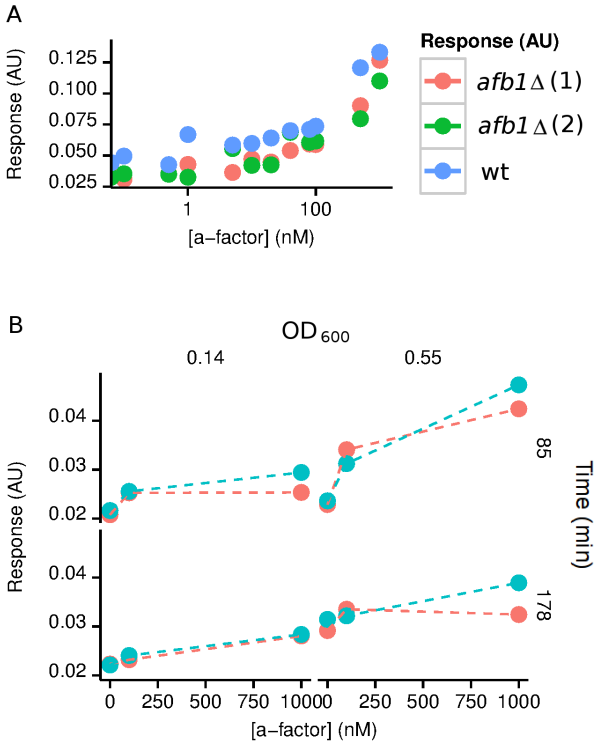

Figure 33: Absence of a-factor degrading activity in $MAT\alpha$ cells. A. Afb1 is not an effective a-factor degrading enzyme. P_{FUS1}-mCherry dose-responses to purified a-factor in wt and *afb1*Δ strains (two different clones). B. Different concentrations of a-factor were incubated with cells carrying a putative a-factor degrading activity (wt $MAT\alpha$ cells, blue) or not ($mat\alpha1\Delta mat\alpha2\Delta$ MAT$\boldsymbol{a}$ cells) set at different densities (columns) and incubated for different times (rows). After cell-filtration, the cell-free media was used to stimulate a $MAT\alpha$ P_{FUS1}-mCherry reporter strain.

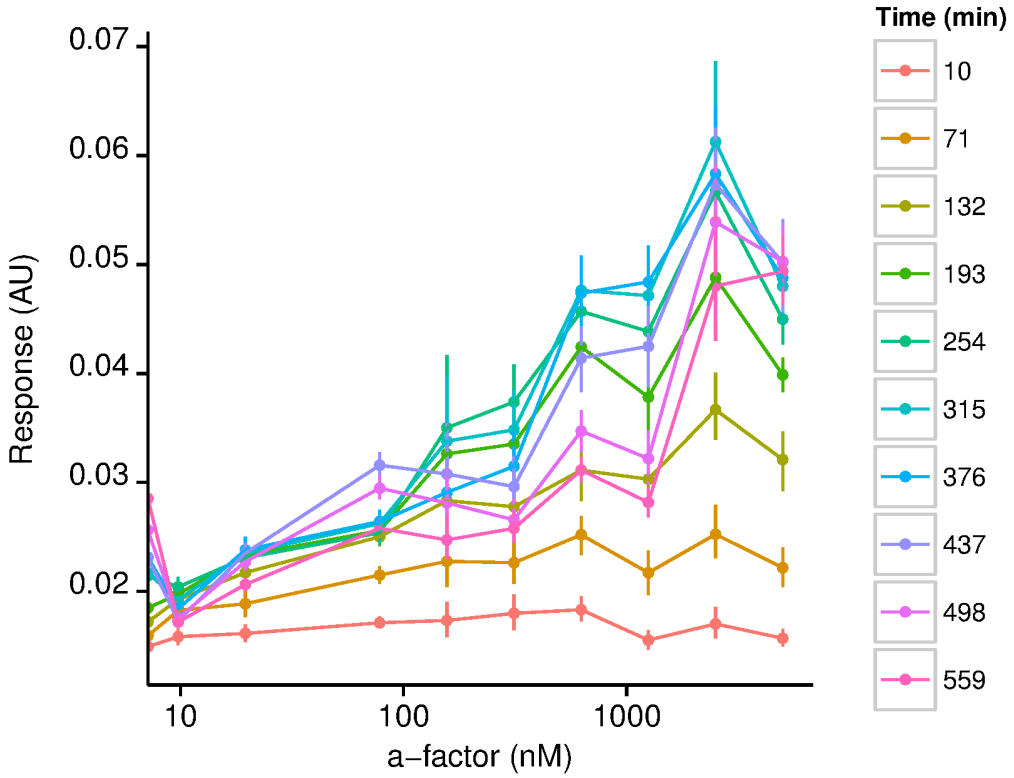

Figure 34: $MAT\alpha$ response to a-factor is downregulated at late times overtime. P_{FUS1}-GFP mean response of a $MAT\alpha$ population to purified a-factor doses at different times (colors) after induction.

14 Mating by chance encounters

Yeast outcrossing is promoted by natural spore dispersal [20] or by germination delays induced by poor fitness in novel environments [72]. In liquid, random sexual pairing of dispersed germinating spores is expected. On the one hand, the length scale at which positional information is useful is reduced by diffusion-mediated gradient homogenization. On the other, the length and time scales of positional change set by fluid displacement processes (e.g. rain, convection) are respectively larger and shorter than those of chemotropism. The existence of the sexual-agglutination system [64] shows a clear adaptation to such conditions. It becomes important as moisture increases in solid-media [95] and critical in liquid media [67, 65]. Together, these facts suggest that under certain conditions, a probabilistic scenario for mating can be expected.

For an effective likelihood-proportional gene-expression response, the likelihood of a $MAT\boldsymbol{a}$ cell forming a mating pair in a random encounter scenario should depend on population parameters in the same way they determine gene expression. Using our assay with normally agglutinating cells (a mating reaction), we demonstrate that the steady state pairing probability for $MAT\boldsymbol{a}$ ($\rho_{\mathrm{MP}}/\rho_a$, see Experimental Methods) matches the value of θ_α (Fig. 36A). This is a non-trivial steady state, because perfectly efficient pair formation should drain completely the minor haploid population at $\theta_\alpha \neq 0.5$ and the whole population at $\theta_\alpha = 0.5$, arguing against

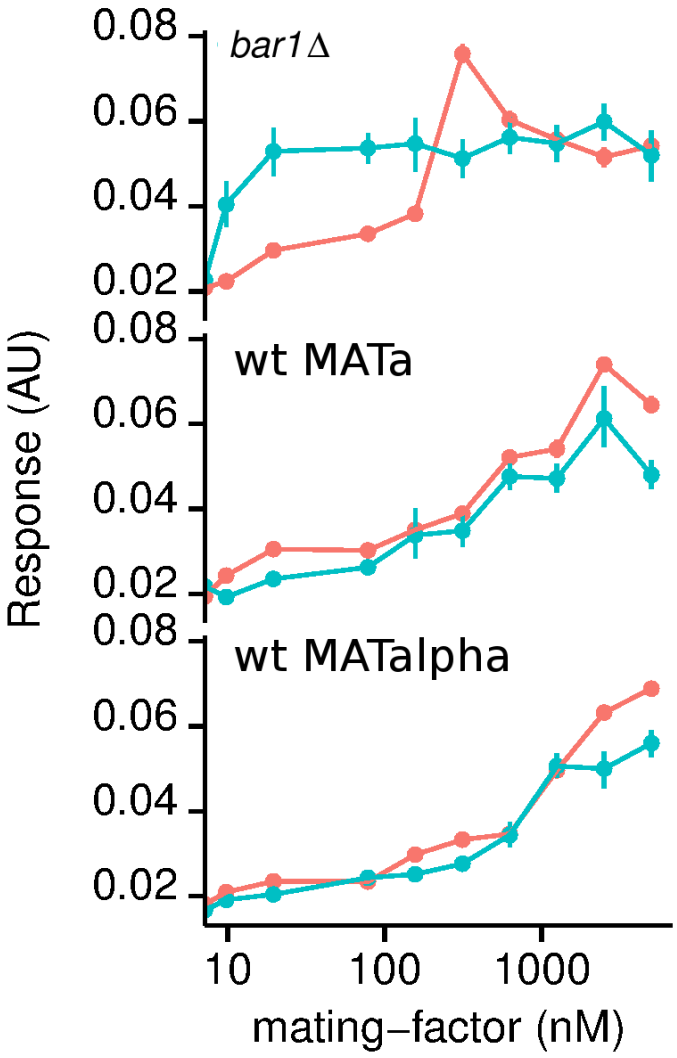

Figure 35: $MAT\alpha$ shows wt sensitivity to mating factor. $MAT\boldsymbol{a}$ ($bar1\Delta$ and wt) and $MAT\alpha$ populations were stimulated with purified mating-factor doses under adsorptive (Concanavalin A 0.06%, Casein 1μM, red) and non-adsorptive (blue) conditions.

complete irreversibility in the process. A similar trend is observed with the fraction of fused cells (Fig 36B, see Experimental methods), suggesting that the likelihood of a fusion event directly depends on mating pair formation. At low ρ_T, Bar1 plays no role in determining the steady state value of the mating probability (Fig 36A, C), however the *bar1*Δ strain does show faster agglutination (Fig 36C, D), as expected from induced agglutinin expression. The invariance in the steady state pairing probability between wt and *bar1*Δ argues against reversibility as the only cause of its tight θ_α dependency, since α-factor induction is at the same time saturated in the knockout (Fig. 36E) and stronger binding affinity should therefore set a higher steady state. This suggests that the enhanced expression of agglutinins does not determine the steady state probability. As density increases, probability keeps nearly the same steady state value across an 8-fold change in density (Fig. 36C and D), in sharp contrast to its linear dependency on sex-ratio (Fig. 36A) and in accordance with the gene expression pattern (Fig 27 E and Fig. 36E). However, probability also shows a small but significant density dependent reduction despite of the expected initial faster pairing at high ρ_T (36C). This reduction might be related to the response down-regulation at high densities (Fig. 25 B). The wt shows less sensitivity to this effect (Fig 36C,D), suggesting that α-factor excess might cause the detriment, with Bar1 as a useful attenuator. Since the *bar1*Δ strain has reduced but comparable pairing and mating likelihood as the wt, we hypothesized that matching gene expression to θ_α might also confer a control mechanism to avoid other phenotypes associated with overstimulation. Since a general trade-off between haploid growth and α-factor induced gene expression exists (Fig. 31), we analyzed how severe is the effect at moderate pairing likelihood (θ_α=0.25) by performing mixing experiments with the non-agglutinating control *MAT****a*** strain. As expected, we found that growth is impaired when mating partners are present (Fig. 36F), with a more severe effect in the *bar1*Δ strain. There, lack of growth reveals a reduction in the initial population density, which is compensated by normal growth in the wt. The reduction is due to a general loss in the population count, a phenomenon probably related to pheromone-induced cell wall degradation and death [112]. In summary, we demonstrated that disentanglement of absolute and relative mate abundance as separate sensory cues allows yeast to robustly sense the sex ratio of the population and to induce mating genes accordingly. The mechanism relies on the diffusible peptidase Bar1 that attenuates the mating signal dependent on the density of receiver cells. The observed response pattern mirrors the measured dependence of the mating encounter probability on both population parameters, suggesting that yeast cells predictively adjust investment of resources into mating by (active) measurement of the mating likelihood.

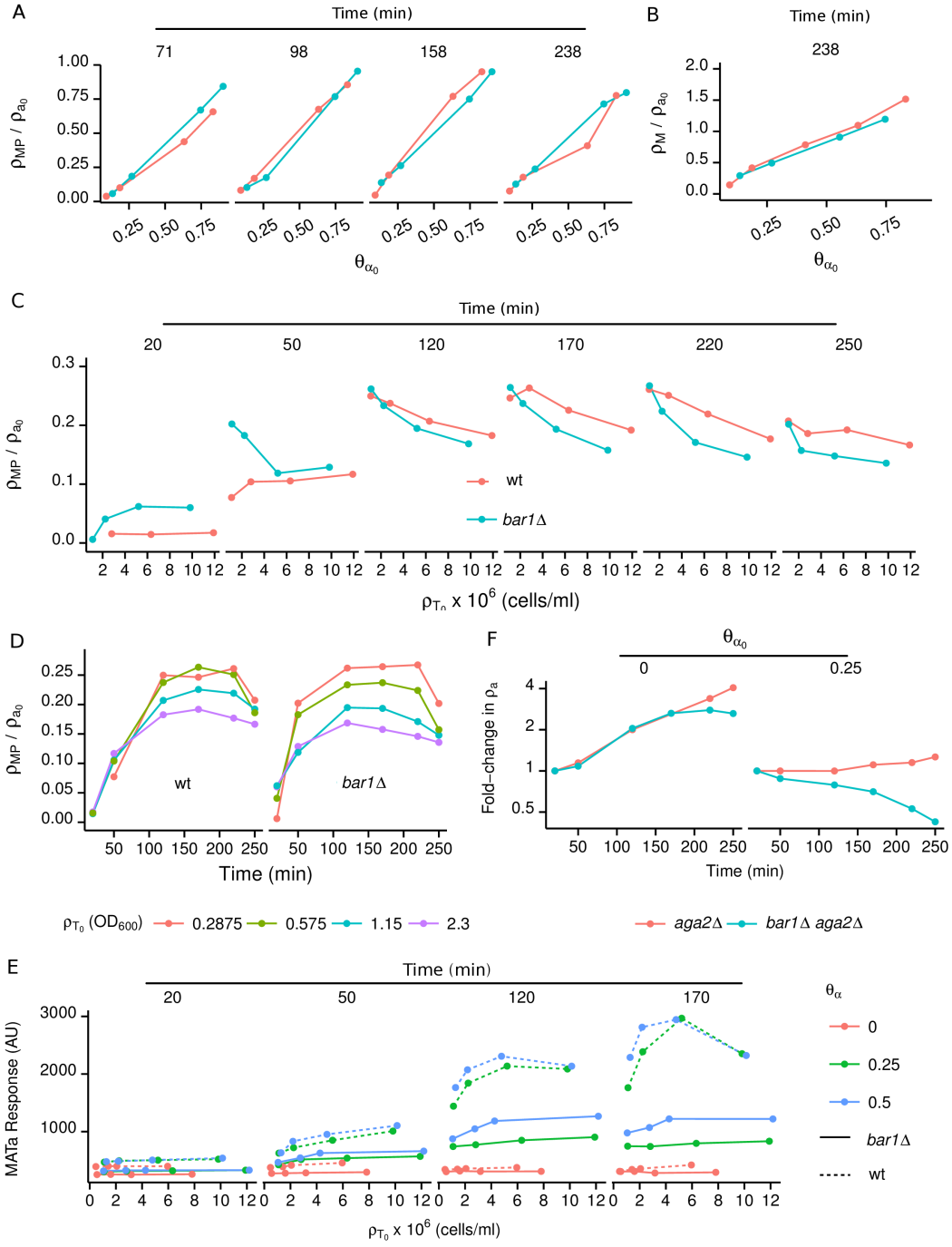

Figure 36: Mating likelihood and growth in liquid mating reactions. A, B. Paired fraction (A) and mated fraction (B) of the initial $MAT\boldsymbol{a}$ population as a function of the initial θ_α (θ_{α_0}) at a fixed low ρ_T of OD_{600}=0.34. C, D. Paired fraction of the initial $MAT\boldsymbol{a}$ population as a function of the initial population density (ρ_{T_0}) at different times (C) or as a function of time at different ρ_{T_0} values (D) at a fixed θ_{α_0}=0.25. E. Gene expression data for the wt (solid lines) and *bar1*Δ (dashed lines) as a function of ρ_{T_0}. F. Effect of mating partners ($\theta_{\alpha 0}$=0.25) on $MAT\boldsymbol{a}$ growth under non-agglutinating conditions.

Part IV

Discussion

The two main results from this work are: The first one is that the input magnitude generated by the number of potential mates is sensed as a constant fraction of the number of competitors and that sensitivity to potential mates is a decreasing non-linear function of competitors. The described system requires absolute pheromone concentration sensing in each cell and an extracellular sensory adaptation mechanism, i.e. input-attenuation. As a consequence different sensitivities to the population sex ratio and the absolute number of potential mates are achieved. The second main result is that indeed the sensory response and the sexual-pairing probability have similar dependencies on sex ratio and density. In a mating reaction, the probability to find a $MAT\boldsymbol{a}$ cell forming part of a sexual pair depends linearly on the sex ratio (θ). The slope of the described function is nearly $\sim$1, suggesting that the dynamic range of gene expression as a function of sex ratio is fine tuned for a form of likelihood-sensing. We discuss first the more unrelated FRET results and then the rest of the results.

15 Bleach-FRET interaction map

The main idea of the FRET interaction map we constructed was to find a suitable pathway expression reporter that could measure fast changes in physical proximity. Even though many protein pairs tested interacted with each other, when we tried to stimulate the pathway with α-factor the interactions, a general absence of stimulus dependency was found. Or when found it could not be reproduced observing oven opposite stimulus dependence. One explanation is that our levels of protein expression are too high, creating artefactual interactions. However, the existence of a variety of FRET efficiencies, including no interaction at all (0% FRET efficiency), argues against this possibility. Given the central role of Fus3 in transduction, we can take it as a problem in case. Among the tested interactions, Fus3 is known to interact with Far1 and Sst2 upon pheromone stimulation. We did not observe FRET for the Fus3-Far1 pair and only a weak interaction for the Fus3-Sst2 pair, and no stimulus dependency. Speculating, it would simply be needed for the bound states of Fus3 and its partners to be in a steady state insensitive to pheromone activation in order to measure a constant FRET signal at the time scale of seconds under either stimulation condition. Indeed, Drogen et al. [100] showed through FRAP experiments that rapid nucleo-cytoplasmic shuttling of Fus3 occurs independently of pheromone, Fus3 phosphorylation and presence of Ste5. No clear stimulus-dependency in FRET efficiency in our pairs that included Fus3 could be simply due to the fact that physical proximity for

these pairs is indeed invariant to stimulation changes. Knowing that some binding partners of Fus3 locate in the nucleus (Dig2 for example), and further assuming that protein numbers are constant, transduction in the MPP could be simply seen as a constant flow of Fus3 in and out of the nucleus interacting at steady state with Dig2 or others. Stimulation only changes the situation in that Fus3 molecules are phosphorylated. Our screen is indeed not exhaustive, both in terms of the number of interactions screened and in terms of optimization of conditions for precise measurement. Stimulus dependent-interactions could be widespread. In the literature, there is one FRET pair that seems to work [106]. It is a reporter of the interaction of the G-protein α-subunit with the $\beta\gamma$ complex. and a valuable tool. Nevertheless, it is surprising that more FRET pairs have not been discovered yet for this pathway.

16 Phenotype development

Our dose-response measurements at the single cell level suggest that initial (minutes after stimulation) gene-expression rate increases gradually with pheromone concentration. This rate is a measure of pathway activation, its dynamic range is between 3 to 4 orders of magnitude and apart from the natural EC_{50} shift expected from degradation of a constant fraction of the initial α-factor dose, it is equivalent in the wt and *bar1*Δ strains. However, at the mating-relevant sensory region of the dose-response, deceleration of the GFP accumulation rate within the first 200 minutes of stimulation depends entirely on Bar1. By noting the phenotypes the two strains generate, we suggest that shmooing development obeys a threshold set by the initial response rate. The threshold is the maximum response rate, corresponding to receptor saturation. On the other hand, elongation requires a sub-threshold activation rate but also longer sustained activation. If attenuated, the elongation phenotype does not develop and simply returns to growth, explaining the difference in phenotypic transitions for the wt and *bar1*Δ strains. Considering also the direct relation between arresting time and pheromone concentration it can be argued that the more time the cells stay arrested, the further development of cellular enlargement. To put our results in context, we next analyze our observations within the known transductional mechanisms for shmooing and transcription.

Malleshaiah et al. [69] describe the operation of an ultrasensitive dose-responsive molecular switch for the Ste5-Fus3 interaction. They used wt strains (harboring the *BAR1* gene) under equivalent experimental conditions as our stimulation experiments, i.e cells at a low optical density (OD_{600}=0.05) stimulated in glass-bottom 96-microwell plates coated with the lectin Concanavalin A for cell adhesion (which we know avoids ligand adsorption), to show that the molecular mechanism underlying the "shmooing switch" is the α-factor dependent ultrasensitive dissociation of the MAPK Fus3 form the Ste5 scaffold. We first confirmed ultrasensitivity in

the shmooing response in the wt strain under conditions replicating Malleshaiah et al. (Fig. 11 and Fig. 16). We must note that under these experimental conditions, Bar1 causes an underestimation of pathway dose-sensitivities (Fig. 11), making the reported values for the transition in Malleshaiah et al. overestimated. Second, we note that the reported value for pheromone-dependent Ste5-Fus3 dissociation EC_{50} in Malleshaiah et al. is 150 nM. This value differs significantly from the EC_{50} value observed for the shmooing frequency switch in the same work (200-300 nM). At 150 nM the phenotypic data in Malleshaiah et al. shows a clear coexistence of phenotypes, in the same way as our data for transitional phenotypes (Fig 16). Then, the Ste5-Fus3 dissociation switch might reflect the transition to a different state from shmooing. Three separate facts support this idea. First, in the data from Malleshaiah et al. the maximum frequency of volume increased cells attainable (the phenotype composition at exactly the concentration generating the dissociation switch) also appears to be switch-like (See very well-resolved dose region in Fig. 1B in reference [69]), as in our wt data (Fig 16). Second, the fold change in pheromone concentration to go from transitional phenotypes (coexistence of cells with bipolar budding, volume increased and mild elongation) to shmooing in our wt data ($\sim$2 fold) corresponds roughly to the fold-change misalignment of shmooing with Ste5-Fus3 dissociation in Malleshaiah et al. (Fig 16, Fig. 1B in reference [69]). Third, disruption of the Fus3-Ste5 binding causes not a loss of shmooing in single cells but instead a gradual increase in their frequency in the population and a general sensitization of mating phenotypes (Fig 1C in [69]). The authors suggest the possibility that lack of Fus3 sequestration can produce the activation of a downstream unknown switch which causes stochastic fate decision, reflected in the coexistence of multiple stable phenotypes. Importantly, disruption of the interaction does not linearize the switch-response in their measured parameter (levels of complexed Fus3·Ste5 at the cell population level) but rather eliminates it. This means that another pathway output has to be measured to confirm linearity. Indeed, the authors observed in immunoblots that double-phosphorylated Fus3 shows the linearization when the Fus3-Ste5 interaction is disrupted. This contrasts with the finding that Ste5 induces Fus3 activation in vitro [36], and also with the fact that the transcriptional response is fundamentally gradual [80, 79, 98] precisely due to Ste5 scaffolding and membrane tethering properties [80]. Moreover, gradual Fus3 activation dose-responses have also been measured for the native pathway with immunoblots [109]. Our data suggests that developmental transitions are switch-like and that it is receptor saturation what marks the transition to shmooing. It is reasonable to think that the Ste5-Fus3 dissociation switch might not necessarily occur at the shmooing transition. If aided by the Ste5-Fus3 dissociation switch, any dose-threshold for the appearance of a sub-saturating mating morphology, e.g. elongation, must also produce a change in the transcriptional output, otherwise a selective pool of released active Fus3 needs to be invoked. It seems plausible that the Ste5-Fus3 switch [69] is different from the shmooing switch

and rather works at the onset of saturation causing cell elongation, which we know from this study, is only downregulated by Bar1-dependent attenuation. In order for the elongation mating response to remain sensitive, i.e. to respond to further increases in pheromone concentrations, it has to occur below receptor saturation. In summary we suggest that shmooing development is fast and determined by a threshold activation level that corresponds to signalling saturation, on the other hand elongation requires long arrest and correlates with sustained activation. The Fus3-Ste5 dissociation could be involved not only in the shmooing-frequency switch but also in the appearance of transitional phenotypes.

17 A non-adaptive sensitivity-preserving sensory system

The full analysis of the mating pathway input-output relationship led us to the conclusion that, if any, adaptive mechanisms play a minor role in the sensitivity of pheromone sensing in the relevant input range, i. e. the one in which mating-phenotypes are expressed. We showed that the response amplitude remains mostly unchanged after prolonged exposure, even though the reporter is perfectly capable of responding to changes in the external concentrations of pheromone. Crucially, sensitivity to α-factor remains unchanged after pre-exposure to sub-saturating pheromone stimulations when attenuation is absent. The yeast's ability to respond in a non-adaptive manner to the current pheromone concentration makes the presence of the Bar1 protease determinant for response dynamics, only that "adaptation" can be said to be external to the cell, occurring at the input level (hence better defined as input attenuation). Total dependence on the Bar1 protease to achieve effective response down-regulation differs dramatically from the commonly observed internal adaptation mechanisms which seem to work well for specific pre-established environmental input distributions in other processes and organisms [91] and grounds the hypothesis that it is population parameters determining the response maximal amplitude and dynamics (See Sec. 13.1).

17.1 Fractional sensing in mate number perception

Next, we discuss parameter sensing in the context of cellular sensory system biophysics. First we note that Paliwal et al. [79] describe for the chemotropic response of yeast to gradients of α-factor in the form of $\frac{\gamma}{\bar{\alpha}} = C$ (in [79]) where γ is the spatial gradient, $\bar{\alpha}$ is the mean α-factor concentration and C is a constant corresponding to precision of alignment (a binary output in their measurements). This description is another example of the molecular version of Weber's law of sensory thresholds [30] (See Sec. 2.3). To our knowledge, the work by Paliwal et al. is the only account in *S. cerevisiae* where fractional sensing has been considered (but see also "dose-to-duration encoding" 2.1). We observed that at the single cell level, mating-relevant

transcriptional responses to pheromone are not adaptive, which results in absolute rather than fractional pheromone sensing, i.e. the background pheromone concentration does not alter the sensitivity to further pheromone concentration changes when measured within the sensitive range of the response. Fractional sensing in precision of protrusion alignment and absolute sensing in transcription are not mutually exclusive.

Input attenuation allows fractional sensing at the population level, i.e. the sensitivity to mate number depends on the density of competitors (same-sex cells) and single cell transduction uses an absolute pheromone sensing mechanism. In other words, what requires the control of an adaptive process in this system is signal production and not signal transduction. The number of potential mates is only a cue for mating likelihood when compared to the number of competitors. As a sensory system, attenuation-based population-parameter sensing might well fit into one of the well-known simple biophysical descriptions of the sensory-response process. The three widely accepted descriptions are, first, Weber's empirical law for sensory thresholds is $S_{min} = kS_0$, where S_{min} is the minimal stimulus level producing a detectable response, k is a constant called the Weber fraction and S_0 is the background stimulus to which the system is adapted to. Second, The Weber-Fechner relationship, also called logarithmic sensing is $F = a \ln \frac{S}{S_0}$, where F is now an internal sensation scale, S is the stimulus and S_0 is the background stimulus. And third the more general Stevens power law [2, 93] ($F = kS^n$, where k and n are constants). Steven's power law is more general because it explains a plethora of sensory modalities including non-compressive (non-converging) relations, e.g. electroshock sensation lowers the threshold for sensation at higher basal stimulus (with the highest n=3.5), opposite to the Weber-Fechner relationship and length visual perception (n=1) rather keeps a linear relationship with no changes in the threshold. The exponent can be as low as 0.5 for brightness perception in humans. Two processes, namely changes in the number of competitors and changes in the number of potential mates generate non-linear and linear changes in response magnitude. When the density of $MAT\alpha$ cells is constant, our attenuation function can be mathematically described as α_{max} being a negative power law function of recipient density ($\alpha_{max} = \rho_\alpha {\rho_a}^{-0.5}$). On the other hand, at constant density of $MAT\boldsymbol{a}$ cells, Weber's law holds, with the Weber constant (k) being equal to $1/\sqrt{\rho_a}$. Since α-factor signal transduction does not process the signal further in the relevant time, in the yeast mating system α_{max} is equivalent to the response magnitude. The response sensitivity to potential mates can be defined as $\frac{\Delta\alpha_{max}}{\Delta\rho_\alpha} = \frac{1}{\sqrt{\rho_a}}$. On the the hand, the non-linear response to competitors is a power law. A power law results in a straight line in a log-log plot (with a slope equal to 0.5 in this case), unlike similar trends (e.g., a converging exponential or a or a Michaelis-Menten curve have a similar shape, however these are not linear in the log-log plane). Steven's account of sensory data allows interpreting the attenuation model in terms of an established empirical law. It is similar to Weber-Fechner curves, but cannot be

called logarithmic sensing. In summary the yeast population-parameter sensing system is well described by sensory-biophysical functions.

17.2 Shmooing control in mixing experiments

From dose-response stimulation experiments we suggest that the reason for shmooing avoidance in the wt strain in density-ratio experiments is that the necessary signal concentration is not reached. Input attenuation allows the wt strain to align its dynamic range of sensing with the sex-ratio. As a consequence, the shmooing phenotype is not expressed, unlike *the bar1*Δ strain which has a compact and unspecific (unable to distinguish absolute from relative mate number) dynamic range. As shown with purified α-factor stimulations, the fact that the wt can show response values sufficient for shmooing does not imply that shmooing must be developed. On the other hand, showing sub-maximal response values does not imply that the shmooing threshold has not been crossed.Sex-ratio generates a dose-response similar to purified pheromones, but unlike in the latter, in the former the wt is indeed able to visit the elongation state (not shown). When varying the ratio at constant densities in the wt strain the contribution of Bar1 to response-rate attenuation is kept across sex ratios, because shmooing is not observed in a wide range. However, signalling can be persistent because α-factor is constantly secreted, so wt cells can elongate and high gene-expression values can be attained which explains the high response values at high ratios. Absence of a clear overshoot in the sex ratio curves suggests that pheromone concentrations generated are not higher than those causing the overshoot in stimulation experiments. Unlike the wt strain, in *bar1*Δ the responses are determined by the abundance of $MAT\alpha$ and independent of the abundance of $MAT\boldsymbol{a}$, so shmooing is naturally more sensitive to $MAT\alpha$ cells abundance. Hence, the *bar1*Δ strain shows the characteristic dose-dependent overshoot and dose-dependent downregulation observed in stimulation experiments already at low ratios. If the sex ratio is pushed to extreme high values, the wt indeed can show shmooing an dose-dependent downregulation (characteristic of shmooing) (Fig. 41). On the other extreme, wt cells seem to be sensitive to very low concentrations of opposite cells (Fig. 28), in agreement with high sensitivity to pheromones (Fig. 38), reduced Bar1 attenuation at early stimulation times (Fig. 22) and lack of adaptation to basal autocrine signalling (Fig. 20).

17.3 Relation of sex-ratio with encounter probability

Our results demonstrate that Bar1-dependent input attenuation allows cells to prevent overstimulation, premature commitment to mating and unproductive growth arrest at higher density of $MAT\alpha$ cells, as well as to ensure controlled induction of the costly mating response dependent on the density and the sex ratio of the population in the same way mating-pair formation is

determined by those parameters. In an active mating population, sex ratio changes the mating probability in all organisms going through sexual reproduction, i.e. the underlying probability of an encounter with a mate depends not much on their number but rather on their availability, i.e. the degree of competition in the population. Instant knowledge of the sex-ratio as a determinant of mating behavior (and hence, sexual selection strength) is often assumed but not explained. By sensing it, organisms can bias the imposed probability on their favor by searching mates, killing competitors, performing courtship, choosing etc. We propose that yeast can sense the sex ratio, and provide an example mechanism. The problem of using a chemosensory system to know the proportion of mates to same-sex individuals (unlike visual counting) is entanglement with density, signal attenuation being one possible solution. Because or the above reasons, yeast resulted an attractive model to perform detailed quantitative studies of general principles that may underlie mating behavior and its regulation. The mass action model shows that pathway activation and cell cycle arrest increase proportionality to pairing probability, however it also predicts that in the long run a trivial steady state where all cells in the minority finds a mate, making ratio sensing only effective transiently. Our measurements on aggregation and mating likelihood confirm that dependence of pairing probability on sex-ratio has in reality a non-trivial steady state that matches perfectly the gene-expression response to sex-ratio. The fact that a steady-state is not equal to exhaustion of mates was observed before by Sena [89] by counting zygotes. She attributed the effect to differences to phenotypic variability, i.e. not all cells are ready to mate in the mating reaction. Since we measure aggregation, heterogeneity could play a role in the expression of agglutinins (possibly related to the arrest state of the cell), so there would be always a fraction of "less-sticky" cells. Another explanation could be that the rate constant of the inverse process "de-agglutination" could increase with ratio. This agrees with a clear downregulation of the *AGA2* gene at the mRNA level at high pheromone doses (Alexander Anders, unpublished), which could be responsible for the effect. The rules we propose for sensory disentanglement (independent of the mechanism by which produce them) might be valid for any pheromonal (vomeronasal in animals) system under unbiased conditions (isotropicity). We can think of it as “sex ratio awareness”, or the (basal) response to “background sex ratio” previous to active mating behavior. Sensing collision likelihood would be a useful strategy under all conditions where the timescale of mating encounter is much smaller than the rate of haplo-selfing in growing colonies. Haploid germinated spores can haplo-self ([58]), i.e. change sex and mate with its mother, or mate with a non-kin ([76]). Haplo-selfing is the easiest way of finding a mate after the start of haploid growth. Commonly used lab strains (as ours) cannot haplo-self. The utility of sex ratio sensing to infer likelihood would be expected to be greater in situations where germination and growth are slow. The rate at which encounters occur in nature is expected to depend on biophysical parameters and so does the utility of sensing mating likelihood by

measuring the sex ratio.

18 Predictability and anticipation

Our work shows that chemosensory sex-ratio sensing through input-attenuation mediated disentanglement of mating cues tunes gene expression to match sexual encounter probability. A chemosensory system can only estimate population parameters precisely if it can first disentangle them from the unitary pheromone signal. Once the parameters are disentangled, an effective response to the mating probability P(m) relies on the ability of the sensory system to match its saturation value with P(m)=1 and its basal activity to P(m)=0. For example, the precision with which the center of the maximum possible dynamic range of the P_{FUS1} response to sex ratio hits θ=0.5. Since in nature density is a dynamic variable (as it is θ to a minor extent), to efficiently determine the mating probability a sensory system has to continuously monitor parameters and estimate the current P(m) value. The prediction in yeast is then based on a measurement instead of an internal representation, as described before for *E. coli* [96]. In Tagkoupolos et al. [96], predictability is defined by the coupling of two random events X and Y. In the case of *E.coli* entering its host, the events are the temperature rise in the human mouth and the subsequent pH decrease in the gastrointestinal tract, respectively. In this case *E. coli* simply evolved linked the transcriptional regulatory networks for heat shock and pH-resistance such that the latter get induced when the direct stimulus is the former. In our case it is input disentanglement and evolutionary tuning of the response dynamic range to mating likelihood what allows predictive behavior. Anticipation in yeast might come from evolutionary tuning of responses to the deterministic outcomes of aggregation by random collisions. Mating-likelihood sensing is expected to evolve from cells lineages with superior fitness control, i.e. those lineages that do no get overstimulated arresting growth more than necessary and at the same time are sensitive enough to detect a mating chance whenever it is present.

19 Conclusions

With the results obtained in this study we can formulate the conclusions listed below.

First, extracellular signal degradation by Bar1 is essential to achieve response downregulation to pheromones at the mating-relevant range of the dose-response. When Bar1 is absent, the MPP lacks an effective mechanism for desensitization. In fact, sensitivity to pheromones remains invariant even if the cells are adapted to different background concentration. This property can be called absolute concentration sensing.

Second, when absolute pheromone concentration sensing is coupled with the external Bar1-

dependent attenuation system. A population-level sensory-adaptive response is generated. The response can be described by classical biophysical descriptions of sensory input-output processes. The response magnitude generated is a decreasing function of the number of same-sex cells. Consequently, cell populations adapt their responses to the current level of competition and do not measure simply the absolute number of potential mates. Then, yeast mating can work as a population fractional-sensing system that does rely on internal but rather on external sensory adaptation (better called attenuation).

Third, the ability to respond to the ratio of potential-mates to competitors and distinguishing it from pure total density changes is explained with the fact that the response dependence on sex-ratio is perfectly correlated with the dependence the probability a given cell has to pair (and mate) a cell of the opposite sex has on sex-ratio, hence there is a tight quantitative relation between the response intensity and the mating probability.

Fourth, response amplitude tuning to likelihood allows cells to scape the negative late effects of overstimulation in spite of its immediate kinetic advantage and avoid arrest that's unlikely to succeed. This constitutes an example of biological anticipation.

Fifth, the work provides a novel way of looking at the function of the mating pheromone pathway and Bar1 at the population level. For cell-cell communication the result demonstrate the capacity to perform more complex tasks (ratio of cell-types) than simple density sensing (or quorum sensing) with an extremely simple network topology. Of use for cellular sensory systems, our result suggests that absolute-concentration sensing is an appropriate sensory strategy when the signal concentration has already been processed and carries population level information (mating likelihood in this case). For sexual selection theory, we contribute by providing a plausible mechanism for perception of competition in chemosensory mating systems.

Part V

Appendix: Supporting Figures

Supporting figures (Figures 37 to 42, see next page)

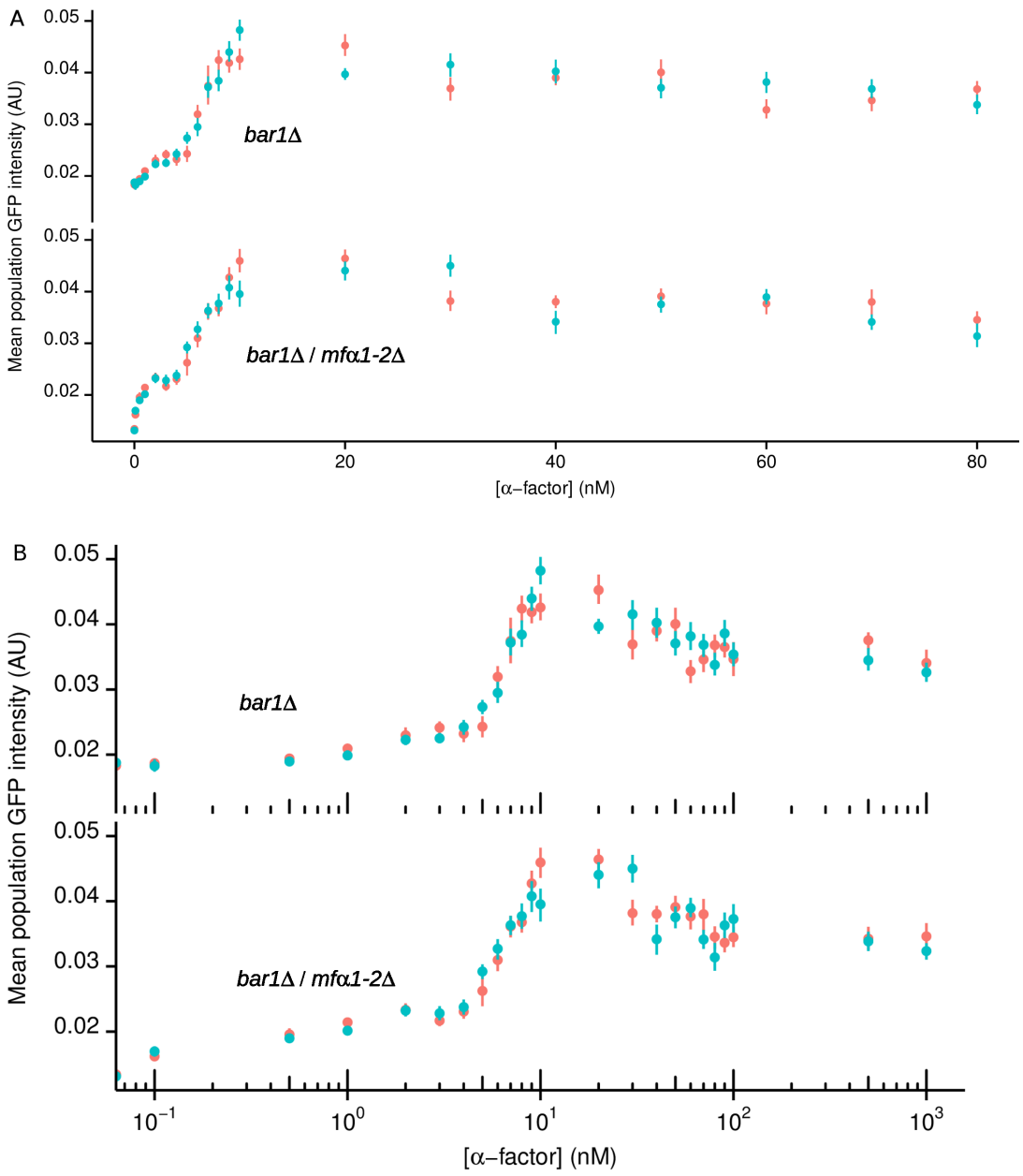

Figure 37: Gene expression response overshoot. Biological replicate from experiment in Fig. 11 in *bar1*Δ strain with (top) or without (bottom) autocrine signalling with technical replicas (a different field of view, colors) shown in linear (A) and logarithmic scales (B). Note the lower basal intensity level of the non-autocrine signaler. Error bars are the standard error of the mean single cell intensity in a field of view (50-100 cells).

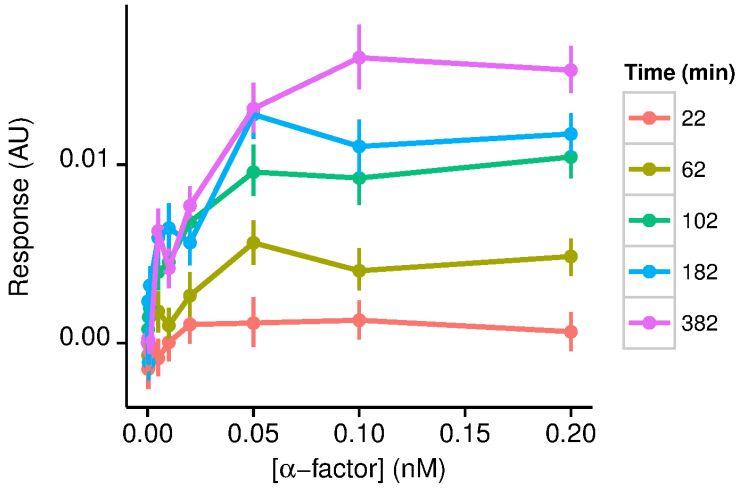

Figure 38: P_{FUS1}-GFP response to picomolar concentrations of α-factor in MAT***a***. α-factor dose response resolving the picomolar range of pheromone concentration at different times after stimulation (colors). Note that dose responses show a plateau at concentrations much lower than the response sensitive range.

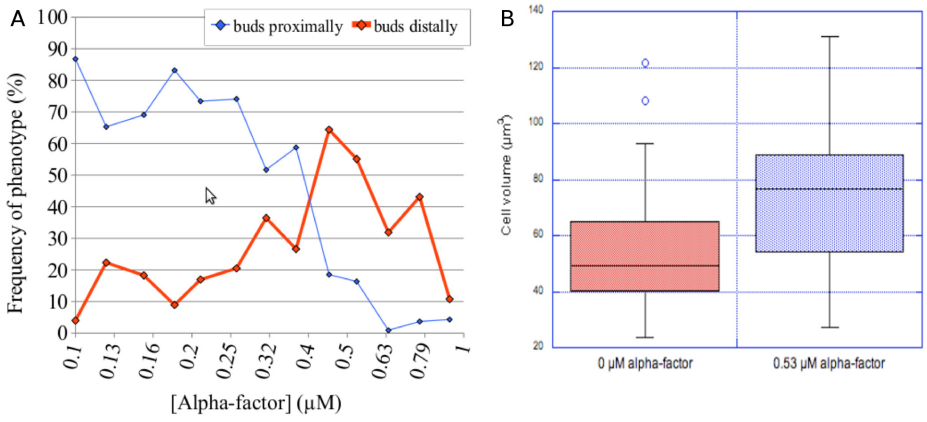

Figure 39: Quantification of transitional phenotypes in the wt strain. Additional mating morphologies are observed below the shmooing threshold. A. Bipolar budding happens when a bud emerges from the opposite site from the previous bud. At low concentrations of pheromone, the budding pattern is altered without influencing the general arresting behavior (Fig. 15) or modifying cell volume. B. Cellular volume increase of 25% (isotropic cell volume increase without elongation) happens only in a narrow range of α-factor concentration. Data is from Fig. 16

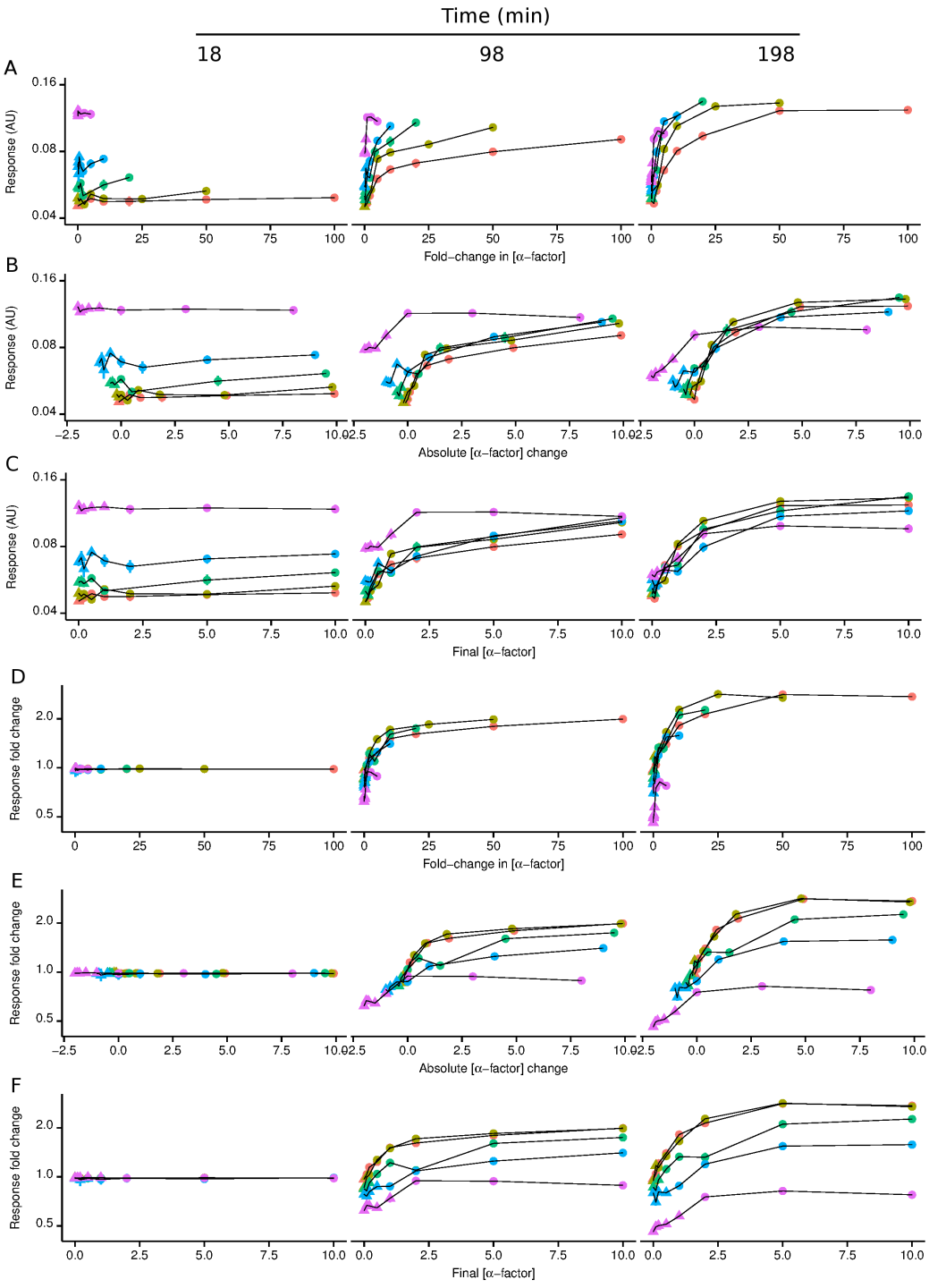

Figure 40: Gene expression response to α-factor on pre-stimulated $MAT\boldsymbol{a}$ populations. P_{FUS1}-GFP expression plotted as the absolute (A, B, C) or fold-change (D, E, F) signal intensity in response to the fold-change (A, D), the absolute change (in nM) (B, E) or the final concentration (in nM) (C, F) of α-factor at 3 different time points in cell populations pre-stimulated with 0.1 (red), 0.2 (yellow), 0.5 (green), 1 (blue) or 2 (pink) nM of α-factor for 320 minutes prior to performing step concentration changes. Response fold-changes correspond to the response normalized to steady state value measured at 18 minutes after changes or additions of α-factor. Note linear y-axis compared with Fig. 21.

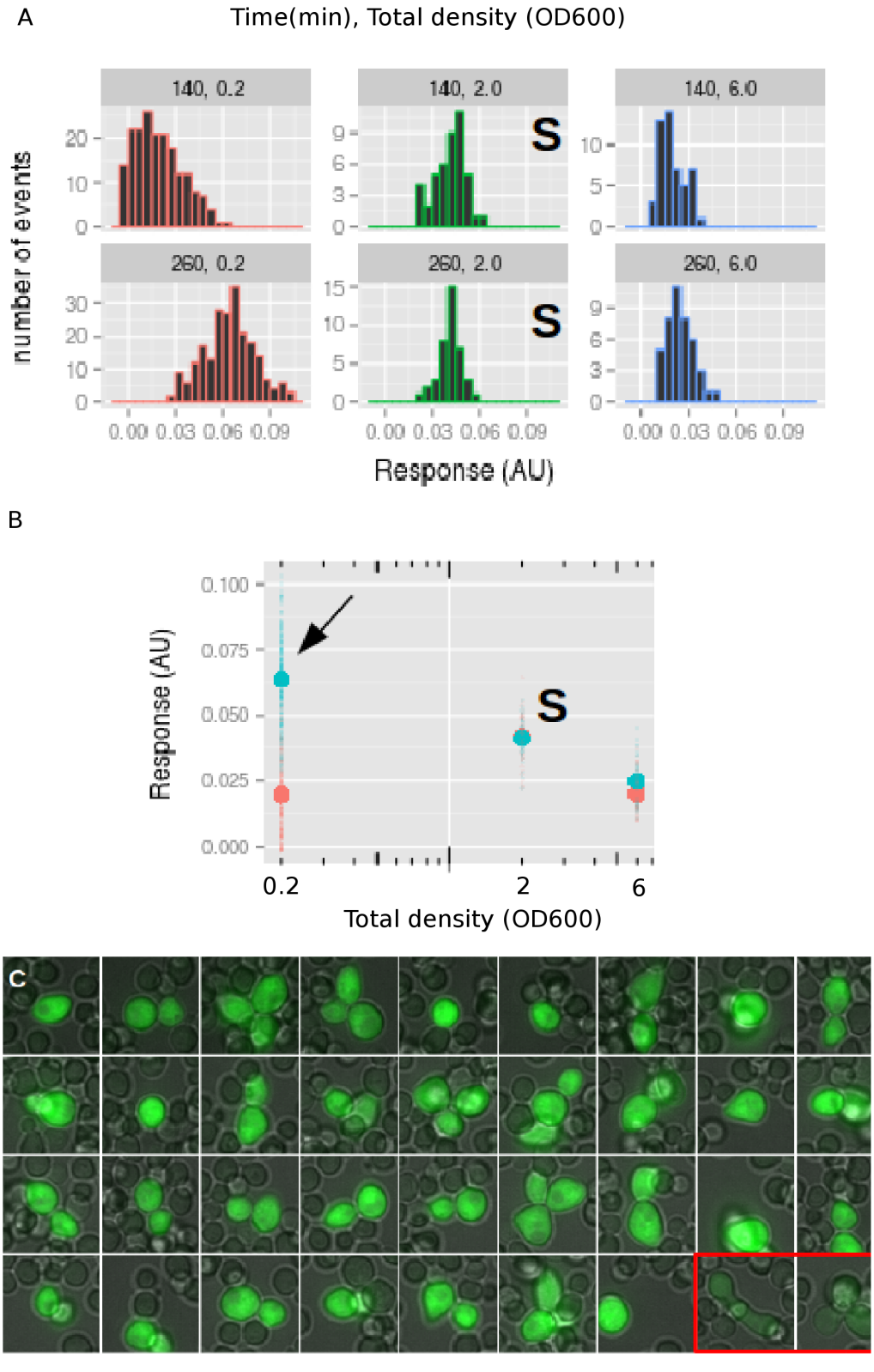

Figure 41: Limit to commitment avoidance in the wt strain. A. GFP intensity distributions in mixing experiments with fixed θ=0.99 and varying total (population) density values at different times. The wt strain only reaches the shmooing threshold at a total population density of OD_{600}=2 ("S" marks shmooing populations). B. Same data as in (A) plotted in the total density axis and different times labeled with colors (red =140 minutes and blue = 260 minutes). The arrow shows the population from where example cells are pictured in panel (C). C. As expected from our dose-response experiments, downregulation of the gene-expression response correlates with shmooing. At OD_{600}=0.2 even though the ratio is high, cells do not shmoo but show "near shmooing" phenotypes. At OD_{600}=6 shmooing is absent, presumably because extreme high densities can be damaging for responding cells.

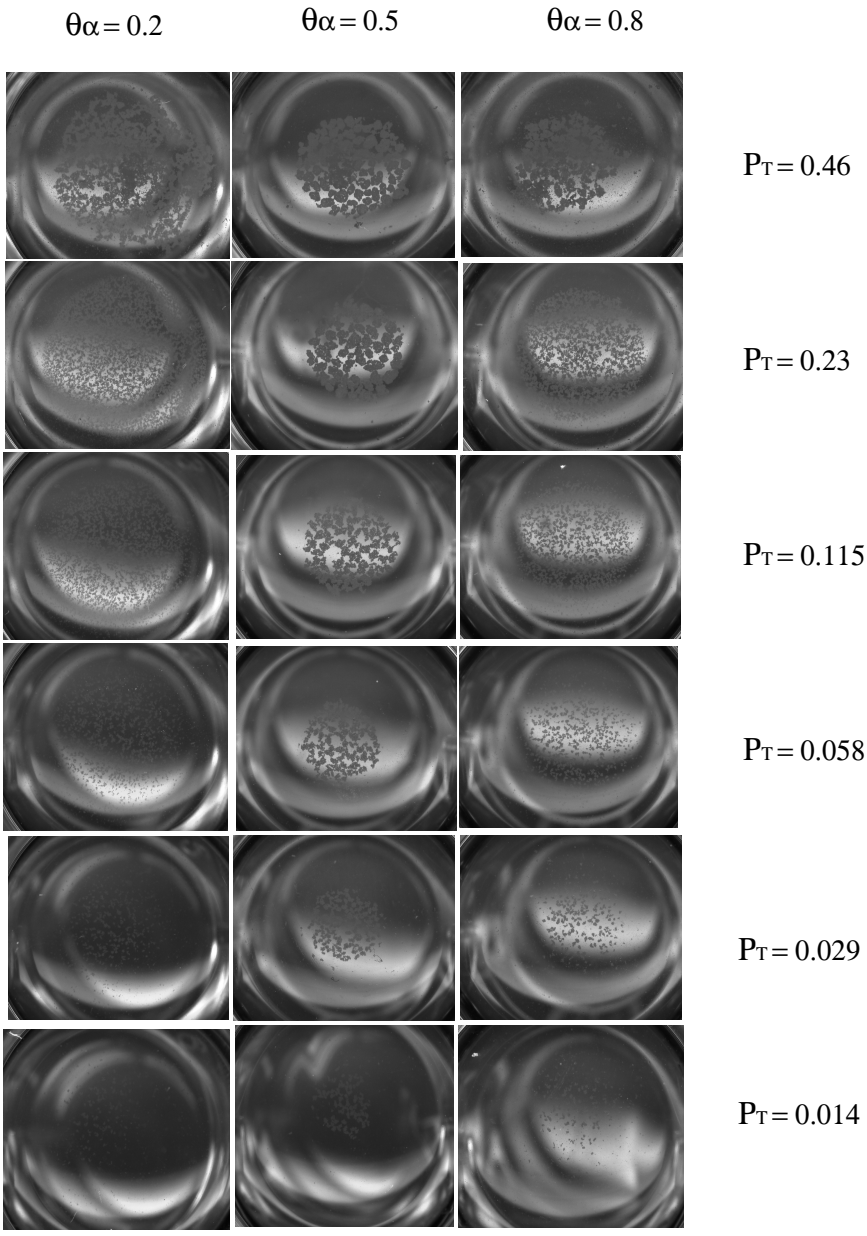

Figure 42: Macroscopic aggregate formation. Mating reactions at different ρ_T values (in OD_{600}) and θ_α values with mild shaking showing macroscopic aggregate formation. The picture was taken 1 hour after incubation, showing the fast aggregation kinetics.

References

[1] T Achstetter. Regulation of alpha-factor production in Saccharomyces cerevisiae: a-factor pheromone-induced expression of the MF alpha 1 and STE13 genes. *Mol Cell Biol*, 9(10):4507–14, October 1989.

[2] Miri Adler, Avi Mayo, and Uri Alon. Logarithmic and power law input-output relations in sensory systems with fold-change detection. *PLoS Comput Biol*, 10(8):e1003781, Aug 2014.

[3] Karin L Akre, Hamilton E Farris, Amanda M Lea, Rachel A Page, and Michael J Ryan. Signal perception in frogs and bats and the evolution of mating signals. *Science*, 333(6043):751–752, Aug 2011.

[4] Karin L Akre and Sönke Johnsen. Psychophysics and the evolution of behavior. *Trends Ecol Evol*, 29(5):291–300, May 2014.

[5] Simon Alberti, Aaron D Gitler, and Susan Lindquist. A suite of gateway cloning vectors for high-throughput genetic analysis in saccharomyces cerevisiae. *Yeast*, 24(10):913–919, Oct 2007.

[6] Uri Alon. *An Introduction to Systems Biology: Design Principles of Biological Circuits (Chapman & Hall/CRC Mathematical and Computational Biology)*. Chapman and Hall/CRC, 2006.

[7] Robert a Arkowitz. Chemical gradients and chemotropism in yeast. *CSH Perspect Biol*, 1(2):a001958, August 2009.

[8] Lee Bardwell. A walk-through of the yeast mating pheromone response pathway. *Peptides*, 26(2):339–350, Feb 2005.

[9] N. Barkai, M. D. Rose, and N. S. Wingreen. Protease helps yeast find mating partners. *Nature*, 396(6710):422–423, Dec 1998.

[10] Marcelo Behar, Nan Hao, Henrik G Dohlman, and Timothy C Elston. Dose-to-duration encoding and signaling beyond saturation in intracellular signaling networks. *PLoS Comput Biol*, 4(10):e1000197, Oct 2008.

[11] Anders Berglund. The operational sex ratio influences choosiness in a pipefish. *Behav Ecol*, 5(3):254–258, 1994.

[12] Ernest Blackwell, Izabel M Halatek, Hye-Jin N Kim, Alexis T Ellicott, Andrey A Obukhov, and David E Stone. Effect of the pheromone-responsive g(alpha) and phosphatase proteins

of saccharomyces cerevisiae on the subcellular localization of the fus3 mitogen-activated protein kinase. *Mol Cell Biol*, 23(4):1135–1150, Feb 2003.

[13] J.W. Boughman. How sensory drive can promote speciation. *Trends Ecol Evol*, 17:571–577, 2002.

[14] Roger Brent. Cell signaling: what is the signal and what information does it carry? *FEBS Lett*, 583(24):4019–4024, Dec 2009.

[15] a. Butty. The Role of Far1p in Linking the Heterotrimeric G Protein to Polarity Establishment Proteins During Yeast Mating. *Science*, 282(5393):1511–1516, November 1998.

[16] Anne-Christine Butty, Nathalie Perrinjaquet, Audrey Petit, Malika Jaquenoud, Jeffrey E Segall, Kay Hofmann, Catherine Zwahlen, and Matthias Peter. A positive feedback loop stabilizes the guanine-nucleotide exchange factor Cdc24 at sites of polarization. *The EMBO journal*, 21(7):1565–76, April 2002.

[17] Fabrice Caudron and Yves Barral. A super-assembly of whi3 encodes memory of deceptive encounters by single cells during yeast courtship. *Cell*, 155(6):1244–1257, Dec 2013.

[18] Song Chou, Shelley Lane, and Haoping Liu. Regulation of mating and filamentation genes by two distinct ste12 complexes in saccharomyces cerevisiae. *Mol Cell Biol*, 26(13):4794–4805, Jul 2006.

[19] E. Ciejek and J. Thorner. Recovery of s. cerevisiae a cells from g1 arrest by alpha factor pheromone requires endopeptidase action. *Cell*, 18(3):623–635, Nov 1979.

[20] Alison E Coluccio, Rachael K Rodriguez, Maurice J Kernan, and Aaron M Neiman. The yeast spore wall enables spores to survive passage through the digestive tract of drosophila. *PLoS One*, 3(8):e2873, 2008.

[21] Karen de Jong, Elisabet Forsgren, Hanno Sandvik, and Trond Amundsen. Measuring mating competition correctly: available evidence supports operational sex ratio theory. *Behav Ecol*, 23(6):1170–1177, 2012.

[22] Christian Diener, Gabriele Schreiber, Wolfgang Giese, Gabriel del Rio, Andreas Schroeder, and Edda Klipp. Yeast mating and image-based quantification of spatial pattern formation. *PLoS Comput Biol*, 10(6):e1003690, Jun 2014.

[23] H. G. Dohlman, J. Song, D. Ma, W. E. Courchesne, and J. Thorner. Sst2, a negative regulator of pheromone signaling in the yeast saccharomyces cerevisiae: expression, localization, and genetic interaction and physical association with gpa1 (the g-protein alpha subunit). *Mol Cell Biol*, 16(9):5194–5209, Sep 1996.

[24] Andreas Doncic and Jan M Skotheim. Feedforward regulation ensures stability and rapid reversibility of a cellular state. *Mol Cell*, 50(6):856–868, Jun 2013.

[25] R. Dorer, C. Boone, T. Kimbrough, J. Kim, and L. H. Hartwell. Genetic analysis of default mating behavior in saccharomyces cerevisiae. *Genetics*, 146(1):39–55, May 1997.

[26] R. Dorer, P. M. Pryciak, and L. H. Hartwell. Saccharomyces cerevisiae cells execute a default pathway to select a mate in the absence of pheromone gradients. *J Cell Biol*, 131(4):845–861, Nov 1995.

[27] E. A. Elion. The ste5p scaffold. *J Cell Sci*, 114(Pt 22):3967–3978, Nov 2001.

[28] R. Keith Esch, Yuqi Wang, and Beverly Errede. Pheromone-induced degradation of ste12 contributes to signal attenuation and the specificity of developmental fate. *Eukaryot Cell*, 5(12):2147–2160, Dec 2006.

[29] G. Fehrenbacher, K. Perry, and J. Thorner. Cell-cell recognition in saccharomyces cerevisiae: regulation of mating-specific adhesion. *J Bacteriol*, 134(3):893–901, Jun 1978.

[30] James E Ferrell. Signaling motifs and weber's law. *Mol Cell*, 36(5):724–727, Dec 2009.

[31] J. E. Ferrell Jr. The Biochemical Basis of an All-or-None Cell Fate Switch in Xenopus Oocytes. *Science*, 280(5365):895–898, May 1998.

[32] R. Fuller, D. Houle, and J. Travis. Sensory bias as an explanation for the evolution of mate preferences. *Am. Nat.*, 166:437–446, 2005.

[33] Martin Funk, Rainer Niedenthal, Dominik Mumberg, Kay Brinkmann, Volker RÃ¶nicke, and Thomas Henkel. Vector systems for heterologous expression of proteins in saccharomyces cerevisiae. *Methods Enzymol*, 350:248–257, 2002.

[34] Daniel M Gelperin, Michael A White, Martha L Wilkinson, Yoshiko Kon, Li A Kung, Kevin J Wise, Nelson Lopez-Hoyo, Lixia Jiang, Stacy Piccirillo, Haiyuan Yu, Mark Gerstein, Mark E Dumont, Eric M Phizicky, Michael Snyder, and Elizabeth J Grayhack. Biochemical and genetic analysis of the yeast proteome with a movable orf collection. *Genes Dev*, 19(23):2816–2826, Dec 2005.

[35] Lea Goentoro, Oren Shoval, Marc W Kirschner, and Uri Alon. The incoherent feedforward loop can provide fold-change detection in gene regulation. *Mol Cell*, 36(5):894–899, Dec 2009.

[36] Matthew Good, Grace Tang, Julie Singleton, Attila RemÃ©nyi, and Wendell A Lim. The ste5 scaffold directs mating signaling by catalytically unlocking the fus3 map kinase for activation. *Cell*, 136(6):1085–1097, Mar 2009.

[37] Albrecht Gruhler, Jesper V Olsen, Shabaz Mohammed, Peter Mortensen, Nils J Faergeman, Matthias Mann, and Ole N Jensen. Quantitative phosphoproteomics applied to the yeast pheromone signaling pathway. *Mol Cell Proteomics*, 4(3):310–327, Mar 2005.

[38] M. C. Gustin, J. Albertyn, M. Alexander, and K. Davenport. Map kinase pathways in the yeast saccharomyces cerevisiae. *Microbiol Mol Biol Rev*, 62(4):1264–1300, Dec 1998.

[39] D. C. Hagen, G. McCaffrey, and G. F. Sprague. Pheromone response elements are necessary and sufficient for basal and pheromone-induced transcription of the fus1 gene of saccharomyces cerevisiae. *Mol Cell Biol*, 11(6):2952–2961, Jun 1991.

[40] Nan Hao, Sujata Nayak, Marcelo Behar, Ryan H Shanks, Michal J Nagiec, Beverly Errede, Jeffrey Hasty, Timothy C Elston, and Henrik G Dohlman. Regulation of cell signaling dynamics by the protein kinase-scaffold Ste5. *Molecular cell*, 30(5):649–56, June 2008.

[41] Nan Hao, Necmettin Yildirim, Yuqi Wang, Timothy C Elston, and Henrik G Dohlman. Regulators of g protein signaling and transient activation of signaling: experimental and computational analysis reveals negative and positive feedback controls on g protein activity. *J Biol Chem*, 278(47):46506–46515, Nov 2003.

[42] Andrew M Hein and Scott A McKinley. Sensory information and encounter rates of interacting species. *PLoS Comput Biol*, 9(8):e1003178, 2013.

[43] Zoe Hilioti, Walid Sabbagh, Saurabh Paliwal, Adriel Bergmann, Marcus D Goncalves, Lee Bardwell, and Andre Levchenko. Oscillatory phosphorylation of yeast fus3 map kinase controls periodic gene expression and morphogenesis. *Curr Biol*, 18(21):1700–1706, Nov 2008.

[44] Lori B Huberman and Andrew W Murray. Genetically engineered transvestites reveal novel mating genes in budding yeast. *Genetics*, 195(4):1277–1290, Dec 2013.

[45] Adam L Hughes and Daniel E Gottschling. An early age increase in vacuolar ph limits mitochondrial function and lifespan in yeast. *Nature*, 492(7428):261–265, Dec 2012.

[46] Won-Ki Huh, James V Falvo, Luke C Gerke, Adam S Carroll, Russell W Howson, Jonathan S Weissman, and Erin K O'Shea. Global analysis of protein localization in budding yeast. *Nature*, 425(6959):686–691, Oct 2003.

[47] John M C Hutchinson and Peter M Waser. Use, misuse and extensions of "ideal gas" models of animal encounter. *Biol Rev Camb Philos Soc*, 82(3):335–359, Aug 2007.

[48] C. L. Jackson and L. H. Hartwell. Courtship in s. cerevisiae: both cell types choose mating partners by responding to the strongest pheromone signal. *Cell*, 63(5):1039–1051, Nov 1990.

[49] C. L. Jackson and L. H. Hartwell. Courtship in saccharomyces cerevisiae: an early cell-cell interaction during mating. *Mol Cell Biol*, 10(5):2202–2213, May 1990.

[50] Carsten Janke, Maria M Magiera, Nicole Rathfelder, Christof Taxis, Simone Reber, Hiromi Maekawa, Alexandra Moreno-Borchart, Georg Doenges, Etienne Schwob, Elmar Schiebel, and Michael Knop. A versatile toolbox for PCR-based tagging of yeast genes: new fluorescent proteins, more markers and promoter substitution cassettes. *Yeast (Chichester, England)*, 21(11):947–62, August 2004.

[51] M. Jin, B. Errede, M. Behar, W. Mather, S. Nayak, J. Hasty, H. G. Dohlman, and T. C. Elston. Yeast Dynamically Modify Their Environment to Achieve Better Mating Efficiency. *Sci Signal*, 4(186):ra54–ra54, August 2011.

[52] Meng Jin, Beverly Errede, Marcelo Behar, Will Mather, Sujata Nayak, Jeff Hasty, Henrik G Dohlman, and Timothy C Elston. Yeast dynamically modify their environment to achieve better mating efficiency. *Sci Signal*, 4(186):ra54, Aug 2011.

[53] Yevgeniy V Kalinin, Lili Jiang, Yuhai Tu, and Mingming Wu. Logarithmic sensing in escherichia coli bacterial chemotaxis. *Biophys J*, 96(6):2439–2448, Mar 2009.

[54] Yukiko Kawanabe, Kazuo Yoshida, and Naohiko Yanagishima. Sexual cell agglutination in relation to the formation of zygotes in saccharomyces cerevisiae. *Plant and Cell Physiology*, 20(2):423–433, 1979.

[55] David Kentner and Victor Sourjik. Dynamic map of protein interactions in the Escherichia coli chemotaxis pathway. *Molecular systems biology*, 5(238):238, January 2009.

[56] Anton Khmelinskii, Philipp J Keller, Anna Bartosik, Matthias Meurer, Joseph D Barry, Balca R Mardin, Andreas Kaufmann, Susanne Trautmann, Malte Wachsmuth, Gislene Pereira, Wolfgang Huber, Elmar Schiebel, and Michael Knop. Tandem fluorescent protein timers for in vivo analysis of protein dynamics. *Nat Biotechnol*, 30(7):708–714, Jul 2012.

[57] Anton Khmelinskii, Matthias Meurer, Nurlanbek Duishoev, Nicolas Delhomme, and Michael Knop. Seamless gene tagging by endonuclease-driven homologous recombination. *PloS one*, 6(8):e23794–e23794, 2011.

[58] Michael Knop. Evolution of the hemiascomycete yeasts: on life styles and the importance of inbreeding. *BioEssays*, 28(7):696–708, July 2006.

[59] Hanna Kokko and Daniel J Rankin. Lonely hearts or sex in the city? density-dependent effects in mating systems. *Philos Trans R Soc Lond B Biol Sci*, 361(1466):319–334, Feb 2006.

[60] B. Kopocinski and T. M. Lachowicz. A probabilistic approach to the analysis of the frequency of diploid formation in yeast (saccharomyces cerevisiae) mating. *Mikrobiol Z*, 56(6):3–16, 1994.

[61] Mohit Kumar and Victor Sourjik. Physical map and dynamics of the chaperone network in escherichia coli. *Mol Microbiol*, 84(4):736–747, May 2012.

[62] C. Kvarnemo and I. Ahnesjo. The dynamics of operational sex ratios and competition for mates. *Trends Ecol Evol*, 11(10):404–408, Oct 1996.

[63] Gregory I Lang, Andrew W Murray, and David Botstein. The cost of gene expression underlies a fitness trade-off in yeast. *Proc Natl Acad Sci U S A*, 106(14):5755–5760, Apr 2009.

[64] P. N. Lipke and J. Kurjan. Sexual agglutination in budding yeasts: structure, function, and regulation of adhesion glycoproteins. *Microbiol Rev*, 56(1):180–194, Mar 1992.

[65] P. N. Lipke, D. Wojciechowicz, and J. Kurjan. Ag alpha 1 is the structural gene for the saccharomyces cerevisiae alpha-agglutinin, a cell surface glycoprotein involved in cell-cell interactions during mating. *Mol Cell Biol*, 9(8):3155–3165, Aug 1989.

[66] M. S. Longtine, A. McKenzie, D. J. Demarini, N. G. Shah, A. Wach, A. Brachat, P. Philippsen, and J. R. Pringle. Additional modules for versatile and economical pcr-based gene deletion and modification in saccharomyces cerevisiae. *Yeast*, 14(10):953–961, Jul 1998.

[67] M. G. Low and A. R. Saltiel. Structural and functional roles of glycosyl-phosphatidylinositol in membranes. *Science*, 239(4837):268–275, Jan 1988.

[68] V. L. MacKay, S. K. Welch, M. Y. Insley, T. R. Manney, J. Holly, G. C. Saari, and M. L. Parker. The saccharomyces cerevisiae bar1 gene encodes an exported protein with homology to pepsin. *Proc Natl Acad Sci U S A*, 85(1):55–59, Jan 1988.

[69] Mohan K Malleshaiah, Vahid Shahrezaei, Peter S Swain, and Stephen W Michnick. The scaffold protein Ste5 directly controls a switch-like mating decision in yeast. *Nature*, 465(7294):101–105, April 2010.

[70] T. R. Manney. Expression of the bar1 gene in saccharomyces cerevisiae: induction by the alpha mating pheromone of an activity associated with a secreted protein. *J Bacteriol*, 155(1):291–301, Jul 1983.

[71] Humberto Martin, Marta Flandez, Cesar Nombela, and Maria Molina. Protein phosphatases in mapk signalling: we keep learning from yeast. *Mol Microbiol*, 58(1):6–16, Oct 2005.

[72] Eric L Miller and Duncan Greig. Spore germination determines yeast inbreeding according to fitness in the local environment. *Am Nat*, 185(2):291–301, Feb 2015.

[73] S a Moore. Comparison of dose-response curves for alpha factor-induced cell division arrest, agglutination, and projection formation of yeast cells. Implication for the mechanism of alpha factor action. *The Journal of biological chemistry*, 258(22):13849–56, November 1983.

[74] Travis I Moore, Ching-Shan Chou, Qing Nie, Noo Li Jeon, and Tau-Mu Yi. Robust spatial sensing of mating pheromone gradients by yeast cells. *PLoS One*, 3(12):e3865, 2008.

[75] I. Moukadiri, L. Jaafar, and J. Zueco. Identification of two mannoproteins released from cell walls of a saccharomyces cerevisiae mnn1 mnn9 double mutant by reducing agents. *J Bacteriol*, 181(16):4741–4745, Aug 1999.

[76] Helen a Murphy and Clifford W Zeyl. Yeast sex: surprisingly high rates of outcrossing between asci. *PloS one*, 5(5):e10461, January 2010.

[77] R. Nath. Properties of barrier, a novel saccharomyces cerevisiae acid protease. *Biochimie*, 75(6):467–472, 1993.

[78] Scott Nolan, Ann E Cowan, Dennis E Koppel, Hui Jin, and Eric Grote. Fus1 regulates the opening and expansion of fusion pores between mating yeast. *Mol Biol Cell*, 17(5):2439–2450, May 2006.

[79] Saurabh Paliwal, Pablo a Iglesias, Kyle Campbell, Zoe Hilioti, Alex Groisman, and Andre Levchenko. MAPK-mediated bimodal gene expression and adaptive gradient sensing in yeast. *Nature*, 446(7131):46–51, March 2007.

[80] M. A. Poritz, S. Malmstrom, M. K. Kim, P. J. Rossmeissl, and A. Kamb. Graded mode of transcriptional induction in yeast pheromone signalling revealed by single-cell analysis. *Yeast*, 18(14):1331–1338, Oct 2001.

[81] Noa Rappaport and Naama Barkai. Disentangling signaling gradients generated by equivalent sources. *J Biol Phys*, 38(2):267–278, Mar 2012.

[82] Nicola O Reilly, Adrian Charbin, Lidia Lopez-serra, and Frank Uhlmann. Facile synthesis of budding yeast a-factor and its use to synchronize cells of a mating type. (May):233–240, 2012.

[83] Max Reuter, Graham Bell, and Duncan Greig. Increased outbreeding in yeast in response to dispersal by an insect vector. *Curr Biol*, 17(3):R81–R83, Feb 2007.

[84] J. S. Robinson, D. J. Klionsky, L. M. Banta, and S. D. Emr. Protein sorting in saccharomyces cerevisiae: isolation of mutants defective in the delivery and processing of multiple vacuolar hydrolases. *Mol Cell Biol*, 8(11):4936–4948, Nov 1988.

[85] David W Rogers and Duncan Greig. Experimental evolution of a sexually selected display in yeast. *Proc Biol Sci*, 276(1656):543–549, Feb 2009.

[86] David W Rogers, Ellen McConnell, and Duncan Greig. Molecular quantification of saccharomyces cerevisiae alpha-pheromone secretion. *FEMS Yeast Res*, 12(6):668–674, Sep 2012.

[87] J E Segall. Polarization of yeast cells in spatial gradients of alpha mating factor. *Proceedings of the National Academy of Sciences of the United States of America*, 90(18):8332–6, September 1993.

[88] E. P. Sena. A and alpha supernatant pretreatment of saccharomyces cerevisiae cells affects both the kinetics and efficiency of mating. *Mol Cell Biol*, 2(8):897–903, Aug 1982.

[89] E. P. Sena, D. N. Radin, and S. Fogel. Synchronous mating in yeast. *Proc Natl Acad Sci U S A*, 70(5):1373–1377, May 1973.

[90] R. S. Sikorski and P. Hieter. A system of shuttle vectors and yeast host strains designed for efficient manipulation of dna in saccharomyces cerevisiae. *Genetics*, 122(1):19–27, May 1989.

[91] Victor Sourjik and Howard C Berg. Receptor sensitivity in bacterial chemotaxis. *Proceedings of the National Academy of Sciences of the United States of America*, 99(1):123–7, January 2002.

[92] Judy A Stamps, Louie H Yang, Vanessa M Morales, and Kyria L Boundy-Mills. Drosophila regulate yeast density and increase yeast community similarity in a natural substrate. *PLoS One*, 7(7):e42238, 2012.

[93] S. S. Stevens. To honor fechner and repeal his law: A power function, not a log function, describes the operating characteristic of a sensory system. *Science*, 133(3446):80–86, Jan 1961.

[94] J. R. Strazdis and V. L. MacKay. Induction of yeast mating pheromone a-factor by alpha cells. *Nature*, 305(5934):543–545, 1983.

[95] Katsunori Suzuki. Roles of sexual cell agglutination in yeast mass mating. *Genes Genet Syst*, 78(3):211–219, Jun 2003.

[96] Ilias Tagkopoulos, Yir-Chung Liu, and Saeed Tavazoie. Predictive behavior within microbial genetic networks. *Science (New York, N.Y.)*, 320(5881):1313–7, June 2008.

[97] Satoe Takahashi and Peter M Pryciak. Membrane localization of scaffold proteins promotes graded signaling in the yeast MAP kinase cascade. *Current biology : CB*, 18(16):1184–91, August 2008.

[98] Satoe Takahashi and Peter M Pryciak. Membrane localization of scaffold proteins promotes graded signaling in the yeast map kinase cascade. *Curr Biol*, 18(16):1184–1191, Aug 2008.

[99] Christof Taxis and Michael Knop. System of centromeric, episomal, and integrative vectors based on drug resistance markers for saccharomyces cerevisiae. *Biotechniques*, 40(1):73–78, Jan 2006.

[100] F. van Drogen, V. M. Stucke, G. Jorritsma, and M. Peter. Map kinase dynamics in response to pheromones in budding yeast. *Nat Cell Biol*, 3(12):1051–1059, Dec 2001.

[101] Alejandra C Ventura, Alan Bush, Gustavo Vasen, MatÃas A GoldÃn, Brianne Burkinshaw, Nirveek Bhattacharjee, Albert Folch, Roger Brent, Ariel Chernomoretz, and Alejandro Colman-Lerner. Utilization of extracellular information before ligand-receptor binding reaches equilibrium expands and shifts the input dynamic range. *Proc Natl Acad Sci U S A*, 111(37):E3860–E3869, Sep 2014.

[102] Peter J Verveer, Oliver Rocks, Ailsa G Harpur, and Philippe I H Bastiaens. Imaging protein interactions by fret microscopy: Fret measurements by acceptor photobleaching. *CSH Protoc*, 2006(6), 2006.

[103] Sebastian Wacker, Kenyon Mobley, Elisabet Forsgren, Lise Cats Myhre, Karen de Jong, and Trond Amundsen. Operational sex ratio but not density affects sexual selection in a fish. *Evolution*, 67(7):1937–1949, Jul 2013.

[104] Laura K Weir, James W A Grant, and Jeffrey A Hutchings. The influence of operational sex ratio on the intensity of competition for mates. *Am Nat*, 177(2):167–176, Feb 2011.

[105] Tau-Mu Yi, Hiroaki Kitano, and Melvin I Simon. A quantitative characterization of the yeast heterotrimeric G protein cycle. *Proceedings of the National Academy of Sciences of the United States of America*, 100(19):10764–9, September 2003.

[106] Tau-Mu Yi, Hiroaki Kitano, and Melvin I Simon. A quantitative characterization of the yeast heterotrimeric G protein cycle. *Proceedings of the National Academy of Sciences of the United States of America*, 100(19):10764–9, September 2003.

[107] T. Yorihuzi and Y. Ohsumi. Saccharomyces cerevisiae mata mutant cells defective in pointed projection formation in response to alpha-factor at high concentrations. *Yeast*, 10(5):579–594, May 1994.

[108] R. C. Yu, O. Resnekov, A. P. Abola, S. S. Andrews, K. R. Benjamin, J. Bruck, I. E. Burbulis, A. Colman-Lerner, D. Endy, A. Gordon, M. Holl, L. Lok, C. G. Pesce, E. Serra, R. D. Smith, T. M. Thomson, A. E. Tsong, and R. Brent. The alpha project: a model system for systems biology research. *IET Syst Biol*, 2(5):222–233, Sep 2008.

[109] Richard C Yu, C Gustavo Pesce, Alejandro Colman-Lerner, Larry Lok, David Pincus, Eduard Serra, Mark Holl, Kirsten Benjamin, Andrew Gordon, and Roger Brent. Negative feedback that improves information transmission in yeast signalling. *Nature*, 456(7223):755–61, December 2008.

[110] Julia Zeitlinger, Itamar Simon, Christopher T Harbison, Nancy M Hannett, Thomas L Volkert, Gerald R Fink, and Richard A Young. Program-specific distribution of a transcription factor dependent on partner transcription factor and mapk signaling. *Cell*, 113(3):395–404, May 2003.

[111] X. L. Zhan, R. J. Deschenes, and K. L. Guan. Differential regulation of fus3 map kinase by tyrosine-specific phosphatases ptp2/ptp3 and dual-specificity phosphatase msg5 in saccharomyces cerevisiae. *Genes Dev*, 11(13):1690–1702, Jul 1997.

[112] Nan-Nan Zhang, Drew D. Dudgeon, Saurabh Paliwal, Andre Levchenko, Eric Grote, and Kyle W. Cunningham. Multiple signaling pathways regulate yeast cell death during the response to mating pheromones. *Mol Biol Cel*, 17(8):3409–3422, Aug 2006.